DESIGN, SIMULATION AND CONTROL OF A 12 DOF BIPED ROBOT

A thesis submitted in partial fulfillment of the requirements for the degree of

MASTERS OF SCIENCE
IN
CONTROL ENGINEERING

By: Andrew Cudowski

Supervisor: Dr. Xiaoping Liu

Lakehead
UNIVERSITY

Department of Graduate Studies

Thunder Bay, Ontario

May, 2009

ABSTRACT

The field of humanoid robotics has in the last several decades taken off as an active area of research. The goal of this field is to build robots which by having a human-like form will be able to work in environments designed for people. An important part of this challenge is the development of biped walking robots. This thesis presents the design, simulation and control of a twelve degree of freedom biped walking robot.

The robot is designed using three dimensional computer aided design software, Solidworks, from which center of mass and inertia tensor data can be extracted and is constructed using an aluminum frame. The electrical controls are performed using two TMS320F2812 digital signal processors (DSP's) on custom designed printed circuit boards and the motors are driven with H-Bridge motor drivers.

A trajectory for each joint is generated offline on a Linux computer using fifth order spline interpolation and the inverse kinematic solution. This trajectory is then transmitted via serial cable to the DSP's. The robot walks by having each joint follow its trajectory using a computed torque scheme consisting of feedback and feedforward terms.

The feedback term is generated by sending joint angle readings from potentiometers mounted on each joint into either proportional-integral-derivative (PID) controllers on some joints and proportional-derivative (PD) controller on other joints. The feedforward term is generated via the Newton Euler Recursive formulation using the center of mass data, inertia tensor data and the joint angle trajectories.

Force sensors located at the four corners of each foot are used to calculate the center of pressure (COP). This is used as an input to an active balance controller which stabilizes the robot in the frontal plane by contributing to the control of the ankles with the use of a proportional-integral (PI) controller.

Acknowledgements

I would like to thank everyone who has given encouragement, advice and guidance with regards to this thesis.

Firstly, I would like to thank my supervisor Dr. Xiaoping Liu for his tireless teaching, insight and direction in this project.

I would also like to thank Haibing Wang for sharing his programming and Linux expertise, Weigang Gu for sharing his experiences working on biped robots, and Kailash Bhatia for helping with machining and allowing the use of the machine shop.

Finally I would like to thank my family and friends for their support and understanding in rarely seeing me during my studies.

Table of Contents

List of Figures

List of Tables

Nomenclature

Acronyms

ADC	Analog-to-Digital Converter
CAD	Computer Aided Design
COM	Centre of Mass
COP	Centre of Pressure
CNC	Computer Numerically Controlled
DOF	Degrees of Freedom
D-H	Denavit-Hartenberg
DS	Double-Support
DSP	Digital Signal Processor
GPIO	General Purpose I/O
IIR	Infinite Input Response
PCB	Printed Circuit Board
PD	Proportional Derivative
PI	Proportional Integral
PID	Proportional Integral Derivative
PWM	Pulse-Width Modulation
RAM	Random Access Memory
SS	SingleSupport
SCI	Serial Communications Interface
ZMP	Zero Moment Point

Variable Definitions

$\vec{a}_{c,i}$:	The linear acceleration of the centre of mass of link i
$\vec{a}_{e,i}$:	The linear acceleration of the end of link i
$\vec{b}_i$:	The axis of rotation of joint i expressed in frame i
$e[n]$:	The discrete error
$\vec{f}_i$:	The force exerted by link $i-1$ on link i
$\vec{g}_i$:	The acceleration due to gravity expressed in frame i
$\overrightarrow{\dot{H}_i}$:	The rate of angular momentum of link i
i:	The link index
I_i:	The moment of inertia of link i taken at the centre of mass and aligned with frame i, (obtained from CAD model)
K_d:	The derivative gain
K_i:	The integral gain
K_p:	The proportional gain
m_i:	The mass of link i
M^{GI}:	The moment about the base reference
$\vec{n}$:	The normal to the plane on which the robot is walking
$\vec{o}_{Li}$:	The location of the centre of mass of link i in the global frame

$\vec{o}_i$: The location of frame i in the global reference frame

$\vec{o}_{zmp}$: The zero moment point with respect to the base frame

$\vec{o}_{COM}$: The centre of mass of a robot with n links

R_i^{i-1}: The rotation matrix from frame $i-1$ to frame i

R_i^0: The rotation matrix from frame 0 to frame i

$\vec{r}_{i,i+1}$: The vector from joint i to joint $i+1$. It is the negative translational part of $(A_i^{i-1})^T$

$\vec{r}_{i,ci}$: The vector from joint i to the centre of mass of link i, obtained from CAD model

$\vec{r}_{i+1,ci}$: The vector from joint $i+1$ to the centre of mass of link i, obtained from CAD model

$r[n]$: The reference angle error

R_i^0: The orthonormal rotation matrix defining frame i orientation with respect to frame 0. It is the upper left 3 by 3 matrix of the transformation matrix T_i^0

$\vec{R}^{GI}$: The resultant of the gravity plus inertia forces for all the links (superscript GI)

$\vec{\tau}_i$: The torque exerted by link $i-1$ on link i

T_s: The sampling period

u_{DS}: The feedforward term for double support phase

u_{slope}: The linear interpolation from the double support feedforward term to the single support

$u_{PID}(s)$: The frequency domain control input from the PID controller

u_{PWM}: The PWM duty ratio during single support phase (found with the Newton Euler formulation)

$u[n]$: The discrete control input.

$\vec{\omega}_i$: The angular velocity of frame i

$\vec{\dot{\omega}}_i$: The angular acceleration of frame i

$y[n]$: The measured angle

$\vec{z}_i$: The direction of the $\vec{z}$ axis located at frame o_i

1 Literature Review

1.1 Motivation

Humans have long created tools to increase their abilities. From early technologies such as spears, bows and arrows, and domesticated animals, we've used our intelligence rather than our brawn to become one of the most successful species on earth. The trend to use ever increasing amounts of technology to increase our ability to produce goods continues today.

One of the technologies, which has become ever prominent in today's factories, is automation through the use of robotics. Figure 1, shows the recent growth in the installation of industrial robots worldwide.

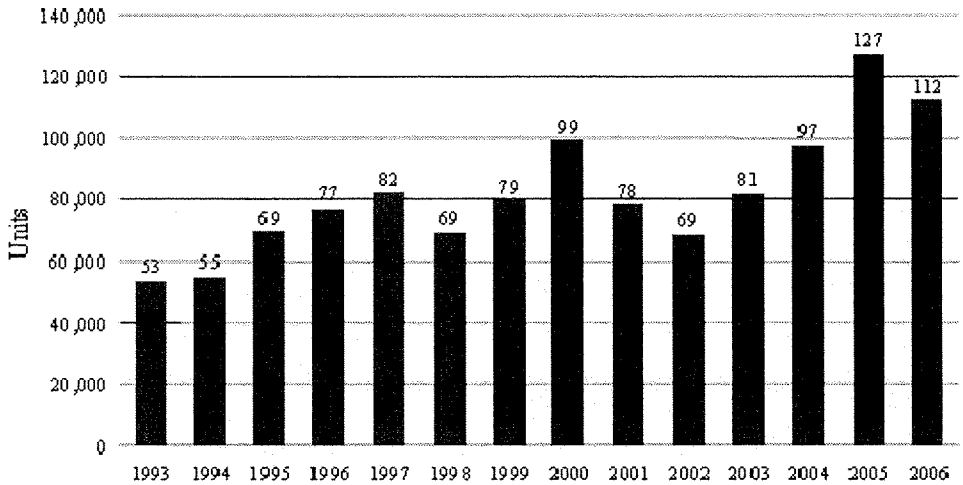

Figure 1.1: Yearly installation of industrial robots worldwide [1]

As a natural extension of the research and development done in industrial automation, the last few decades have also seen an ever increasing focus on developing robots that are able to work in environments designed for people. The biped walking robot is part of this research.

The most advanced walking robots, such as Honda's ASIMO can now run at up to 6 *km/h* [2]. However, this is still slower than people and many animals. Also the efficiency of most biped robots is low when compared to humans or animals. This inefficiency is graphically represented in Figure 1.2, which shows the cost of transport, a unit-less measure of efficiency calculated by dividing the energy consumed by weight and distance travelled [3].

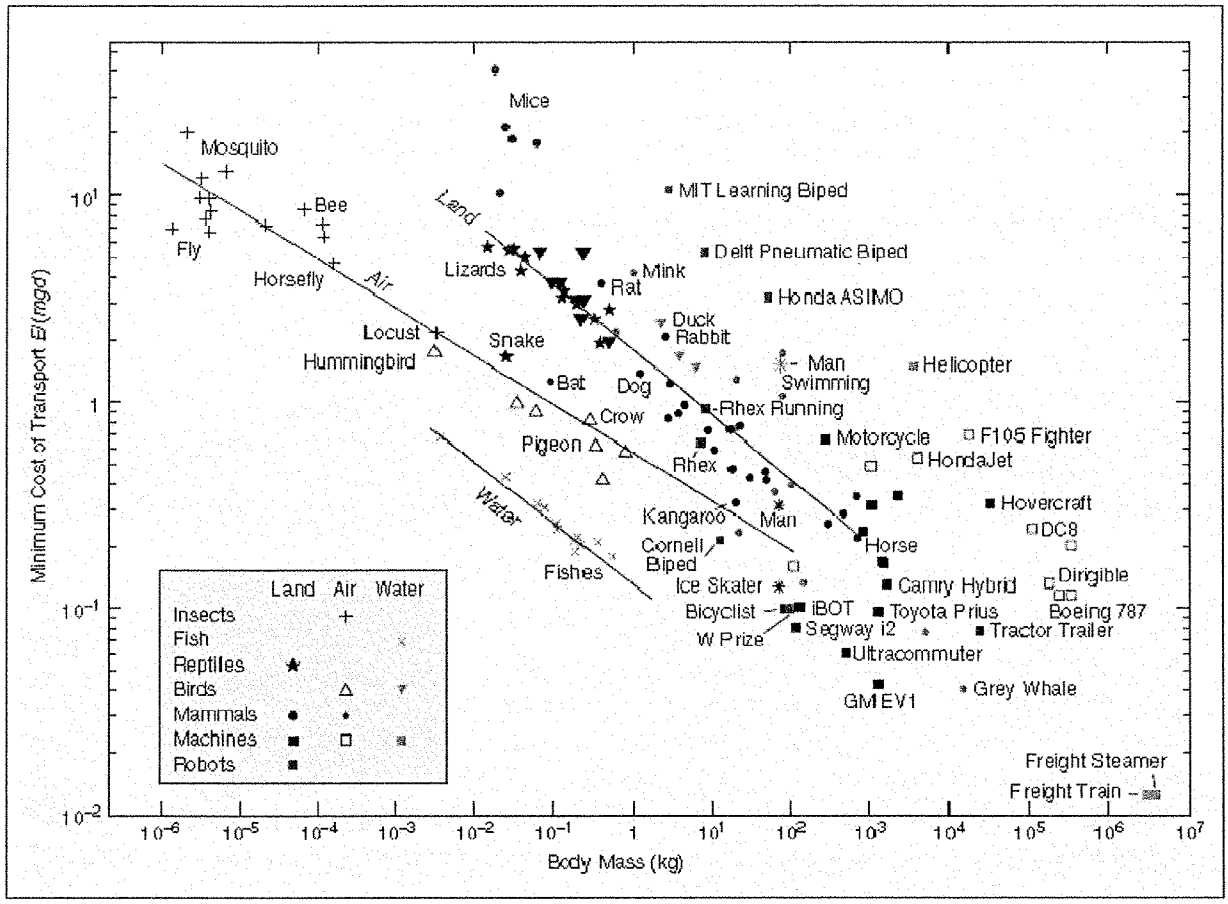

Figure 1.2: Comparison of minimum cost of transport as function of body mass for a variety of robots, animals, and vehicles [3]

Passive robots on the other hand are incredibly efficient and can walk relying on only a gentle slope to power their walking. These walkers have a minimum cost of transport of only 0.2, comparable to human walking [4].

There is also a good deal of research into actuating biped robots with pneumatics with the use of artificial "muscles", or pneumatic cylinder actuators. Some of the first biped robots ever built were done so using this method of actuation at Waseda University [26]. Pneumatic actuation for walking robots is still popular with some university researchers and with companies in the private sector.

Biped robots have also been built using hydraulics for actuation. Because of the greater load that hydraulic robots can bear, they have found considerable interest from the defense research community, a large portion of which is located in the United States.

Although biped robots are still fairly rare today, the technology developed for biped robots is finding uses in developing actuated prosthetics like the MIT prosthetic ankle [52] and exoskeletons for the disabled like the robot suit Hal developed by Cyberdyne [53].

Still, there exist trends that may lead to a greater demand for biped walking robots in the coming decades. This demand will come from the demographics of most developed countries, which if current demographic trends continue will be aging at an alarming rate in the coming years, causing a demand for replacement of human labour and hence a larger demand for biped robots.

A 2005 report published by Statistics Canada [6] predicts that by 2015 the elderly will outnumber children in Canada. In addition, aging of the population is set to continue with the elderly comprising 27% of the population by 2056. These trends are illustrated in Figure 1.3 which shows the age pyramid of Canada in 2005 and 2056. Similar aging is expected in many European countries and is well underway in Japan, perhaps pointing to the cause of the advanced robotic industry currently present in that country.

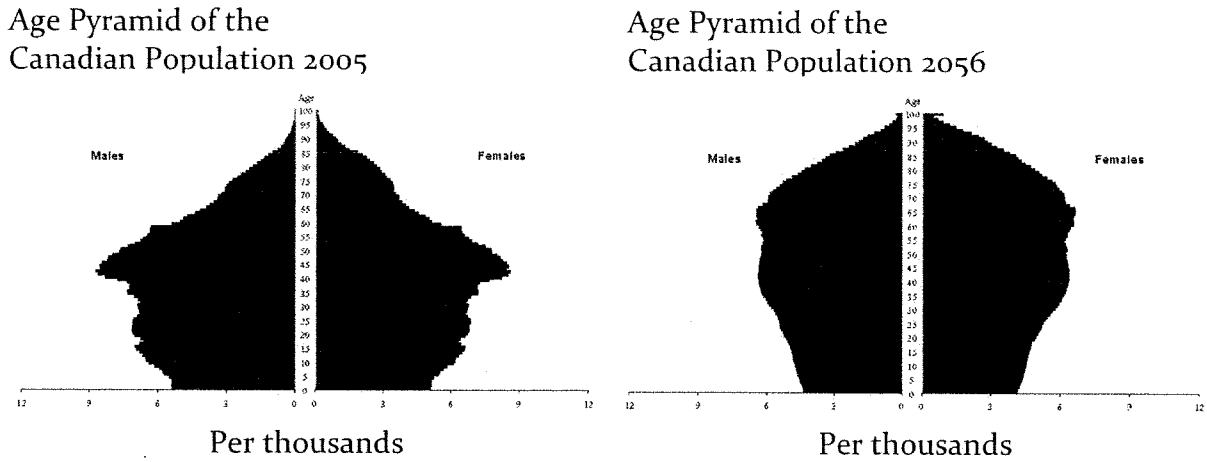

Figure 1.3: Age pyramids of the Canadian population in 2005 and 2056 [6]

1.2 Robot Gait and Trajectory Generation

Designing a suitable gait for biped robots is one of the critical challenges faced in this field of research. While a well planed walking pattern can ensure that the robot does not tip over while walking, further refinement of the gait can improve performance and even energy consumption [46], although solving the problem of an optimally efficient gait is still one for which a solution is being sought.

Many approaches to designing the gait of a biped robot have been undertaken. One of the most basic involves generating trajectories for the robot joints, and then verifying that the given trajectories meets some stability criteria for the robot not to fall over [47], [16]. For a robot which due to slow movement does not build up significant inertia, verifying that the center of mass falls onto the support polygon is a sufficient criterion for stability.

Increasingly, researchers have been using the zero moment point (ZMP) as means of verifying stability. The zero moment point is: *"the point on the ground where the tipping moment acting on the biped, due to gravity and inertia forces, equals zero, the tipping*

moment being defined as the component of the moment that is tangential to the supporting surface."[20].

Another approach commonly found in the literature to develop the walking pattern involves planning the trajectory of the zero moment point and then deriving from this, the corresponding center of mass trajectory. From the center of mass trajectory joint angles can be derived using inverse kinematics. In order to accomplish this approach on-line, the dynamics of the robots are often simplified into an inverted pendulum model [48], [49].

Many of the aforementioned approaches to trajectory generation result in a gait that does not resemble the human one as the knees of the robot are bent to avoid the large disturbance that can arise when a robot lands its foot with the knee locked. To counter this, researchers have started using motion capture from a person walking and then using various techniques to apply this to biped robots, resulting in a hybrid trajectory [56], [57]. Although motion capture from people has been applied to robots, work is still underway to create a more human-like gait for biped robots.

1.3 Trajectory Tracking

Once a trajectory has been generated for the robot, (either off or on-line), the task left to the robot is to follow this trajectory. State space representations of biped robot are generally avoided for all but simplest of robots due to the complexity of the dynamics.

Instead of modern control techniques, at the core of most trajectory tracking schemes is a proportional derivative loop on the tracking error [55] using either a traditional PD controller or a fuzzy logic controller [58]. The controller most often directly controls the joint angle, however controllers have been implemented where the location center of mass is controlled and the joint accelerations and then torques computed through inverse kinematics [52].

To improve performance and to reduce the high gains needed for only a PD controller a computed torque scheme is often implemented where the required torque is calculated and then injected into the control. This method requires a fairly accurate knowledge of the physical parameters of the robot links.

1.4 Postural Stability and Balance Control

For a robot to maintain postural stability by balancing, it must first determine what the effect of the disturbance is on the robot's body. This is done by determining the inclination of the body of the robot with accelerometers and joint sensors or by determining the center of pressure on the feet with the use of load cells or strain gauges in the ankles.

Once a disturbance is detected, biped robots can regain an upright posture in a number of ways. For minor disturbances the robots can use the center of pressure on the foot as

measured by load cell or similar means to control how the robot pushes off the ground, this is called Ground Reaction Control.

For larger disturbances robots can alter their zero moment point trajectories from which a modified walking trajectory is generated for the upcoming steps. This type of control is called Model ZMP Control and can help steady the inclination of the upper body. Because this type of calculation has to be done on-line, the dynamic model of the robot is often simplified to an inverted pendulum model during the single support phase and suspended pendulum model during double support phase [52].

Once the model ZMP control has been activated the landing location of the feet needs to be updated to correct the relative position of the upper body and the feet. This correction is referred to as Foot Landing Control. Honda used all three means of balancing to ensure the balancing of their robot P2 [51].

1.5 Existing Walking Robots

A wide range of walking biped robots has been developed around the world. Since the dynamics of a robot are largely determined by the means of actuation, the following sections provide an overview of robots developed using electric motors, passive walkers, pneumatic robots, and hydraulic motors.

1.5.1 Electric Motor Actuated Walking Robots

The most common form of actuation for walking robots is the electric motor. Electric motors can be easily controlled with solid state electronics, are relatively low cost and most robotics engineers are familiar with them as they are prominent in robotic manipulating arms.

Electric motors are also widely applicable since they can be mounted directly onto a joint if gearing is employed, or used as a linear actuator. Frequently, robot designers use remote control or (RC) servo's, a modularized motor-controller combination, as this negates the need for feedback to the main controller due to the presence of a local controller in the servo. RC servos remain popular with hobby robots, and are still quite widely used in university research robots.

The following sections cover some of the most advanced walking robot projects that have been developing noteworthy prototypes in the recent past. This includes the robots developed by: Honda, Humanoid Robotics Project, and the Korea Advanced Institute of Science and Technology.

1.5.1.1 Honda Humanoid Robots

The Japanese automotive giant Honda has a long history of producing ground breaking biped robot research. This research started in 1986 with the production of Eo, which achieved walking at a speed of five seconds a step [7]. With each following generation of prototypes, the abilities of the walking robots increased. The latest robot Asimo is now

able to run at 6km/h [2] and has intelligence technology that allows the robot to interact with people and its environment [8]. Figure 4 shows the evolution of Honda humanoid robot prototypes.

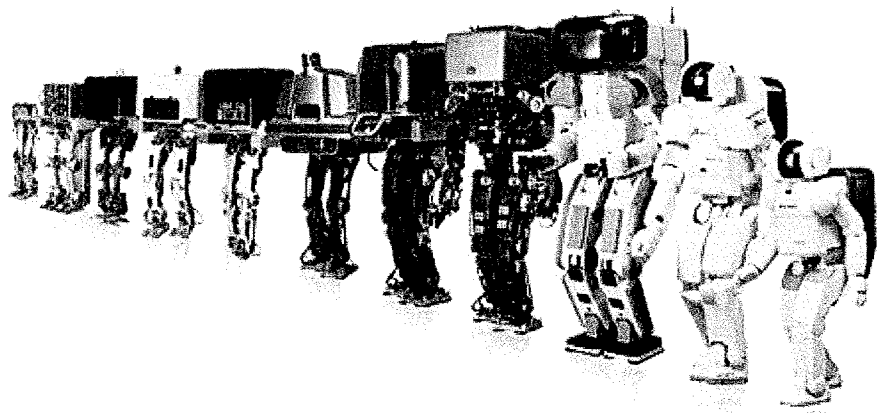

Figure 1.4: Honda walking robots 1986 to present left to right: E0, E1, E2, E3, E4, E5, E6, P1, P2, P3, Asimo [7]

1.5.1.2 Humanoid Robotics Project

The humanoid robotics project is sponsored by the Japanese Ministry of Trade and Industry (METI), New Energy and Industrial Technology Development Organization (NEDO), Kawada Industries, National Institute of Advanced Industrial Science and Technology (AIST), and Kawasaki heavy industries. The project has created an impressive line of robots show in Figure 1.5.

The latest walking robot HRP-4C was built to the average dimensions of a young Japanese female [9] and can closely mimic the movements of humans. The debut of the robot, which occurred at a fashion show, highlights the plan to use this robot in the entertainment industry.

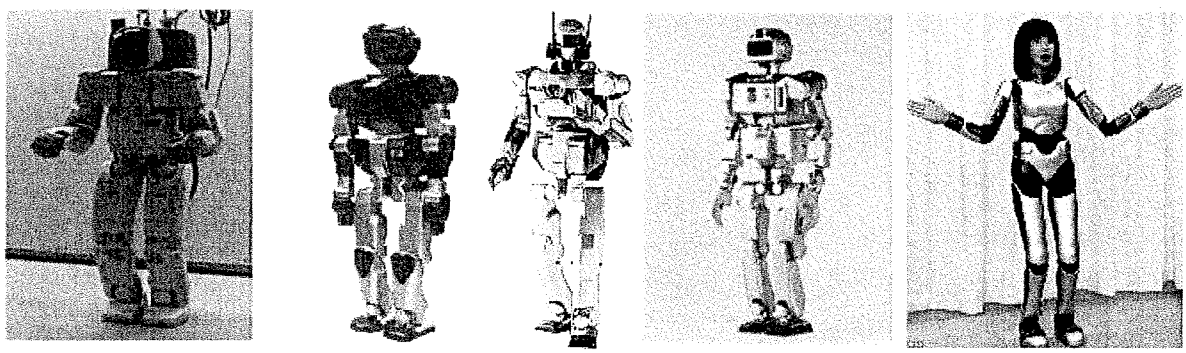

Figure 1.5: Humanoid Robotics Project prototypes, left to right: HRP-1, HRP-2p, HRP-2, HRP-3c, HRP-4C

1.5.1.3 Korea Advanced Institute of Science and Technology (KAIST)

Outside of Japan some of the most impressive research in biped robots has occurred at the Korea Advanced Institute of Science and Technology (KAIST). Since the early 2000's they have developed a line of biped robots including KHR-1, KHR-2, HUBO (KHR-3), HUBO FX-1, Albert HUBO and KHR-4 [23], [24]. The robots have grown in sophistication and capabilities. One of their latest robots, Albert HUBO is thought to be the first un-tethered biped robot with a humanly expressive face [25].

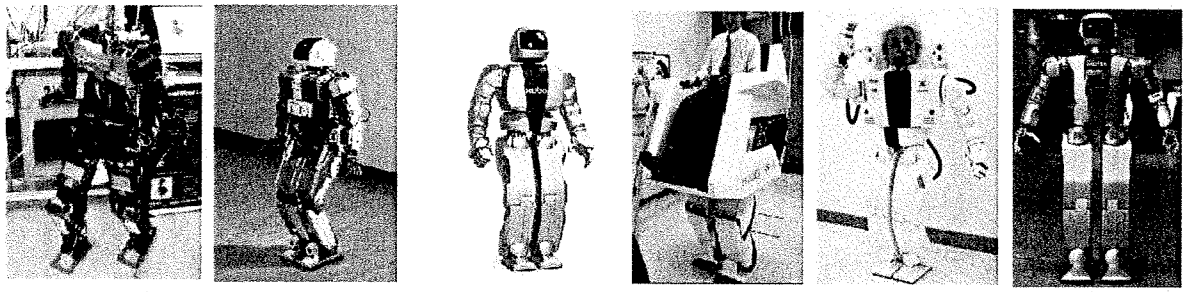

Figure 1.6: Korean Advanced Institute of Science Robots left to right: KHR-1, KHR-2, HUBO (KHR-3), HUBO FX-1, Albert HUBO, KHR-4

1.5.2 Passive Biped Walking Robots

Passive biped robots make up a class of walking robots that unlike active robots can walk with little or no actuation from sources other than gravity and momentum.

One of the earliest documentations of such a robot is the patent by George Fallis in the United States, in 1888, of a Walking Toy that "*consists of a combined pendulum and rocker construction whereby when placed upon an inclined plane it will be caused by the force of its own gravity to automatically step out and walk down said plane*" [27].

The technology was resurrected by McGeer [28] who in 1990 showed that a dynamic gait, otherwise stated as a gait in which the projection of centre of gravity falls outside of the support region of the foot while walking, could be achieved using a only a mechanical structure without any forms of actuation [29].

Further advancement occurred in passive walkers with the addition of light forms of actuation as on the Cornell's Walking Robot with Efficient Human-Like Gait [10]. This robot is able to walk continuously on level ground due two small motors which give the robot enough power to overcome friction. Figure 6 shows the development of passive walking robots from the Fallis Walking Toy to McGeer's Walker and Cornell's Robot with Efficient Human-Like Gait.

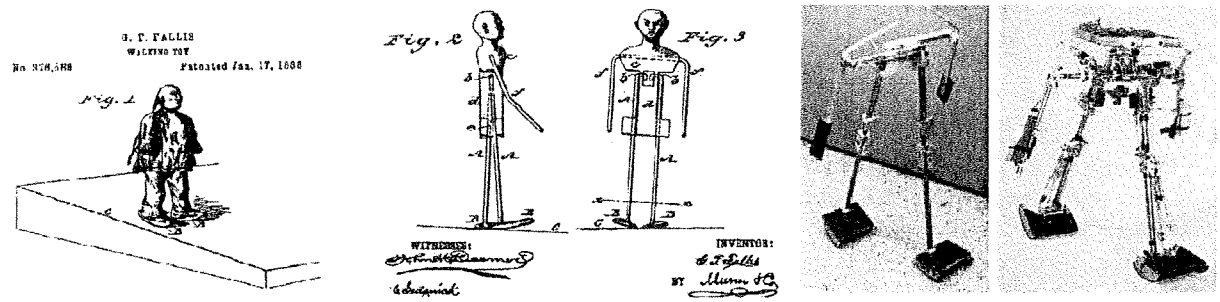

Figure 1.7: Passive biped robot development. From left to right: Fallis Walking Toy (1888), McGeer Walker, Cornell's Walking Robot with Efficient Human-Like Gait

Despite their efficiency, passive robots do not have many practical applications as they cannot yet be controlled to go to a location or perform a given tasks. However their further development is likely to have *"implications for the design of advanced foot prostheses"*[10] as well in the design of actively actuated robots.

1.5.3 Pneumatic Biped Robots

Pneumatic biped robots are rarer than the comparatively ubiquitous electrically powered ones, but the development of this type of robot dates back to the same time as early electrically powered bipeds.

One of the first pneumatic biped robots was Waseda University's WAP-1, built in 1969 [26]. The robot used artificial muscles made of rubber to achieve planar locomotion. More recently in the 1990's, the Shadow Robot Company developed a biped which through a series of tilt switches and accelerometers could balance, but never achieved walking [30].

A recent notable pneumatic powered biped was built at the Vrije University in Brussels. The goal of the project was to *"achieve a lightweight bipedal robot able to walk in a dynamically stable way while exploiting the passive behavior of the pleated pneumatic artificial muscles in order to reduce energy consumption and control efforts."* Slow walking by the robot was achieved and further research is underway to improve speed and control [32].

Another pneumatically actuated biped recently released is the company Anybots' robot Dexter. Unlike most biped robots which rely on Zero Moment Point to guarantee stability, Dexter is completely dynamic, otherwise stated *"there are no stable postures that it can be put in where it can balance without active feedback"*[32]. The robot uses pneumatic cylinders to drive its joints and is capable of walking, jumping and according to the makers will soon be able to run.

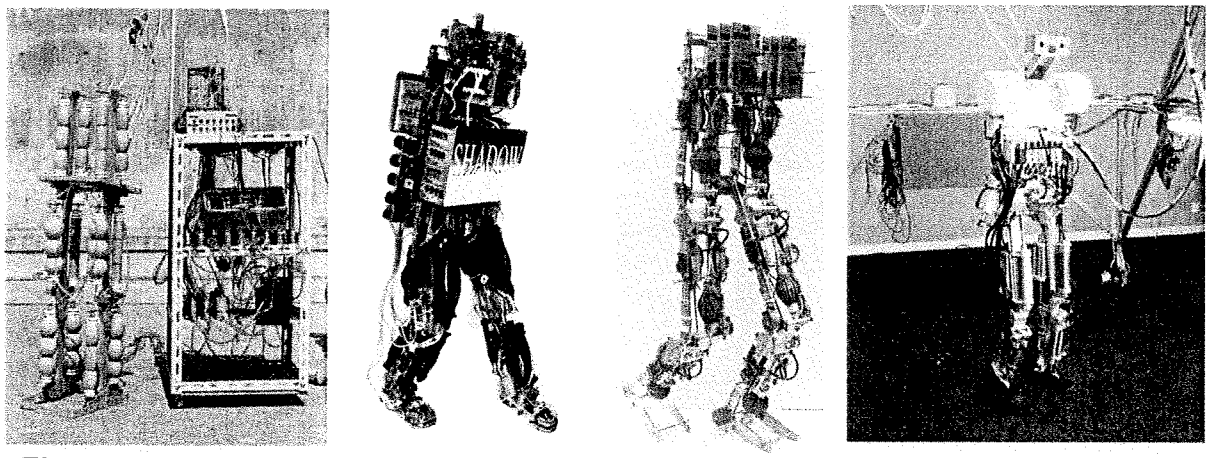

Figure 1.8: Pneumatic actuated robots from left to right: Waseda University's WAP-1, Shadow Company Biped, Vrije University's Lucy and Anybots' Dexter

1.5.4 Hydraulic Robots

Much like pneumatic biped robots, some of the earliest research into hydraulic biped robots occurred at Waseda Universtiy in Japan [26]. One of their early robots WL-3 used electro-hydraulic servo-actuators and was built in 1969 and *"managed human-like movement in a swing phase and a stance phase"* [26].

More recently, most of the development in hydraulic powered bipeds has shifted to the United States where biped robots have found defense applications. Some initial development was done by Sarcos, a Utah based engineering and Robotics Company, that developed products for the medical, entertainment and defense industries. Sarcos developed Primus, a 53 degree of freedom biped [34] as well as the initial development for a military exoskeleton before the company was purchased by the large defense contractor Raytheon [35].

Since the purchase, Raytheon-Sarcos has developed an exoskeleton to enable "a user to easily carry a man on his back or lift 200 pounds several hundred times without tiring" [36]. Raytheon has also stated the goal of developing the exoskeleton into a fully autonomous biped when not occupied by a pilot.

Another notable hydraulically actuated biped is the Boston Dynamics' Petman. The robot *"is an anthropomorphic robot for testing chemical protection clothing used by the US Army"* [33]. The robot has what is arguably the most human-like gait ever developed and can walk at over 5km/h. Delivery for the project is expected sometime in 2011.

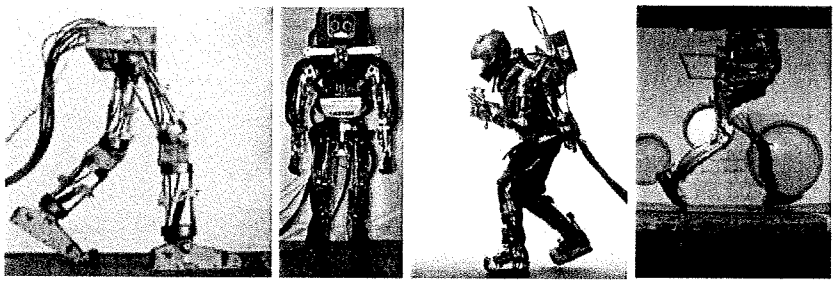

Figure 1.9: Hydraulic actuated robots from left to right: Waseda University's WL-3, Sarcos Primus, Raytheon Exoskeleton and Boston Dynamics Petman

1.6 Biped Robots at Lakehead University

The 12 DOF robot described in this thesis is the fourth biped robot developed at Lakehead University. The fist robot developed had only 6 DOF and was suspended from a track above it. The second robot developed had 7 DOF with 6 DOF on the legs and a seventh controlling a counterweight that allowed it to lift its feet without tipping over. The third robot developed had 10 DOF and walked at a rate 8cm/min. The control of this robot was accomplished by using a PD controller with gain scheduling and gravity compensation terms attained through trial and error. The 12 DOF robot proposed in this thesis can walk at the rate of 25cm/min and is controlled via computed torque scheme with active balance in the frontal plane. Figure 1.10 shows pictures of the biped robots developed at Lakehead.

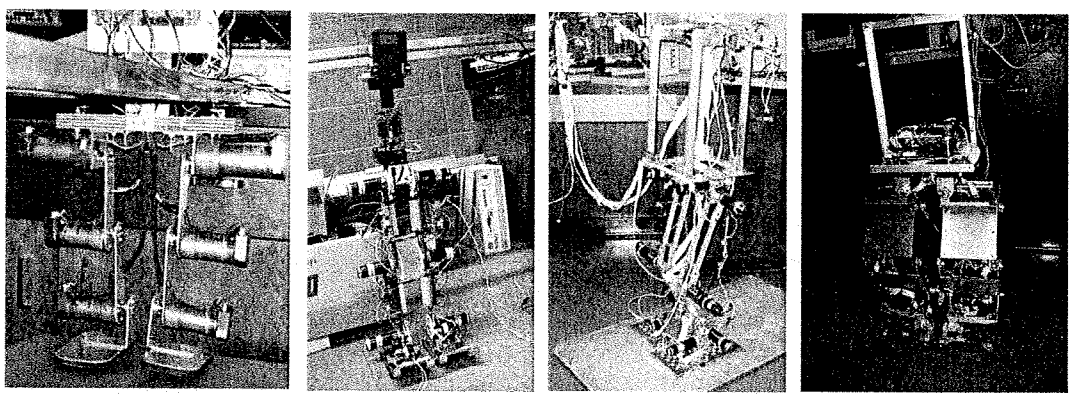

Figure 1.10: Biped robots developed at Lakehead University from left to right: 6 DOF biped robot, 7 DOF biped robot, 10 DOF biped robot and 12 DOF biped robot

1.7 Goal of Thesis

The goal of this thesis is the design, and building of a low-cost biped robot to study the theories of bipedal walking and balance control. This thesis proposes joint control of a biped robot using a PD and PID controllers with feedback from potentiometers mounted on each joint and with a feedforward term generated by the Newton Euler Recursive formulation. Balance control in the frontal plane is achieved using a PI controller which contributes to the control of the frontal ankle motor using feedback from force sensors mounted on the feet.

1.8 Thesis Organization

The thesis is organized into 11 chapters including this introductory one.

Chapter 1 introduces topics associated with biped walking robots and examines various notable walking robots that have been developed.

Chapter 2 covers the forward and inverse kinematics of the biped robot developed in this thesis.

Chapter 3 examines the inverse dynamics calculations, thereby determining torque requirements of the robot.

Chapter 4 delves into topics associated with biped walking such as the zero moment point, centre of mass and trajectory generation for the 12 DOF walking robot.

Chapter 5 goes over simulations results for the joint trajectory, center of mass trajectory and torque requirements.

Chapter 6 covers topics associated with the mechanical design of the robot including means of actuation, material selection and the overall structure.

Chapter 7 gives an overview of the electrical design of the robot including the selection of sensors, motor driver and processor.

Chapter 8 explains the functioning of the control systems on the robot. This includes details regarding the trajectory following controller, the active balance controller as well as the required digital filtering.

Chapter 9 goes over the experimental results from the walking robot prototype.

Chapter 10 summarizes the thesis and proposes future work to improve the robot design.

2 Robot Kinematics

2.1 Introduction

Kinematics is a branch of classical mechanics that studies motion without considering the forces that are causing it [37]. Later sections will deal with the forces acting on the biped robot, but this chapter will examine how to mathematically represent the position, velocity and acceleration, as well as the orientation of the links of the robot. This chapter assumes the reader has some basic knowledge of robotics. As covering this entire topic would go beyond the scope of this thesis, for additional information the reader is referred to two popular texts in on the subject: [5] and [37].

2.2 Denavit and Hartenberg Notation

Unlike a point in space, a three dimensional robotic link is not completely defined by a position with respect to a fixed frame; it is also necessary to describe its orientation. To do this we first dissect the robotic structure into links and the joints that connect the links. To describe the location and orientation of each link a coordinate frame is affixed and parameters assigned that describe the location and orientation of the frame.

Denavit and Hartenberg notation, or D-H notation, is a convention used in robotics which creates a standardized set of axes and parameters which can then be used to create a homogenous transformation matrix A_i that describes the location and orientation of each frame with respect to the previous frame.

In D-H notation, the axis of a revolute joint i is aligned with the z_{i-1} axis. The x_{i-1} axis is directed along the normal from z_{i-1} to z_i, it is parallel to $z_{i-1} \times z_i$. The y axis follows the x and the z axis using the right hand rule. The D-H parameters are shown in Table 2.1.

Symbol	Name	Description
a_i	Link length	The offset distance between the z_{i-1} and z_i axes along the x_i axis.
α_i	Link twist	The angle from the z_{i-1} axis to the z_i axis about the x_i axis
d_i	Link offset	The distance from the origin of frame $i-1$ to the x_i axis along the z_{i-1} axis.
θ_i	Joint angle	The angle between the x_{i-1} and x_i axes about the z_{i-1} axis.

Table 2.1: D-H notation parameters

The homogenous transformation matrix A_i is a product of four basic transformations: a rotation about the z axis by θ, a translation along z axis by d, a translation along x by a, and a rotation about x by α as shown in formulas (2.1-2.3).

$$A_i^{i-1} = Rot_{z,\theta}\, Trans_{z,d}\, Trans_{x,a}\, Rot_{x,\alpha} \tag{2.1}$$

$$A_i^{i-1} = \begin{bmatrix} \cos\theta_i & -\sin\theta_i & 0 & 0 \\ \sin\theta_i & \cos\theta_i & 0 & 0 \\ 0 & 0 & 1 & 0 \\ 0 & 0 & 0 & 1 \end{bmatrix} \begin{bmatrix} 1 & 0 & 0 & 0 \\ 0 & 1 & 0 & 0 \\ 0 & 0 & 1 & d_i \\ 0 & 0 & 0 & 1 \end{bmatrix} \begin{bmatrix} 1 & 0 & 0 & a_i \\ 0 & 1 & 0 & 0 \\ 0 & 0 & 1 & 0 \\ 0 & 0 & 0 & 1 \end{bmatrix} \begin{bmatrix} 1 & 0 & 0 & 0 \\ 0 & \cos\alpha_i & -\sin\alpha_i & 0 \\ 0 & \sin\alpha_i & \cos\alpha_i & 0 \\ 0 & 0 & 0 & 1 \end{bmatrix} \tag{2.2}$$

$$A_i^{i-1} = \begin{bmatrix} \cos\theta_i & -\sin\theta_i\cos\alpha_i & \sin\theta_i\sin\alpha_i & a_i\cos\theta_i \\ \sin\theta_i & \cos\theta_i\cos\alpha_i & -\cos\theta_i\sin\alpha_i & a_i\sin\theta_i \\ 0 & \sin\alpha_i & \cos\alpha_i & d_i \\ 0 & 0 & 0 & 1 \end{bmatrix} \tag{2.3}$$

To describe the biped robot's body in terms D-H parameters, the body of the robot can be considered as one large chain consisting of twelve revolute joints connecting thirteen links. The base of this chain is located on the stationary foot and the end-effector on the swing foot.

Table 2.2, shows the D-H parameter for the robot's legs with the right foot planted and the left foot swinging. The variables for link lengths and joint angles are indicated on Figure 2.1, a wire frame robot. Figure 2.2 explains which joint on the robot shown in Figure 2.1 corresponds to the roll, pitch and yaw terms.

Local Frame Origin	a_i	α_i	d_i	θ_i
0	0	90	l_1	90
1	l_2	-90	0	θ_1+90
2	l_3	0	0	θ_2
3	l_4	0	0	θ_3
4	l_5	90	0	θ_4
5	0	-90	0	θ_5+90
6	l_6	0	0	θ_6
7	0	90	0	θ_7
8	l_5	90	0	θ_8+90
9	l_4	0	0	θ_9
10	l_3	0	0	θ_{10}
11	l_2	-90	0	θ_{11}
12	l_1	0	0	θ_{12}

Table 2.2: D-H parameter table from right leg to left

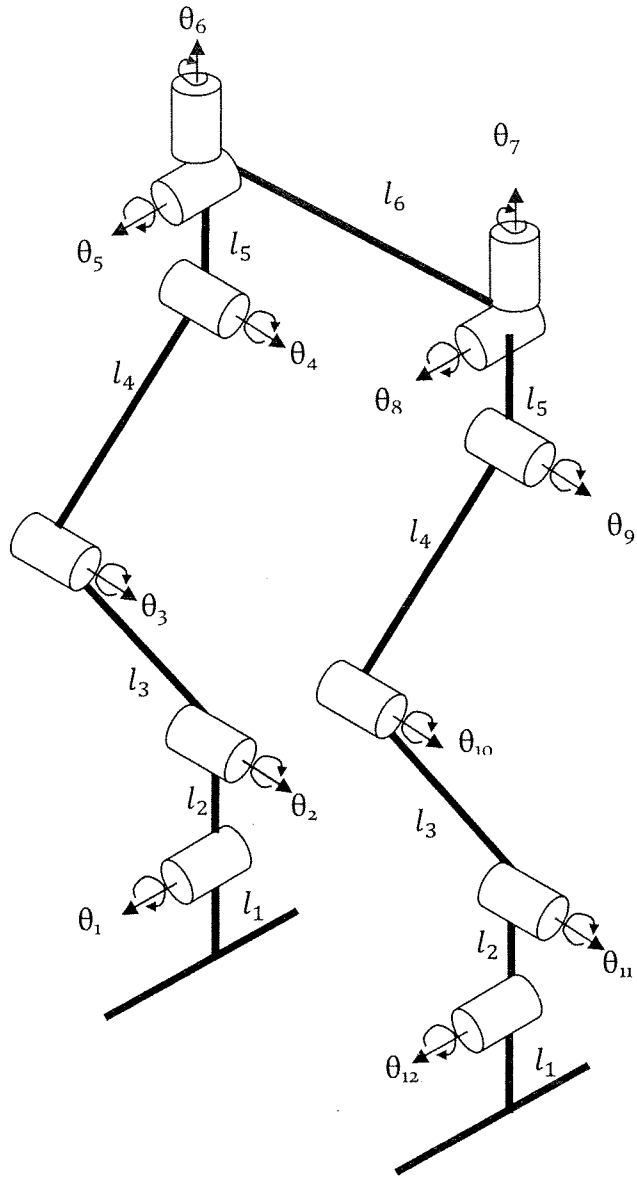

Figure 2.1: Joint and link locations on wire frame robot

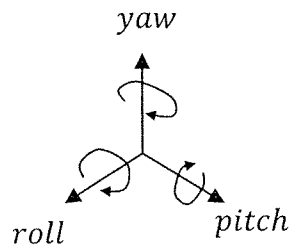

Figure 2.2: Yaw pitch and roll definitions in reference to the robot frame

2.3 Forward Kinematics

Forward kinematics finds the Cartesian location of the end effector given the joint angles. Mathematically this requires multiplying the homogenous transformation matrices A_1 through to A_n where n is the number of frames. This yields the transformation matrix for the end effector T_0^n as shown in formula (2.4).

$$T_n^0 = A_1^0 A_2^1 A_3^2 \dots A_n^{n-1} \tag{2.4}$$

Multiplying the homogenous transformation matrices 0 to i where i is the frame from 0 to n yields the transformation matrix for frame i. This is also the location of (joint i+1). The first three rows of the fourth column of the transformation matrix represent the x, y and z coordinates of frame i in the base reference frame.

$$o_i = (x, y, z)^T = \begin{bmatrix} T_i^0(1,4) \\ T_i^0(2,4) \\ T_i^0(3,4) \end{bmatrix} \tag{2.5}$$

Thus, by calculating the forward kinematics using the link lengths listed in Table 2.3, it is possible to plot a graphical representation of the robot as shown Figure 2.3. It should be noted that the reference frame is at the base of the right foot while frame 1 is on right ankle.

Link	Length (mm)
l_1	33
l_2	64
l_3	170
l_4	160
l_5	71
l_6	114

Table 2.3: Designed robot link lengths

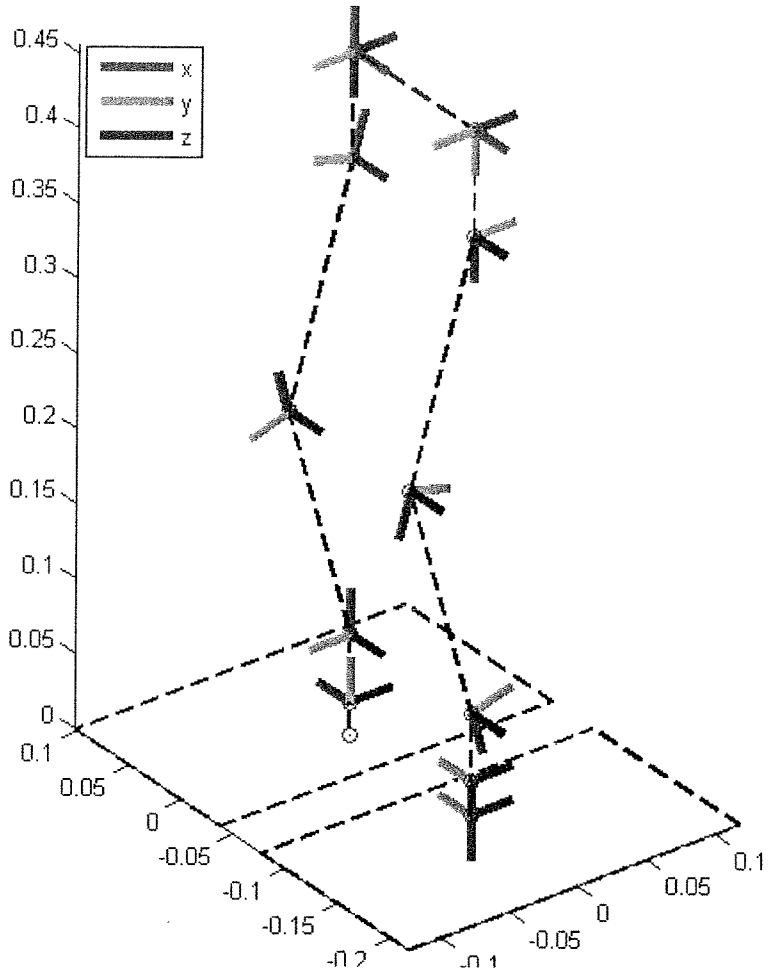

Figure 2.3: Reference frame locations

2.4 Inverse Kinematics

If instead of knowing the joint angles and requiring the Cartesian coordinates, the Cartesian coordinates are known and the joint angles required, the mathematical method that needs to be applied is inverse kinematics. Figure 2.4 shows graphically the relationship between inverse and forward kinematic.

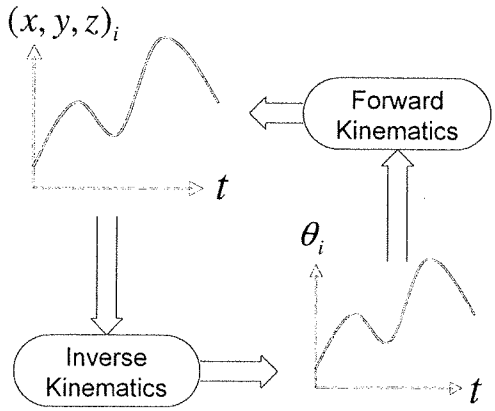

Figure 2.4: Relation between forward and inverse kinematics

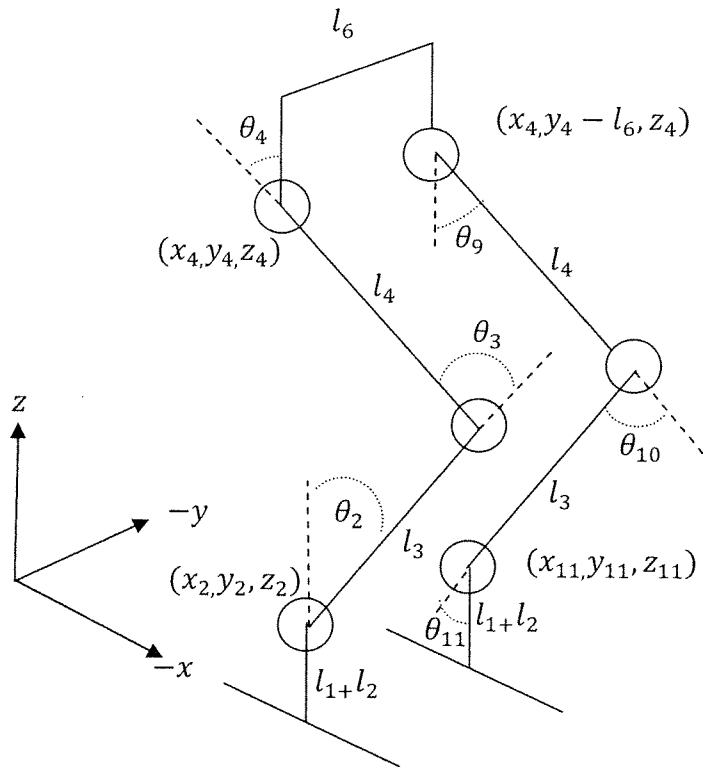

Figure 2.5: The variables for the robot's right leg that will be used in deriving the inverse kinematic solution

2.4.1 Inverse Kinematic Calculation for the Right Leg Knee Angle

To find the inverse kinematic solution for the right leg in the sagittal plane, we first find the joint angle for the knee θ_3 given Cartesian location for the hip and ankle. The Cartesian location of the ankle and hip in the sagittal plane are known since trajectories for these are generated directly.

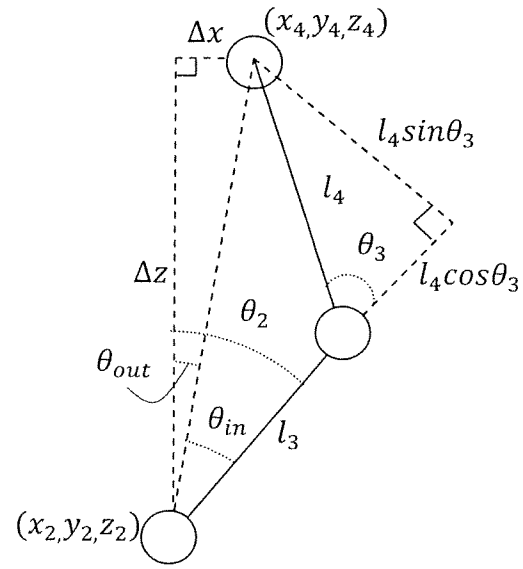

Figure 2.6: Diagram for solving right leg inverse kinematics

Applying the law of cosines, Equation (2.6), to the triangle bounded by l_3 and l_4 in Figure 2.6, yields Equation (2.7). Rearranging Equation (2.7) produces Equation (2.8). Using Equation (2.8) and trigonometric identity (2.9) allows the use of the four-quadrant inverse tangent resulting in one solution: Equation (2.10).

$$a^2 = b^2 + c^2 - 2bccos\theta \tag{2.6}$$

$$\left(\sqrt{(x_4 - x_2)^2 + (z_4 - z_2)^2}\right)^2 = l_2^2 + l_3^2 - 2l_2l_3\cos(180 - \theta_3) \tag{2.7}$$

$$\cos\theta_3 = \frac{(x_4 - x_2)^2 + (z_4 - z_2)^2 - l_2^2 - l_3^2}{2l_2l_3} \tag{2.8}$$

$$\sin\theta_3 = \sqrt{1 - \cos^2\theta_3}\ ,\ (0 \le \theta_3 < \pi) \tag{2.9}$$

$$\theta_3 = atan2(\sin\theta_3, \cos\theta_3) \tag{2.10}$$

2.4.2 Inverse Kinematics for the Right Leg Ankle and Hip Angles

Once the knee angle θ_3 is calculated the next step is to find the ankle and hip angles. To find the ankle angle the it can be seen from Figure 2.7 that summing angles θ_{in} and θ_{out}, calculated in equations (2.11) and (2.12) yields the right ankle angle (2.13).

$$\theta_{in} = atan2(l_3 + l_4\cos\theta_3, l_4\sin\theta_3) \tag{2.11}$$

$$\theta_{out} = atan2(x_4 - x_2, z_4 - z_2) \tag{2.12}$$

$$\theta_2 = \theta_{in} + \theta_{out} - \pi/2 \tag{2.13}$$

With the ankle and knee angles calculated we can now calculate the hip angle. From geometry we know that if we wish to keep the abdomen of the robot in a vertical position the ankle knee and hip angles need to sum to zero. Hence we can find the hip angle with Equation 2.14.

$$\theta_4 = -\theta_2 - \theta_3 \tag{2.14}$$

2.4.3 Inverse Kinematics Calculation for the Left Leg Knee Angle

The inverse kinematics for the left leg can be solved with a similar approach as those for the right leg. To find the knee angle the law of cosines, Equation (2.6), is applied to Figure 2.7 , yielding Equations 2.15-2.18.

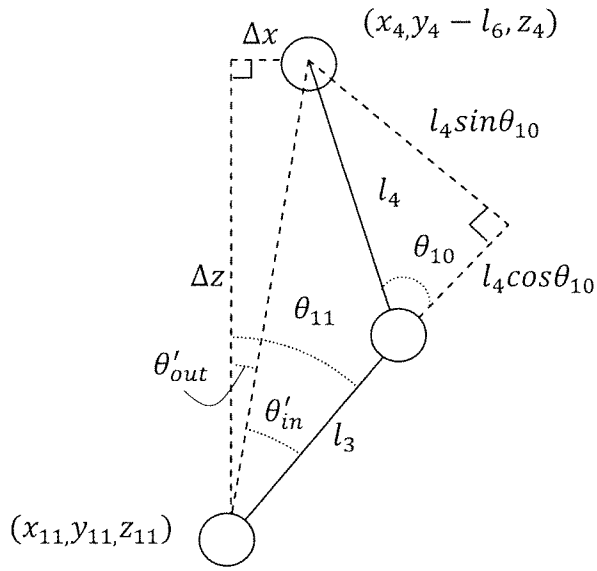

Figure 2.7: Diagram for solving left knee angle

$$\left(\sqrt{(x_4 - x_{11})^2 + (z_4 - z_{11})^2}\right)^2 = l_2^2 + l_3^2 - 2l_2 l_3 \cos(180 - \theta_{10}) \tag{2.15}$$

$$\cos\theta_{10} = \frac{(x_4 - x_{11})^2 + (z_4 - z_{11})^2 - l_2^2 - l_3^2}{2l_2 l_3} \tag{2.16}$$

$$\sin\theta_{10} = \sqrt{1 - \cos^2\theta_0}\ ,\ (0 \le \theta_{10} < \pi) \tag{2.17}$$

$$\theta_{10} = atan2(\sin\theta_{10}, \cos\theta_{10}) \tag{2.18}$$

2.4.4 Inverse Kinematics for the Left Leg Ankle and Hip Angles

To solve the ankle and hip angles on the left leg the same approach can be applied as on the right leg. The solution of Figure 2.7 yields equations (2.19)-(2.22).

$$\theta'_{in} = atan2(l_3 + l_4 \cos\theta_{10}, l_4 \sin\theta_{10},) \tag{2.19}$$

$$\theta'_{out} = atan2(x_4 - x_{11}, z_4 - z_{11}) \tag{2.20}$$

$$\theta_9 = \theta'_{in} + \theta'_{out} - {}^{\pi}/_{2} \tag{2.21}$$

$$\theta_9 = -\theta_{10} - \theta_{11} \tag{2.22}$$

3 Inverse Dynamics

3.1 Introduction

Robot dynamics studies the equations relating the motions of the links of a robot with respect to applied forces such as those coming from robot actuator or those external to the robot. The two main problems associated with robot dynamics are forward dynamics and inverse dynamics.

Forward dynamics involves determining the motion of the robot links given a set of forces while inverse dynamics involves determining joint torques for a given set of joint angles, velocities and accelerations.

Hence by using inverse dynamics the torques required from the robot's motors can be determined. From this simulation the robot's trajectory or mechanical structure can be adjusted appropriately.

Many methods have been developed to address the problem of inverse dynamics, with two of the more popular methods being: the Lagrangian, which is based on finding the kinetic and potential energy of the robot and the Recursive Newton Euler formulation. Depending on the application, both have their advantages; however for robots with a high number of degrees of freedom, Hollerbach [17] has shown that the computational load for the Recursive Newton Euler method is far lighter than the Lagrangian. Table 3.1 shows the computational burden of the Lagrangian compared to the Newton Euler. At $O(n^4)$ computational cost, the Lagrangian method would require 1.5 million floating point calculations per iteration, enough to burden even today's powerful computers. Meanwhile the Newton Euler Recursion at $O(n)$ computational cost can be calculated on-line with a modern personal computer.

Method	Multiplications	Additions
Lagrangian	$32.5n^4 + 86\frac{5}{12}n^3 + 171\frac{1}{4}n^2 + 53\frac{1}{3}n - 128$	$25n^4 + 66\frac{1}{3}n^3 + 129\frac{1}{2}n^2 + 42\frac{1}{3}n - 96$
Newton Euler	$150n - 48$	$131n - 48$

Table 3.1: Computational comparison between Recursive Newton Euler and Lagrangian inverse dynamics [17]

3.2 Recursive Newton Euler Formulation

The Recursive Newton Euler formulation finds the joint torques by propagating information such as angular momentum, angular acceleration and liner acceleration from the base to the end-effector[5]. It then propagates from the end effector back down to the base the forces and moments exerted on each link from the previous one. Equations (3.1) to (3.13) outline the Recursive Newton Euler formulation. The output of the formulation is the torque expressed as a 3 x 1 vector with each row representing the torque about the x, y and z axis.

The Newton Euler formulation also makes use of the tensor matrix and vectors associated with the centre of mass and joint location. Figure 3.1 shows the location and orientation of these vectors with respect to joints i , $i + 1$, $i + 2$ and frames o_{i-1}, o_i and o_{i+1} .

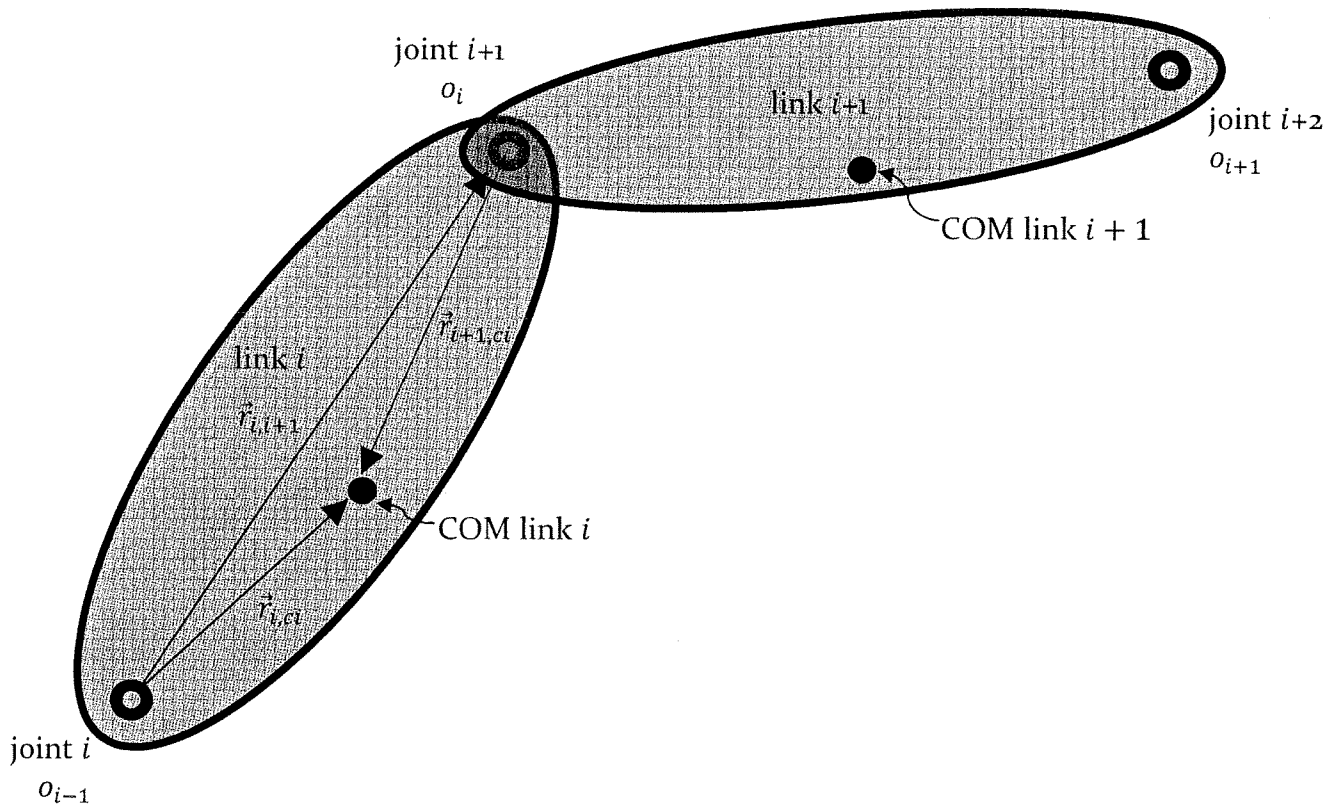

Figure 3.1: Frame and vector locations

Initial conditions for outward iterations:

$$\vec{\omega}_0 = \begin{bmatrix}0\\0\\0\end{bmatrix}, \dot{\vec{\omega}}_0 = \begin{bmatrix}0\\0\\0\end{bmatrix}, \vec{a}_{e,0} = \begin{bmatrix}0\\0\\0\end{bmatrix}, \vec{a}_{c,0} = \begin{bmatrix}0\\0\\0\end{bmatrix}, \vec{z}_0 = \begin{bmatrix}0\\0\\1\end{bmatrix} \tag{3.1}$$

Outward Iterations ($i = 0$ *to* n):

$$\vec{\omega}_{i+1} = R_i^{i-1}\vec{\omega}_i + \vec{b}_i\dot{\theta}_i \tag{3.2}$$

$$\dot{\vec{\omega}}_{i+1} = R_i^{i-1}\dot{\vec{\omega}}_i + \vec{b}_i\ddot{\theta}_i + \vec{\omega}_i \times (\vec{b}_i\dot{\theta}_i) \tag{3.3}$$

$$\vec{a}_{e,i+1} = R_i^{i-1}\vec{a}_{e,i} + \dot{\omega}_i \times r_{i,i+1} + \vec{\omega}_i \times (\vec{\omega}_i + \times \vec{r}_{i,i+1}) \tag{3.4}$$

$$\vec{a}_{c,i+1} = R_i^{i-1}\vec{a}_{e,i} + \dot{\vec{\omega}}_i \times r_{i,ci} + \vec{\omega}_i \times (\vec{\omega}_i \times \vec{r}_{i,ci}) \tag{3.5}$$

Initial conditions for inward iterations:

$$\left.\begin{aligned}\vec{f}_{n+1} &= \begin{bmatrix}0\\0\\0\end{bmatrix}\\ \vec{\tau}_{n+1} &= \begin{bmatrix}0\\0\\0\end{bmatrix}\end{aligned}\right\} \tag{3.6}$$

Inward Iterations ($i = n$ *to* 1):

$$\vec{f}_i = R_i^{i+1}\vec{f}_{i+1} + m_i\vec{a}_{ci} - m_i\vec{g}_i \tag{3.7}$$

$$\vec{\tau}_i = R_i^{i+1}\vec{\tau}_{i+1} - \vec{f}_i \times \vec{r}_{i,ci} + (R_i^{i+1}\vec{f}_{i+1}) \times \vec{r}_{i+1,ci} + I_i\dot{\vec{\omega}}_i + \vec{\omega}_i \times (I_i\vec{\omega}_{i+1}) \tag{3.8}$$

Variable Definitions:

i: The link index

I_i: The moment of inertia of link i taken at the centre of mass and aligned with frame i, (obtained from CAD model)

$\vec{\omega}_i$: The angular velocity of frame i

$\dot{\vec{\omega}}_i$: The angular acceleration of frame i

$$\vec{z}_i = T_0^i(1{:}3,3) \tag{3.9}$$

$\vec{z}_i$: The direction of the $\vec{z}$ axis located at frame o_i

$$R_{i-1}^{i} = A_i(1:3,1:3) = \begin{bmatrix} \cos\theta_i & -\sin\theta_i \cos\alpha_i & \sin\theta_i \sin\alpha_i \\ \sin\theta_i & \cos\theta_i \cos\alpha_i & -\cos\theta_i \sin\alpha_i \\ 0 & \sin\alpha_i & \cos\alpha_i \end{bmatrix} \tag{3.10}$$

$$R_i^{i-1} = \left(R_{i-1}^{i}\right)^T \tag{3.11}$$

R_i^{i-1}: The rotation matrix from frame $i-1$ to frame i

$$\vec{b}_i = R_i^0 \vec{z}_{i+1}$$

$\vec{b}_i$: The axis of rotation of joint i expressed in frame i

$$R_i^0 = \left(R_0^i\right)^T = \left(T_0^i(1:3,1:3)\right)^T \tag{3.12}$$

R_i^0: The rotation matrix from frame 0 to frame i

$$\vec{r}_{i,i+1} = \begin{bmatrix} a_i \\ d_i \sin a_i \\ d_i \cos a_i \end{bmatrix} \tag{3.13}$$

$\vec{r}_{i,i+1}$: The vector from joint i to joint $i+1$. It is the negative translational part of $(A_i^{i-1})^T$

$\vec{a}_{c,i}$: The linear acceleration of the centre of mass of link i

$\vec{a}_{e,i}$: The linear acceleration of the end of link i

$\vec{r}_{i,ci}$: The vector from joint i to the centre of mass of link i, obtained from CAD model

$\vec{r}_{i+1,ci}$: The vector from joint $i+1$ to the centre of mass of link i, obtained from CAD model

$\vec{g}_i$: The acceleration due to gravity expressed in frame i.

$\vec{f}_i$: The force exerted by link $i-1$ on link i

$\vec{\tau}_i$: The torque exerted by link $i-1$ on link i

m_i: The mass of link i

I_i: The inertia matrix of link i about a frame parallel to frame i whose origin is at the centre of mass of link i (Tensor matrix)

4 Biped Robot Walking

4.1 Introduction

One of the most basic ways to maintain stability of the robot is by ensuring that the projection of the centre of mass of the robot falls under the supporting foot if standing on one leg, or the area bounded by two supporting feet (otherwise known as the support polygon). This is referred to as static walking [12]. In static walking, if the motion of the robot is stopped at any time, the robot should remain stable in its position.

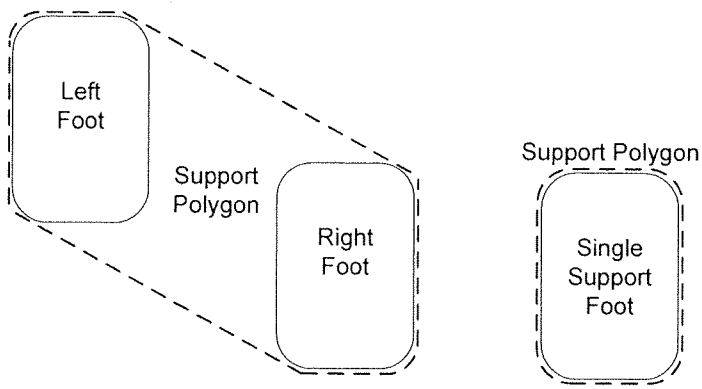

Figure 4.1: Support polygon boundaries for double support and single support

As the speed of a biped walking robots is increased, momentum plays an ever increasing role and the projection of the centre of gravity can no longer act as the lone criterion for stability. For this reason a stability criterion is required that includes both the gravity term as well as the momentum term. This criterion is referred to as the zero-moment point (ZMP) and robots that make use of zero moment point are referred to as dynamic robots. Dynamic walking allows the projection of the centre of mass of the robot to fall outside the robot's support polygon, though the ZMP still falls within the boundary. This type of walking has led to the development of faster and more nimble walking robots.

Recently robots have been developed which go beyond the zero moment point principle and can be referred to as fully dynamic. One such robot is Dexter from the company Anybots[31]. Because of the small feet and sophisticated balance algorithm the robot's zero moment point can momentarily land outside of its support polygon yet the robot maintains stability through reactive stepping.

4.2 Centre of Mass Calculation

For biped robots that move slowly, the projection of the centre of mass (COM), also known as the centre of gravity (COG), is a sufficient criterion to ensure that the robot does not tip over. Equation (4.1) shows how to calculate the centre of mass of the robot. The projection of the centre of mass onto a flat surface is simply the x and y components of the vector $\vec{o}_{COM}$.

$$\vec{o}_{COM} = \frac{\sum_{i=0}^{n-1} m_i \vec{o}_{Li}}{\sum_{i=0}^{n-1} m_i} \tag{4.1}$$

Variable Definitions:

$\vec{o}_{COM}$: The centre of mass of a robot with n links

m_i: The mass of link i

$r_{i+1,ci}$: The vector from joint $i+1$ to the centre of mass of link i in frame i. Frame i is located at joint $i+1$

$$\vec{o}_{Li} = \vec{o}_i + R_0^i r_{i+1,ci} \tag{4.2}$$

$\vec{o}_{Li}$: The location of the centre of mass of link i in the global frame

$$R_i^0 = T_i^0(1{:}3,1{:}3) \tag{4.3}$$

R_i^0: The orthonormal rotation matrix defining frame i orientation with respect to frame 0. It is the upper left 3 by 3 matrix of the transformation matrix T_i^0

$$\vec{o}_i = (x,y,z)^T = \begin{bmatrix} T_i^0(1,4) \\ T_i^0(2,4) \\ T_i^0(3,4) \end{bmatrix} \tag{4.4}$$

$\vec{o}_i$: The location of frame i in the global reference frame Equation (2.5), repeated here for convenience

4.3 ZMP Calculation

The formula for the Zero-Moment point is given in Equation (4.5), with supporting calculations given in Equations (4.6)-(4.8). In order to implement this formula the centre of mass of each link needs to be known. As finding this value can be difficult for complex structures manually a three dimensional computer aided design (CAD) programs is used for this function.

$$\vec{o}_{zmp} = \frac{\vec{n} \times M_i^{GI}}{\vec{R}^{GI} \cdot \vec{n}} \tag{4.5}$$

$$\overrightarrow{H_i} = R_i^0 \left(I_i \vec{a}_{c,i} - I_i \vec{\omega}_i \times \vec{\omega}_i \right) \tag{4.6}$$

$$M^{GI} = \sum_{i=0}^{n-1} \left(\vec{o}_{Li} \times m_i R_i^0 \vec{g} - \vec{o}_{Li} \times m_i R_i^0 \vec{a}_{c,i} - \overrightarrow{H_i} \right) \tag{4.7}$$

$$\overrightarrow{n} = \begin{bmatrix} 0 \\ 0 \\ 1 \end{bmatrix} \tag{4.8}$$

$$\vec{R}^{GI} = \sum_{i=0}^{n-1} R_i^0 m_i \left(\vec{g}_i - \vec{a}_{c,i} \right) \tag{4.9}$$

Variable Definitions:

$\vec{o}_{zmp}$: The zero moment point with respect to the base frame

$\vec{R}^{GI}$: The resultant of the gravity plus inertia forces for all the links (superscript GI).

$\vec{g}_i$: The acceleration due to gravity expressed in frame i

$\vec{a}_{c,i}$: The linear acceleration of the centre of mass of link i in frame i, this can be found using the Newton Euler Recursive formulation

m_i: The mass of link i

$\overrightarrow{\dot{H}_i}$: The rate of angular momentum of link i

I_i: The inertia matrix of link i about a frame parallel to frame i whose origin is at the centre of mass of link i (Tensor matrix), attained using CAD model

$\vec{\omega}_i$: The angular velocity of frame i. This can be found using the Newton Euler Recursive formulation

M^{GI}: The moment about the base reference

$\vec{n}$: The normal to the plane on which the robot is walking, for a horizontal plane it is listed in (4.8)

4.4 Trajectory Generation

For biped locomotion to take place, the robot's joints follow through a pre-determined trajectory. For the current robot frame some of the joint trajectories will be generated directly, as for the frontal plane motors, while other will be result of inverse kinematics.

Overall the gait of the robot developed in this thesis is passive as the robot does not move fast enough to generate a significant inertia. The robot gait is composed of phases outlined in Table 4.1. To start walking the robot needs to shift its weight to one side then take half a step listed as items 1-3 in Table 4.1. To continue walking it shifts its weight to the supporting leg, takes a step with the swing leg then shifts its weight back to the centre alternating between the right and the left leg acting as the supporting and swinging leg. This typical gait is composed of items 4-9 in Table 4.1. Finally to finish walking the robot takes half a step with the opposite leg that it stated walking with.

Item	Description
1	Shift weight onto right leg
2	Take a half step with left
3	Shift weight back to centre
4	Shift weight to left side
5	Take step with right leg
6	Shift weight back to centre
7	Shift weight on right leg
8	Take a step with left leg
9	Shift weight to centre
10	Shift weight to the left
11	Take half step with right leg
12	Shift weight to the centre

Table 4.1: Components of basic gait for biped walking

Humans walk with the heal striking the ground first; this is impractical for a robot with a foot structure currently consisting of only a flat surface. Until a foot with more elasticity and degrees of freedom is developed, the robot will make steps keeping the sole of the foot parallel to the ground.

4.4.1 Polynomial Trajectory Generation

To generate trajectories for the robot joints, whether that trajectory is in Cartesian space or joint space a polynomial equation is used to generate that trajectory. This is done by applying a fifth order, or quintic polynomial, to generate the trajectory. Typically, cubic polynomial is used in robotics; however with only a slight increase in computation, quintic polynomial allows the starting and ending velocity and acceleration to be specified.

For the ankle and hip roll joints the trajectory is generated directly by connecting a series of spline interpolations. For the joints in the sagittal plane, a trajectory is generated for ankles and hips in Cartesian space using spline interpolation and inverse kinematics is used to find joint angles for the ankle pitch, knee and hip pitch joints.

To solve the six unknown coefficients for the quintic polynomial shown in Equation (3.7), the six constraint equations listed in Equation (3.8) are solved. The resulting coefficients are listed in Equation (3.9) [37].

$$\theta(t) = a_0 + a_1 t + a_2 t^2 + a_3 t^3 + a_4 t^4 + a_5 t^5 \tag{3.7}$$

$$\left.\begin{aligned}
\theta(0) &= a_0 \\
\theta(t_f) &= a_0 + a_1 t_f + a_2 t_f^2 + a_3 t_f^3 + a_4 t_f^4 + a_5 t_f^5 \\
\dot{\theta}(0) &= a_1 \\
\dot{\theta}(t_f) &= a_1 + 2a_2 t_f + 3a_3 t_f^2 + 4a_4 t_f^3 + 5a_5 t_f^4 \\
\ddot{\theta}(0) &= 2a_2 \\
\ddot{\theta}(t_f) &= 2a_2 + 6a_3 t_f + 12a_4 t_f^2 + 20a_5 t_f^3
\end{aligned}\right\} \tag{3.8}$$

$$\left.\begin{aligned}
a_0 &= \theta_0 \\
a_1 &= \dot{\theta}_0 \\
a_2 &= \frac{\ddot{\theta}_0}{2} \\
a_3 &= \frac{20\theta_f - 20\theta_0 - (8\dot{\theta}_f + 12\dot{\theta}_0)t_f - (3\ddot{\theta}_0 - \ddot{\theta}_f)t_f^2}{2t_f^3} \\
a_4 &= \frac{30\theta_0 - 30\theta_f + (14\dot{\theta}_f + 16\dot{\theta}_0)t_f - (3\ddot{\theta}_0 - 2\ddot{\theta}_f)t_f^2}{2t_f^4} \\
a_5 &= \frac{120\theta_f - 12\theta_0 - (6\dot{\theta}_f + 6\dot{\theta}_0)t_f - (\ddot{\theta}_0 - \ddot{\theta}_f)t_f^2}{2t_f^5}
\end{aligned}\right\} \tag{3.9}$$

4.4.2 Frontal Plane (Roll) Joint Angle Trajectory Generation

All joints on the robot have a trajectory generated for them. For the ankle and hip joints in the frontal plane, the joint space trajectories to make the robot shift its weight from one leg to the other are generated directly using the polynomial trajectory generation.

The magnitude of the shifting is determined by verifying the centre of mass and zero moment point simulations. An additional three degree of shifting is done by the swing leg to ensure that the leg does not touch the supporting leg. Figure 4.2 and Figure 4.3 show the generated trajectories for the ankles and hips for the robot.

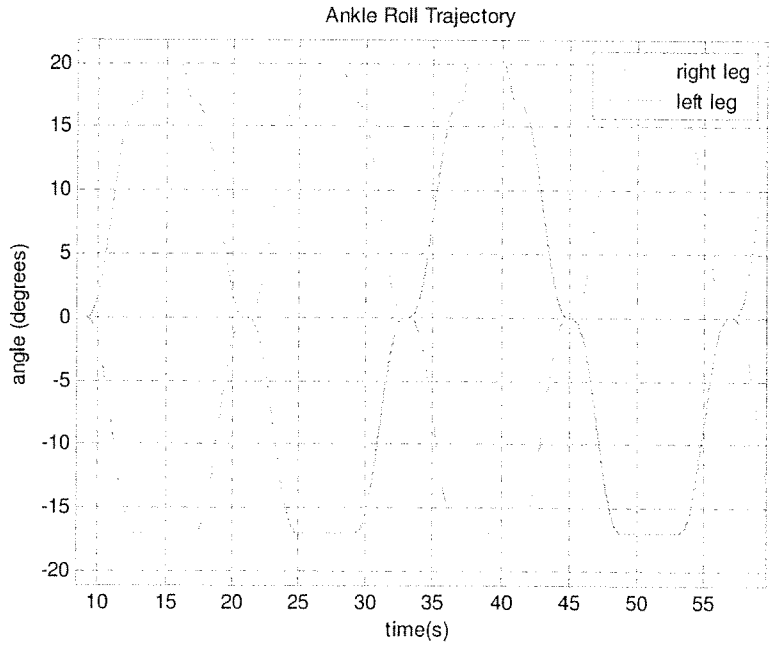

Figure 4.2: Ankle roll trajectories

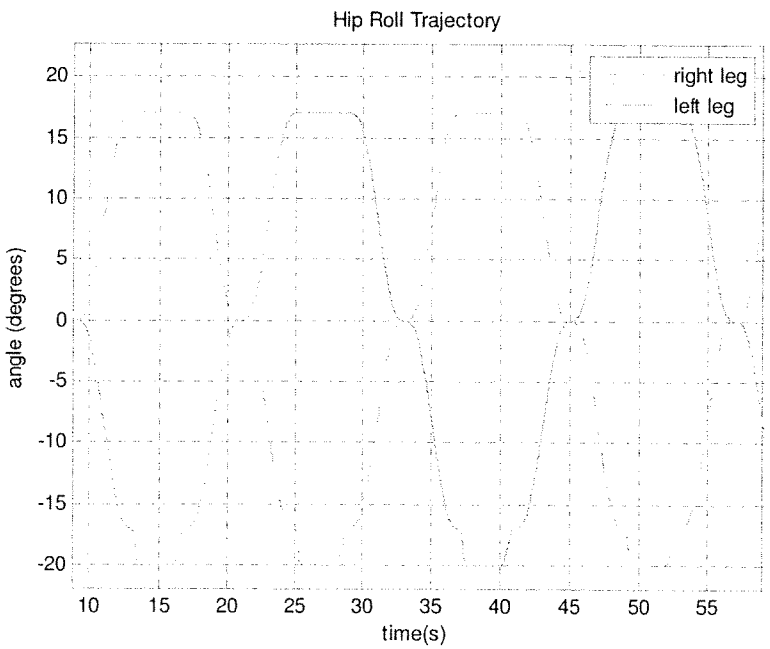

Figure 4.3: Hip roll trajectories

4.4.3 Sagittal Plane (Pitch) Cartesian Trajectory Generation

For the hip and ankles in the sagittal plane, the Cartesian trajectory is first generated for the ankle and hip joints, then inverse kinematics are applied to solve for the joint angles of the joints in sagittal Plane. Figure 4.4 to Figure 4.7 show the x and z trajectories for the hip and ankles for the robot taking a starting step, two full steps and a finishing step.

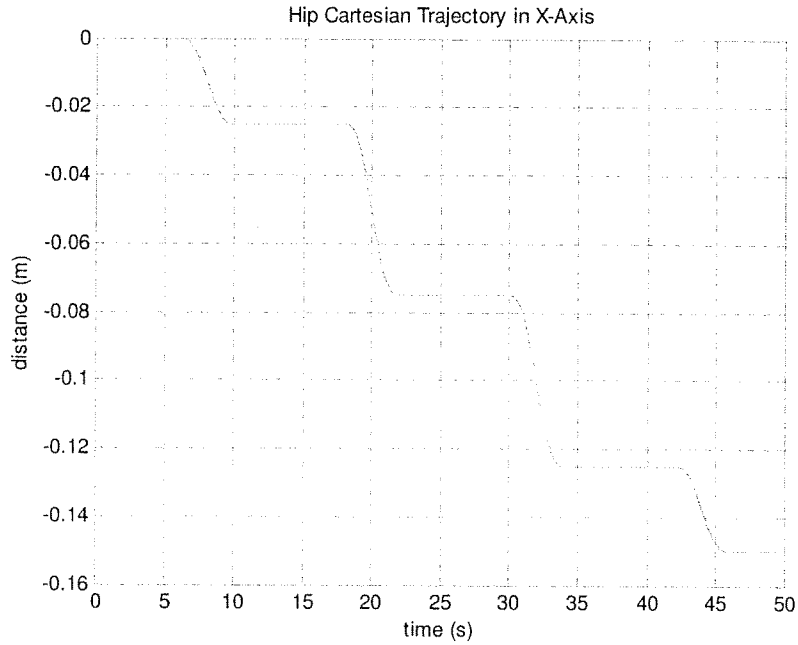

Figure 4.4: Cartesian trajectory for the hip in the x-axis

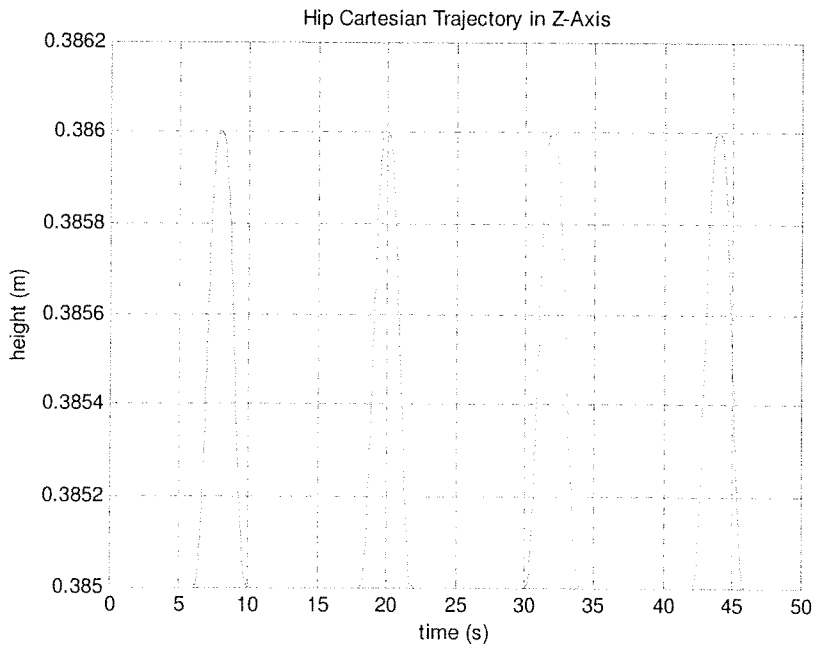

Figure 4.5: Cartesian trajectory for the robot hip in the z-axis

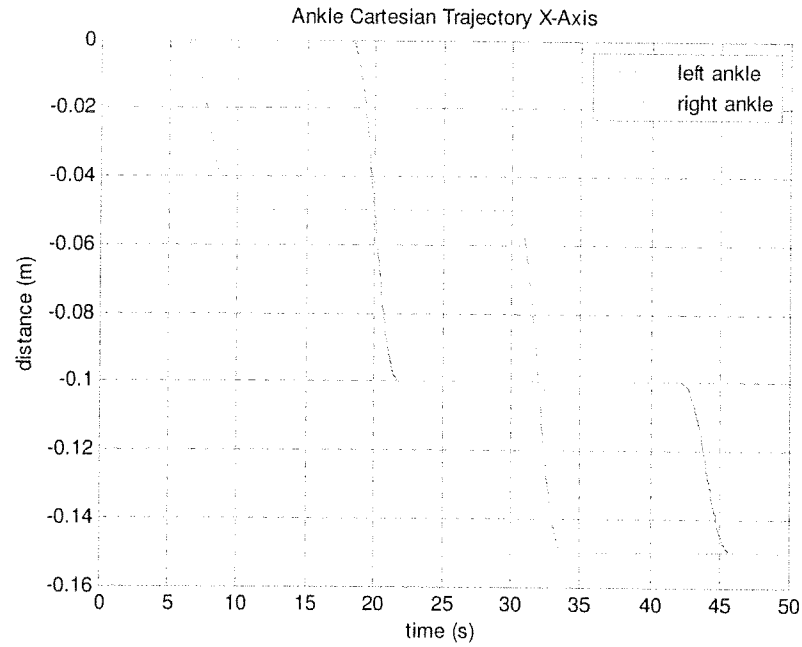

Figure 4.6: Cartesian trajectory for the robot ankles in the x-axis

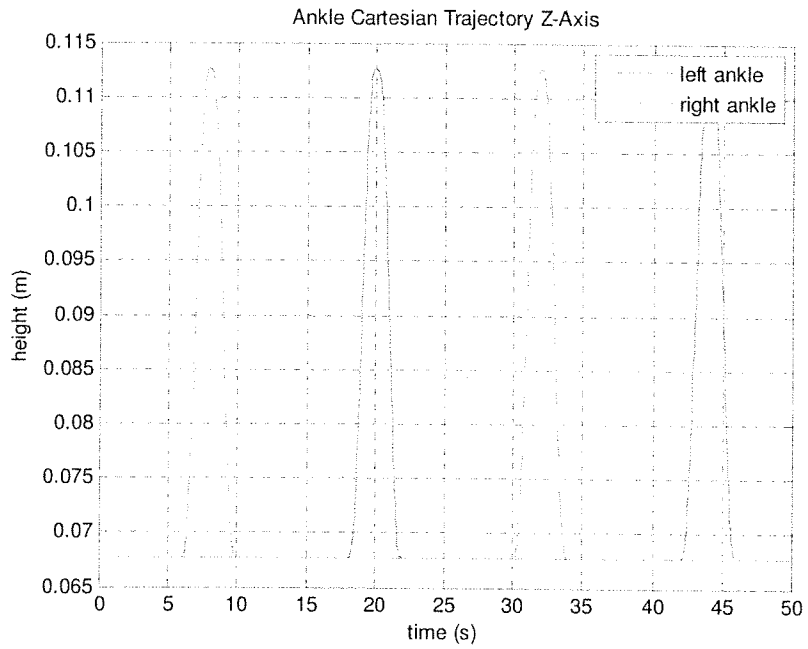

Figure 4.7: Cartesian trajectory for robot ankles in the z-axis

4.4.4 Sagittal Angle Joint (Pitch) Trajectories

Once the Cartesian trajectories are generated for the ankles and hips in the sagittal plane, inverse kinematics is used to find the joint angles of the ankle, knee and hip joints. Figure 4.8 to Figure 4.10 shows the trajectories of the joints in the sagittal plane outputted from the inverse kinematic solution.

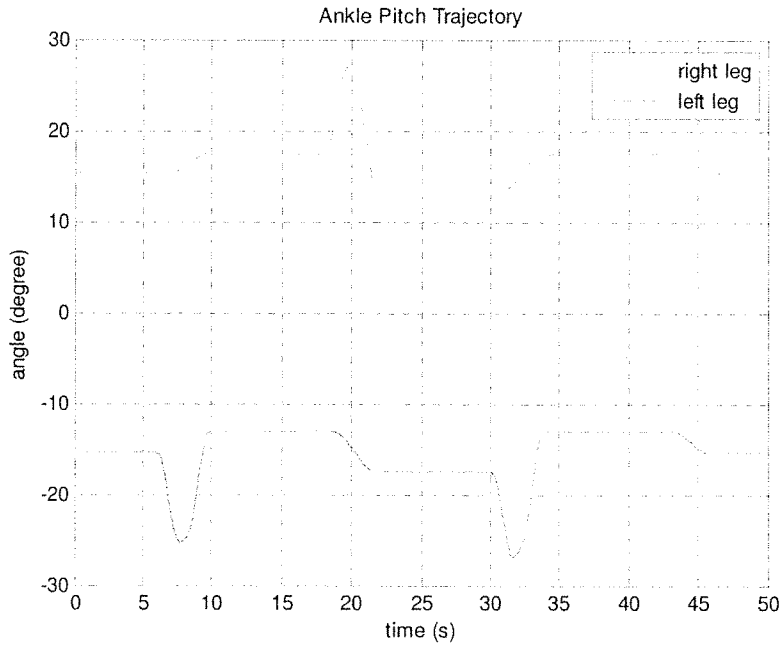

Figure 4.8: Ankle pitch trajectories

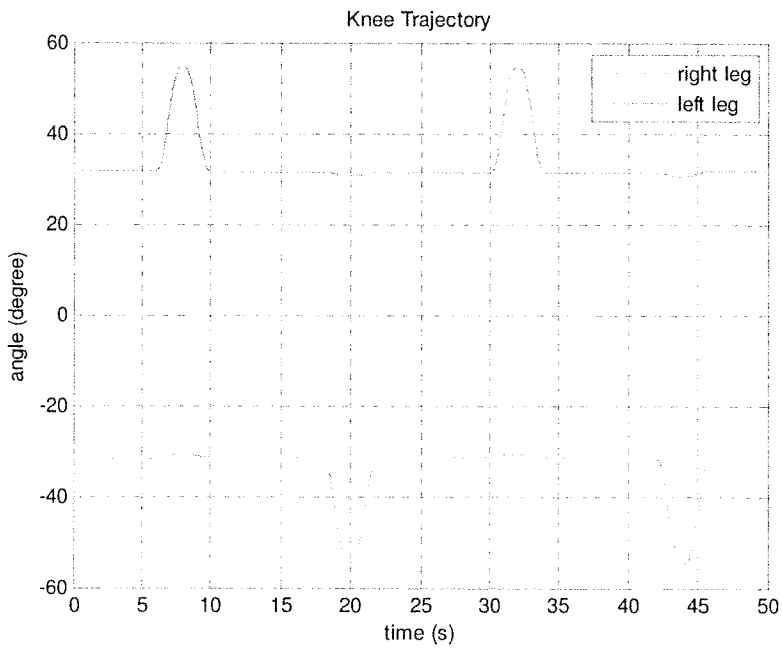

Figure 4.9: Knee joint trajectories

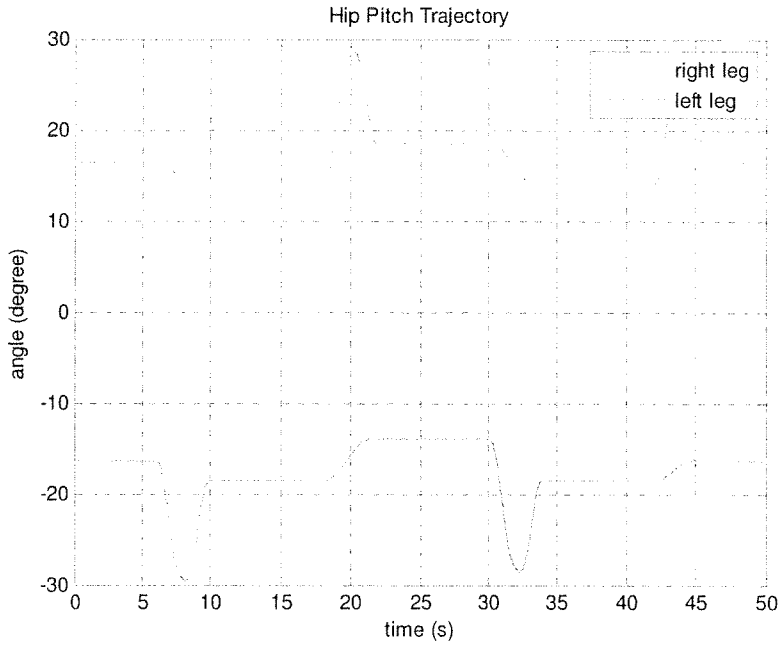

Figure 4.10: Hip pitch trajectories

5 Walking Simulation

5.1 Trajectory Generation Simulation

Using the generated trajectory and forward and inverse kinematics the trajectory can be verified by plotting a wireframe robot with respect to time using formula (2.5) which yields the Cartesian coordinates of each frame. Figure 5.1 shows snapshots of a wireframe visualization of the robot going through the motions of walking. The magenta circle represents the projection of the centre of mass.

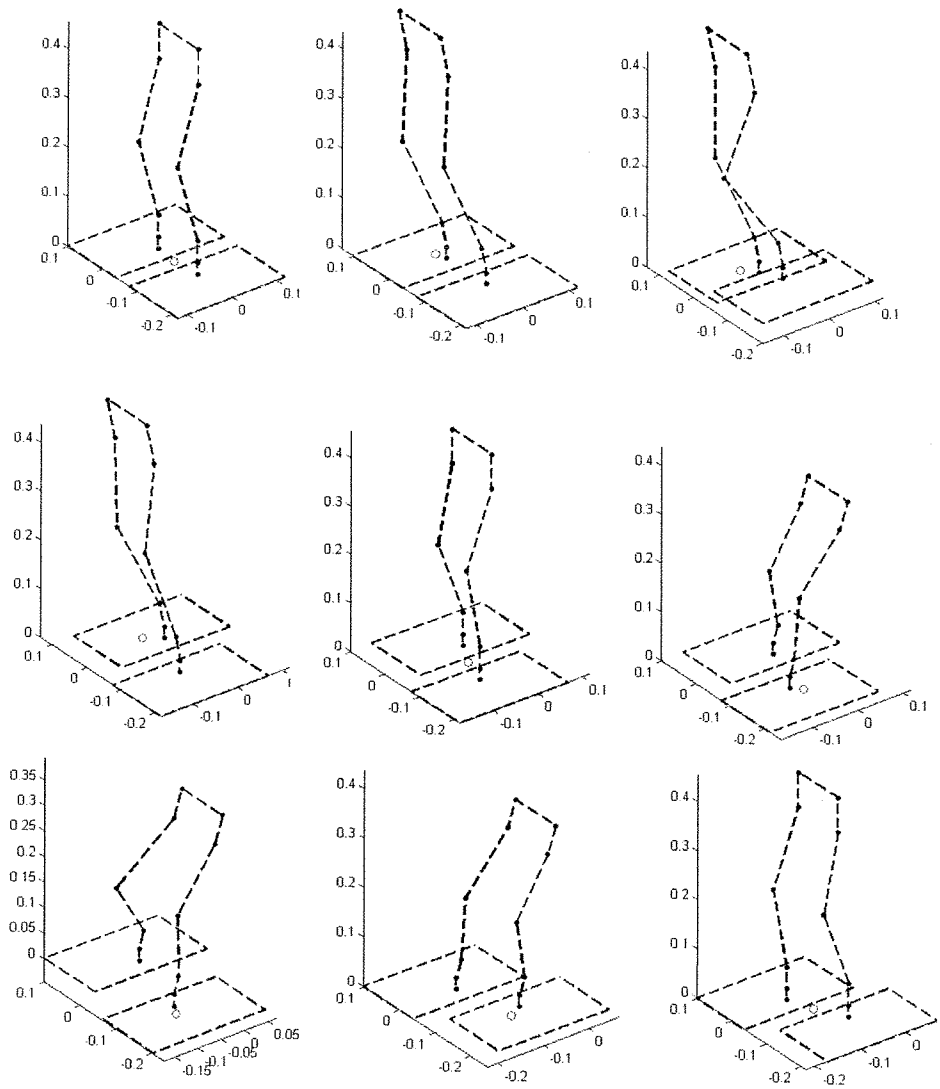

Figure 5.1: Plotted trajectory generation of robot walking ordered left to right and top to bottom; the magenta circle represents the projection of the centre of mass

5.2 COM and ZMP Simulation

In order to verify that the centre of mass of the robot follows a desirable path for a given generated trajectory, the centre of mass projection is plotted with respect to the feet of the robot as shown in Figure 5.2 and 5.3. For a robot moving as slowly at this robot the zero moment point and the projection of the centre of mass are approximately the same so the zero moment point is not shown.

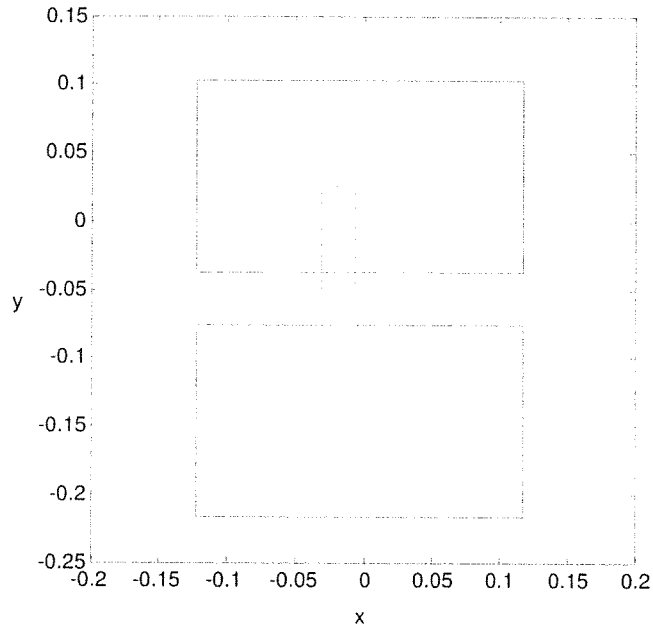

Figure 5.2: Path of centre of mass projection, half step with left leg (right leg support)

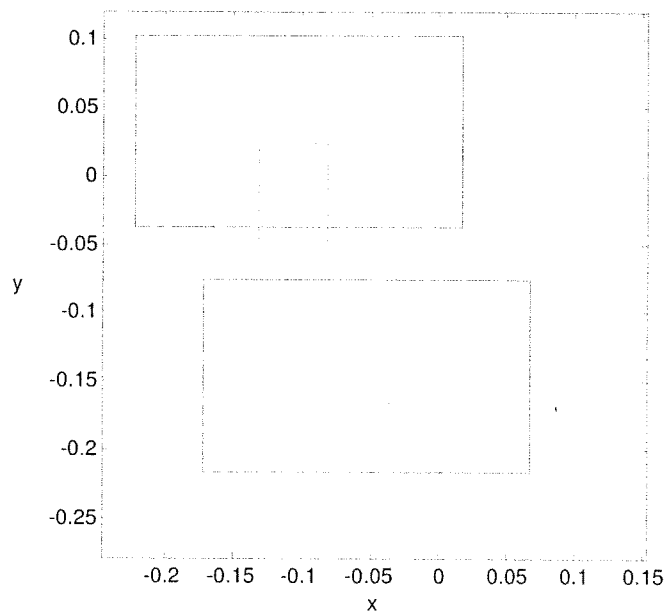

Figure 5.3: Path of centre of mass projection, full step left leg (right leg support)

5.3 Torque Requirement Simulation

In order to gage the torque requirement for the designed mechanical structure and planned walking gait, the torque is calculated using the recursive Newton Euler formulation. Figure 5.4 Figure 5.8 show the torque requirements during single support phase for the robot's walking gait.

The torque requirements are only shown for single support phase since the Recursive Newton Euler formulation requires the robotic structure to have a base (the planted foot) and an end effector (the swing foot).

The torque plots show that the motors that take the largest load are the hip roll motors, since during single support phase they support the abdomen as well as the swing leg. Because of this large torque it is important that the distance between the legs be kept to a minimum, and that a sufficiently strong motor is used for this joint.

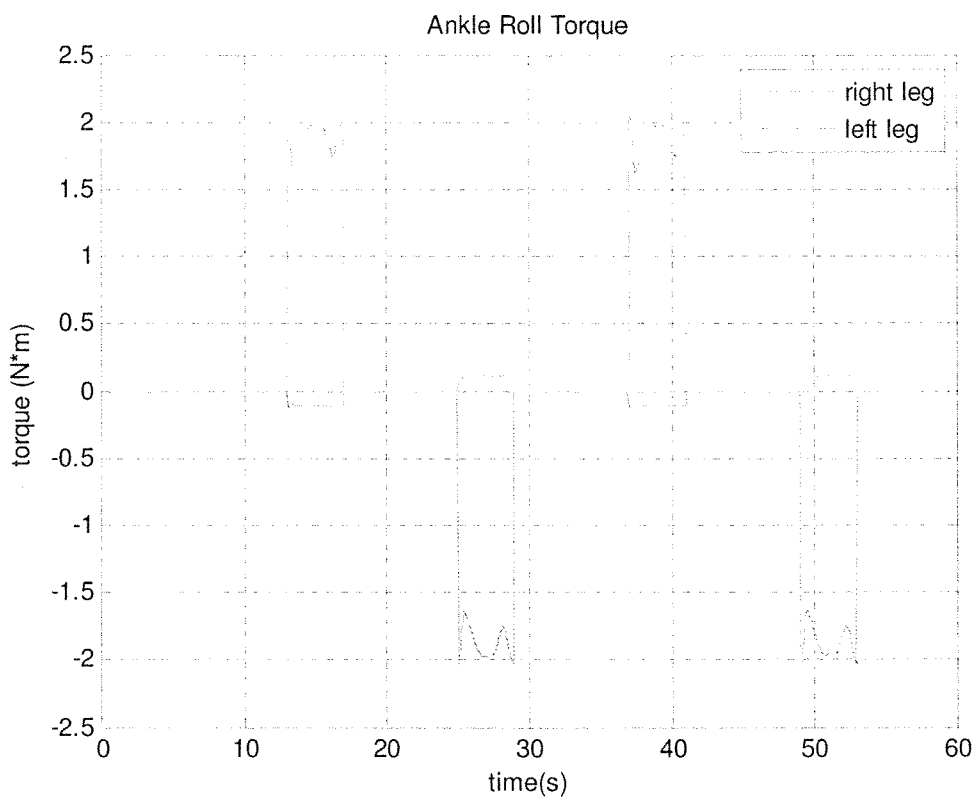

Figure 5.4: Ankle roll torque

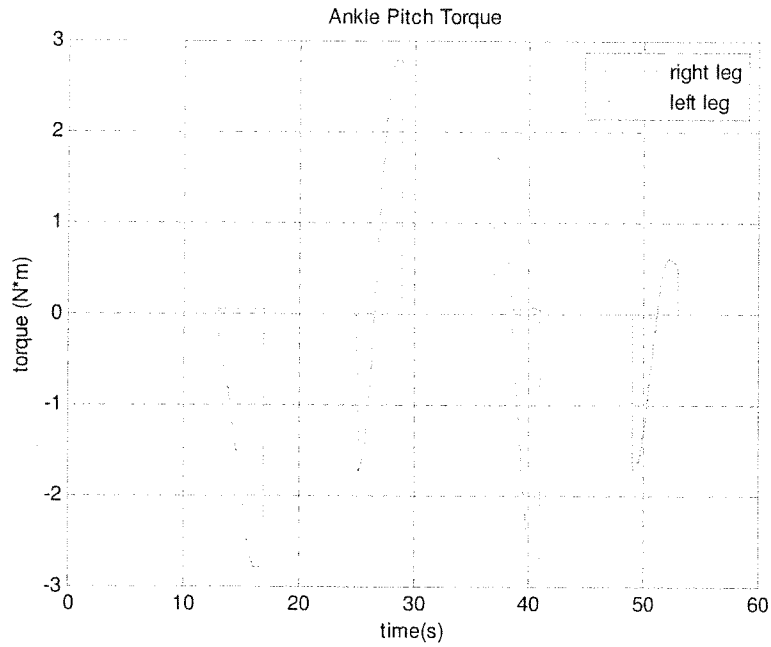

Figure 5.5: Ankle pitch torque

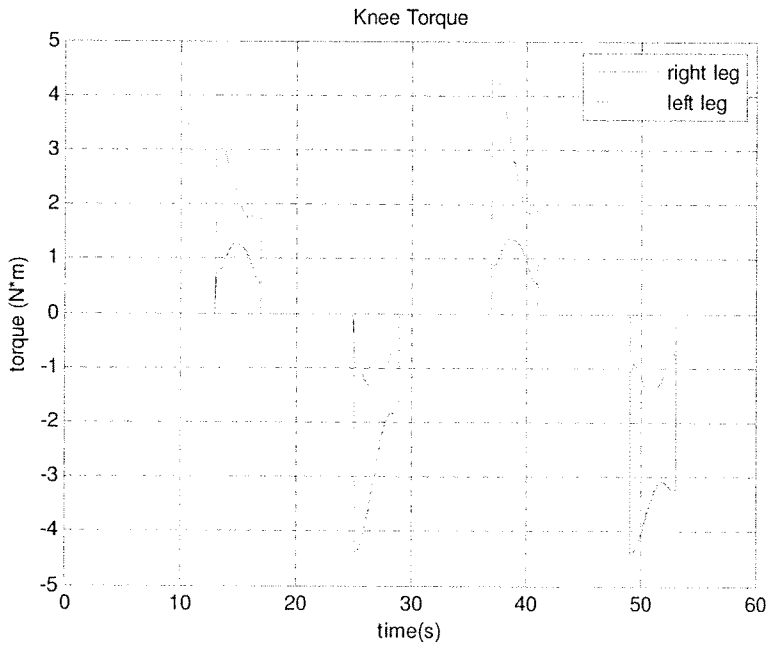

Figure 5.6: Knee torque

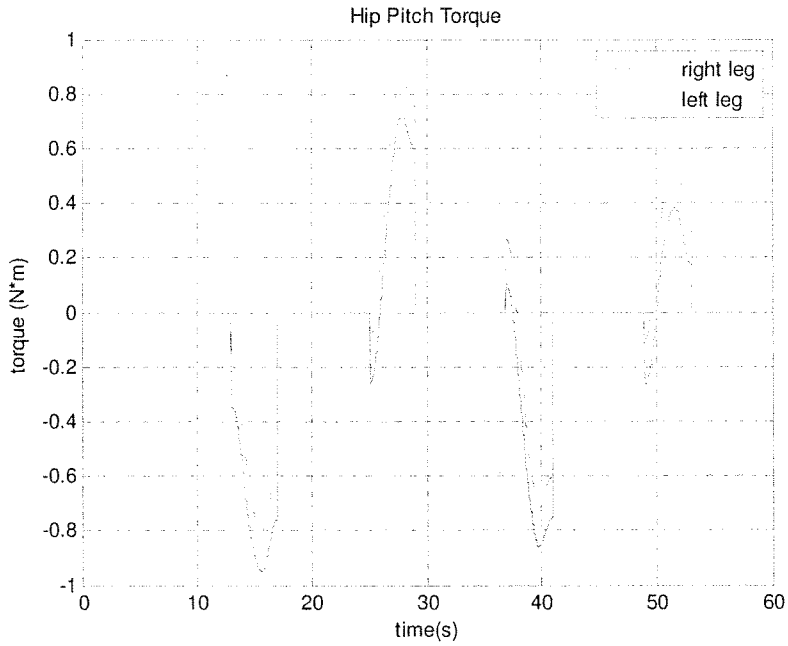

Figure 5.7: Hip pitch Torque

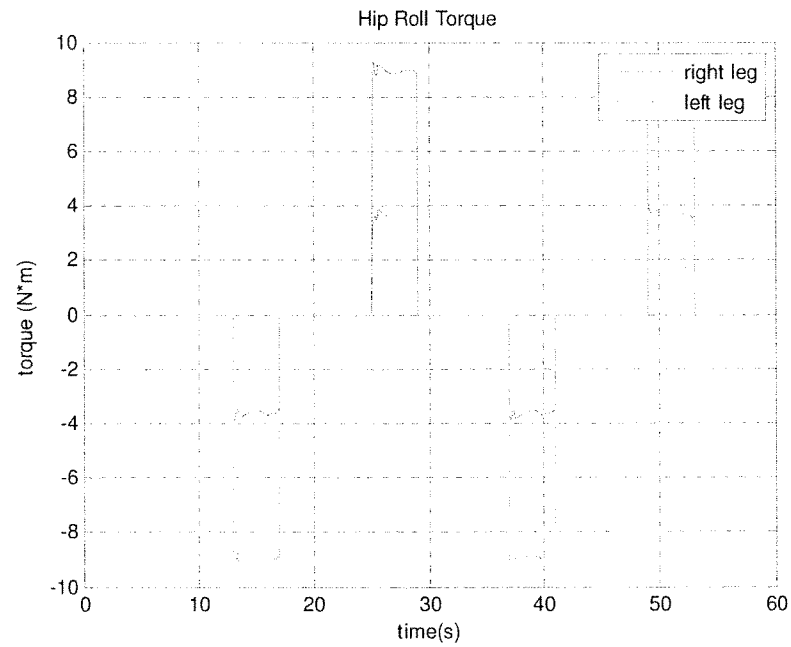

Figure 5.8: Hip roll torque

6 Mechanical Design

6.1 Introduction

For a robot to achieve stable biped locomotion it must have a reliable well proportioned mechanical structure. The design of passive walker robots like those described in references [27],[28] and [29]has shown that a properly designed mechanical structure can be made to walk with little or no actuation at all, highlighting the importance of a good mechanical design.

The location of the centre of mass is also important in how the robot performs. Clearly a low centre of mass is inherently more stable, however requires a larger shifting angle in order for the robot to take a step. Meanwhile a higher centre of mass, though less inherently stable, allows the robot to shift its centre of mass or zero moment point more easily.

All of these factors, as well as the means of actuation, construction material, degrees of freedom and sensors used come into consideration when designing a robot. Modern computer aided design software has greatly helped in this endeavor as it is now possible to quickly design three dimensional structures and to check for conflicts when assembling all of the parts.

6.2 Means of Actuation

The first decision in the mechanical design is to select the means of actuation. Electric motors are used since if geared properly, they can have a high enough torque output for the robot joints, and for an engineer with an electrical background like the author, are straight forward to control joints using only a potentiometer as feedback.

The two main other forms of actuation for robots, pneumatic and hydraulic, have been successfully implemented on robots such as Dexter from Anybots [31] and Petman from Boston Dynamics [33]. Although they have some advantages like a similar actuation to human muscles and controllable compliance [11], they require a more complicated control system which includes a hydraulic pump or compressor, pressure sensors, and linear distance transducers. All of these additional complications add the expense and complexity of the project, helping build the case for electric motors.

The electric motors for this thesis are selected in combination with gears such that the maximum torque of the motor-gear combination would meet the demands of the robot as calculated using the Recursive Newton Euler formulation. Higher gear ratios are used for the ankles joints to allow them enough stiffness to control the inertia of the robot's body while standing on one leg. The motors-gear combinations used on the robot are outlined in Table 6.1.

The current gears have a backlash of roughly 1°. This may seem small, however even 1° of backlash is enough to hinder performance of the robot and add to instability. Harmonic drive gearing, a gearing mechanism with no backlash, is the "de-facto standard for humanoid robots"[43], however due to its high cost is not employed in this project.

	Electric Motor		Gearhead	
	Model	**Power**	**Model**	**Gear Ratio**
Hip (Yaw)	Maxon RE-max 214581	18W	Maxon Planetary Gearhead 166949	246:1
Hip (Roll)	Maxon RE-max 268214	60W	Maxon Planetary Gearhead 166947	159:1
Hip (Pitch)	Maxon RE-max 268214	60W	Maxon Planetary Gearhead 166947	159:1
Knee (Pitch)	Maxon RE-max 268214	60W	Maxon Planetary Gearhead 166947	159:1
Ankle (Pitch)	Maxon RE-max 268214	60W	Maxon Planetary Gearhead 166951	318:1
Ankle (Roll)	Maxon RE-max 268214	60W	Maxon Planetary Gearhead 166952	411:1

Table 6.1: Electric motors and gears selection the 12-DOF freedom robot.

6.3 Mechanical Structure

6.3.1 Material Selection

The mechanical structure is designed and built using aluminum alloy primarily due to the ease with which it can be machined, low cost and its low density of approximately 2.70 g/cm^3, which is 34% of the density of steel.

One of the drawbacks of using aluminum is that it is not the most rigid material available. Since the shear modulus or modulus of rigidity of aluminum is only 25.5 GPa, compared to steel's 79.3GPa, a link made of aluminum can be expected to deform over three times

as much as a comparable link made of steel. This makes it important to properly size certain load bearing links so that the robotic structure is rigid.

Since thin pieces of aluminum deform considerably when welded, the mechanical structure is connected using small bolts, locking washers and nuts. The nut and bolt construction also makes assembly and disassembly easier than permanent fastening systems like blind rivets.

6.3.2 Shaft Connection

In order to attach the motor shafts to the various links, clamping hubs, as seen in Figure 6.1, are used since unlike set screw hubs, they do not damage the motor shaft and offer more holding power in high torque situations. For joints where the holding power is insufficient and the motor slips within the hub, locktite adhesive is used to prevent slipping.

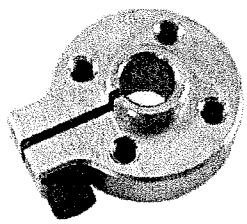

Figure 6.1: Clamping hubs employed on robot

6.3.3 Passive Shaft Design

On the side opposite from the motor shaft, the passive shaft joint is composed of a steel shaft, locking hub, brass bushing, shaft collar and potentiometer. A typical joint is shown in Figure 6.2.

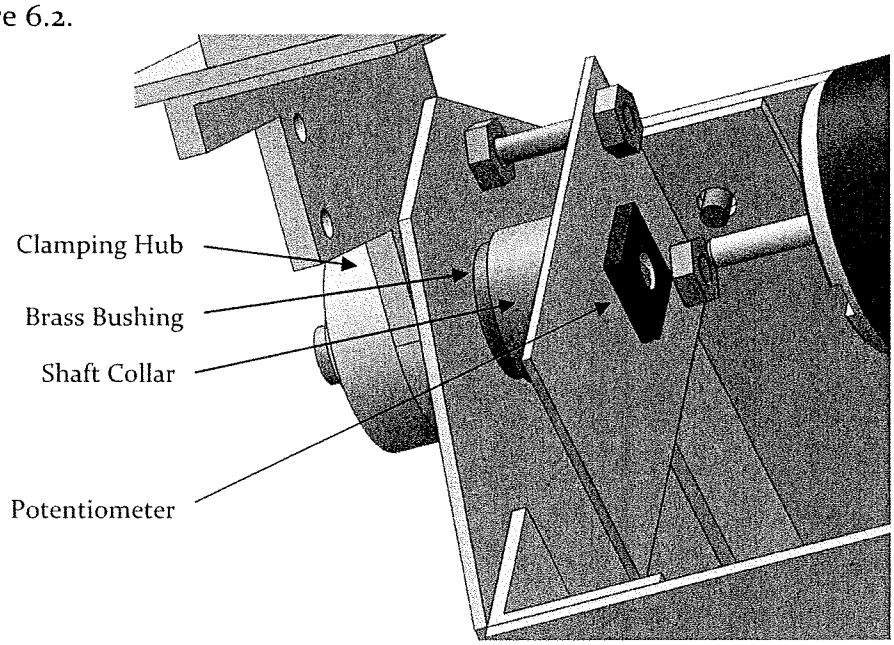

Figure 6.2: Typical passive shaft design detail

6.3.4 Overall Structure

The robot is designed to have a form similar to a human. However, with only twelve degrees of freedom and each electric motor actuating each degree of freedom, the form is greatly influenced by the size and shape of the motors used. This is most evident in the ankles and hip joint where two and three motors respectively are used to mimic ball joints present on humans.

The motor which bears the largest amount of torque is the hip roll joint. When the robot takes a step this motor supports the abdomen as well as the opposite leg. To keep torque on this joint to a minimum the distance between the legs is kept to a minimum, only 114mm.

Figure 6.3 shows a completed mechanical design of the robot consisting of thirteen links and twelve degrees of freedom. The design also shows potentiometers and motors mounted on each joint as well as force sensors installed on the feet.

6.3.5 Construction

The components of the robot's mechanical structure were machined using a CNC machine, band saw, sheet metal shears and a drill press. The parts were assembled using bolts, locking washers, and nuts. Figure 6.4 shows the constructed robot with electronics mounted in the abdomen.

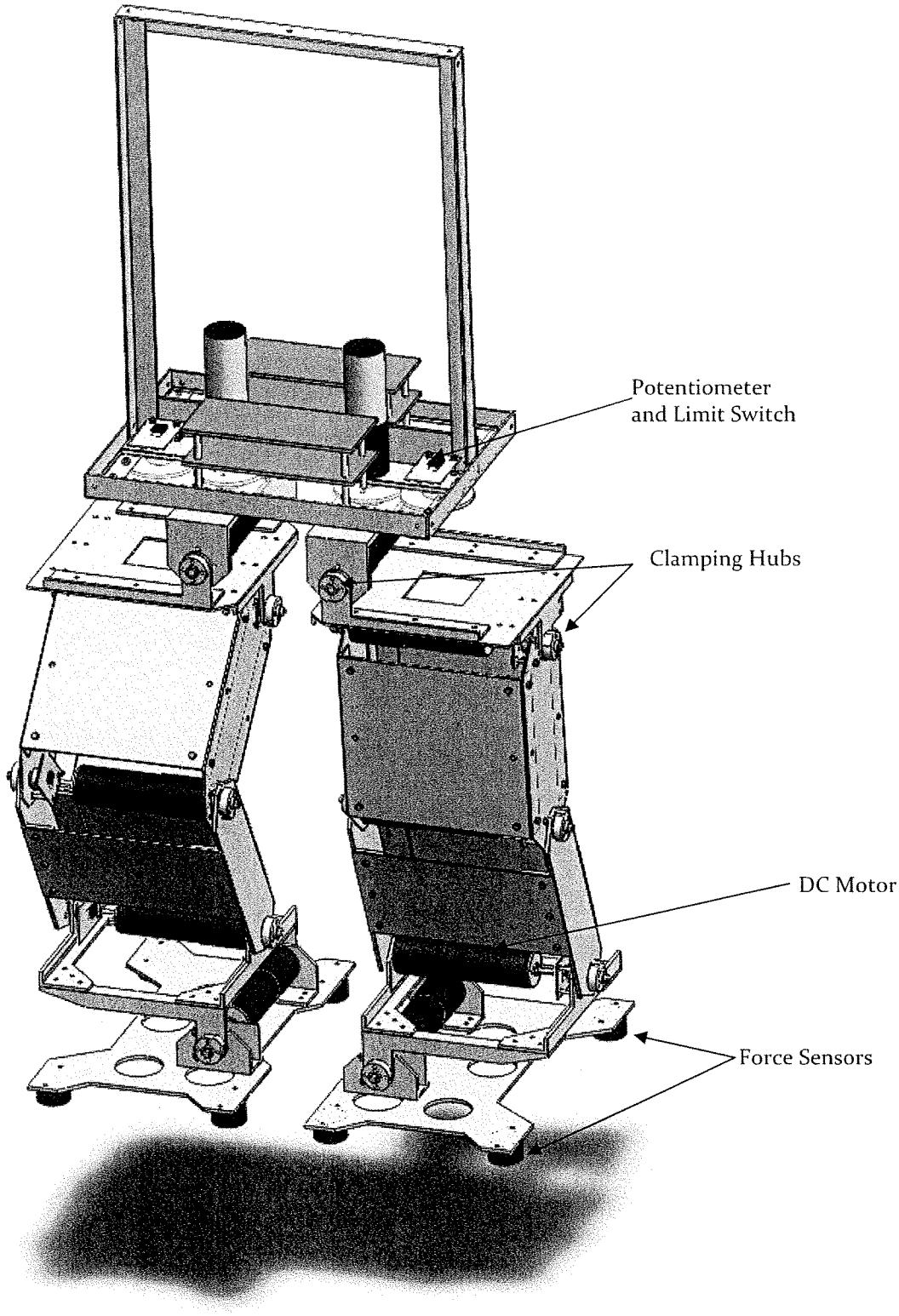

Figure 6.3: CAD model of biped robot

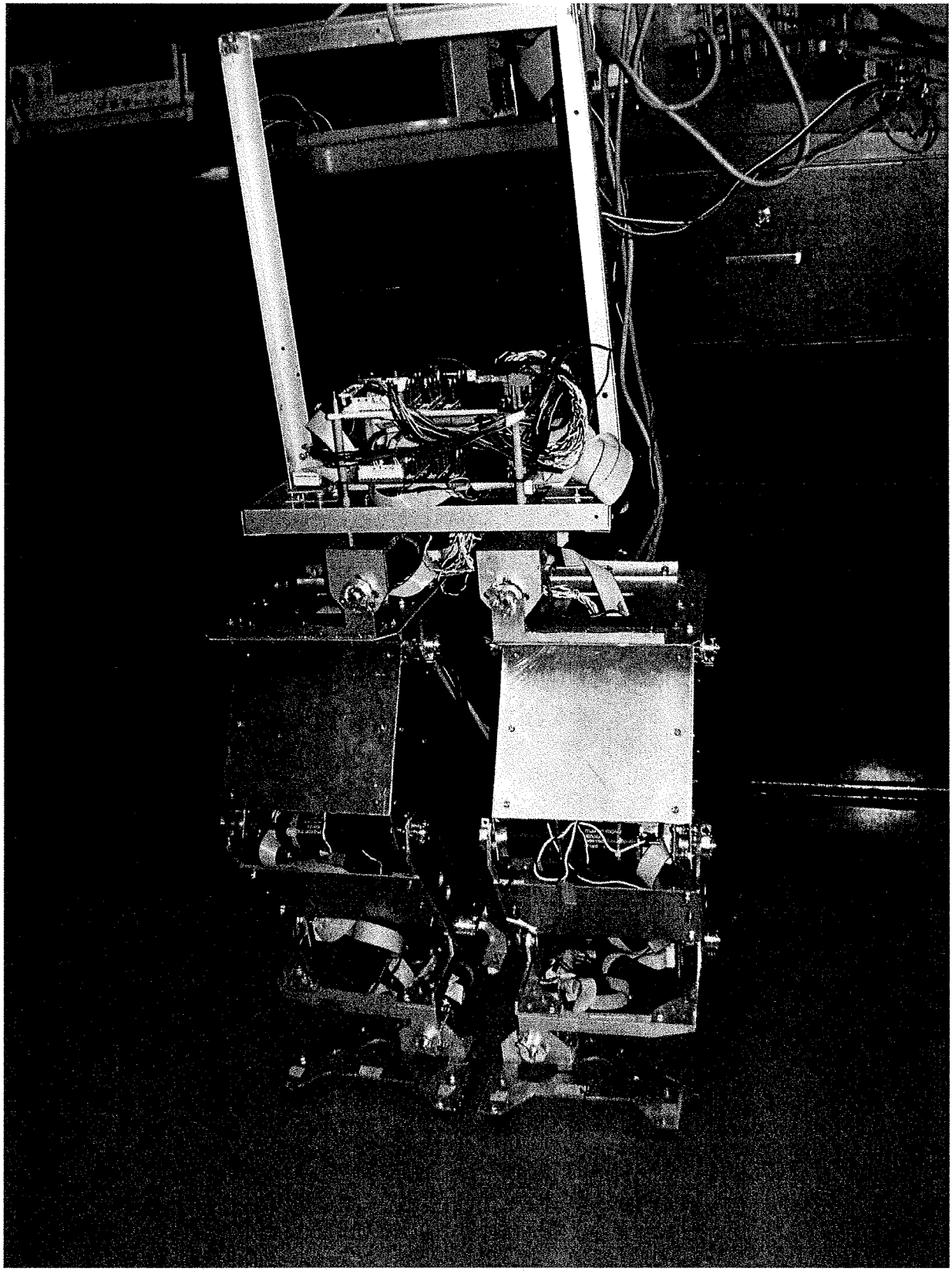

Figure 6.4: Photograph of constructed 12-DOF walking robot

6.4 Link Parameters

Using the 3D CAD program Solidworks the parameters that are required for the Newton Euler Recursion, the centre of mass calculation and the zero moment point are easily attained, and are listed in Table 6.2 and Table 6.3.

Link Number	Link Description	Mass (kg)	$\vec{r}_{i+1,ci}$ (mm)	$\vec{r}_{i,i+1}$ (mm)
1	foot	0.646	(8.82 ,-6.99 ,19.7)	(0, 22.6, 0)
2	ankle	0.564	(-4.36 ,2.62 ,-27.79)	(65.3, 0, 0)
3	shin	0.392	(-88.63 ,-0.37 ,-59.91)	(170, 0, 0)
4	thigh	1.224	(-82.93 ,-0.02 ,-25.59)	(160, 0, 0)
5	lower hip	0.229	(-35.63 ,-59.91 ,-0.52)	(71, 0, 0)
6	upper hip	0.671	(-0.08 ,-25.59 ,-8.85)	(0, 0, 0)
7	abdomen	1.860	(-56.64 , -3.25, -106.44)	(114, 0, 0)
8	upper hip	0.671	(-0.08 ,-8.85 ,-14.13)	(0, 0, 0)
9	lower hip	0.229	(-35.35 ,-0.51 ,52.26)	(71, 0, 0)
10	thigh	1.224	(-77.07 ,-0.02 ,25.49)	(160, 0, 0)
11	shin	0.392	-84.98, 0.01, 7.62)	(170, 0, 0)
12	ankle	0.564	(-40.64 ,-27.79 ,-2.57)	(65.3, 0, 0)
13	foot	0.646	(-11.18 ,27.59 ,43.41)	(22.6, 0, 0)

Table 6.2: Mass and centre of mass locations for robot links

Link Number	Link Description	Inertia Tensor (g*mm²)
1	foot	$\begin{bmatrix} 1830950.43 & -91559.15 & -104215.93 \\ -91559.15 & 2213772.77 & 78621.04 \\ -104215.93 & 78621.04 & 579380.56 \end{bmatrix}$
2	ankle	$\begin{bmatrix} 2292134.59 & 794.06 & -12903.57 \\ 794.06 & 1637642.22 & 5737.41 \\ -12903.57 & 5737.41 & 1068580.16 \end{bmatrix}$
3	shin	$\begin{bmatrix} 2098163.66 & 44269.45 & -323.75 \\ 44269.45 & 3000992.32 & 797.89 \\ -323.75 & 797.89 & 1190933.39 \end{bmatrix}$
4	thigh	$\begin{bmatrix} 3006750.60 & -72.91 & 259609.69 \\ -72.91 & 8591311.73 & 2260.29 \\ 259609.69 & 2260.29 & 6667178.05 \end{bmatrix}$
5	lower hip	$\begin{bmatrix} 2361441.77 & 52721.73 & 3485.92 \\ 52721.73 & 1163049.86 & 16081.48 \\ 3485.92 & 16081.48 & 1319604.34 \end{bmatrix}$

6	upper hip	$\begin{bmatrix} 1407520.02 & 4391.21 & -520.51 \\ 4391.21 & 363006.66 & 93366.65 \\ -520.51 & 93366.65 & 1406684.46 \end{bmatrix}$
7	abdomen	$\begin{bmatrix} 12520278.48 & 39739.52 & 1778.45 \\ 39739.52 & 20490455.48 & 279362.43 \\ 1778.45 & 279362.43 & 13505805.89 \end{bmatrix}$
8	upper hip	$\begin{bmatrix} 1407520.02 & -520.51 & -4391.21 \\ -520.51 & 1406684.46 & -93366.65 \\ -4391.21 & -93366.65 & 363006.66 \end{bmatrix}$
9	lower hip	$\begin{bmatrix} 2360959.48 & -2429.53 & 52786.24 \\ -2429.53 & 1319620.54 & -16983.15 \\ 52786.24 & -16983.15 & 1163514.80 \end{bmatrix}$
10	thigh	$\begin{bmatrix} 3006750.60 & 72.91 & 259609.69 \\ 72.91 & 8591311.73 & -2260.29 \\ 259609.69 & -2260.29 & 6667178.05 \end{bmatrix}$
11	shin	$\begin{bmatrix} 2098163.65 & 44269.54 & 179.43 \\ 44269.54 & 3000992.33 & -836.50 \\ 179.43 & -836.50 & 1190933.39 \end{bmatrix}$
12	ankle	$\begin{bmatrix} 2287848.09 & 45680.34 & -79319.39 \\ 45680.34 & 1231953.53 & -61778.08 \\ -79319.39 & -61778.08 & 1581903.32 \end{bmatrix}$
13	foot	$\begin{bmatrix} 5342488.64 & -196855.96 & -130416.14 \\ -196855.96 & 4226955.44 & 196535.24 \\ -130416.14 & 196535.24 & 1434123.54 \end{bmatrix}$

Table 6.3: Robot link tensor matrices

7 Electrical Design

7.1 Electric Design Overview

The electrical design of the biped robot is centreed around two TMS320F2812 digital signal processor (DSP) from Texas Instruments mounted on custom designed printed circuit boards. Each of the DSP's controls one of the legs of the robot and performs all of the real time control functions including: reading the potentiometers and foot sensors; computing the control signal; and sending out a control signal via pulse width modulation (PWM) and direction signals to motor driver boards.

The motor driver board uses the PWM and direction signals to drive the DC motors using LMD18200 integrated circuits. The Motor driver board also includes a safety interlock circuit wired to joint overextension limit switches to prevent the robot from damaging itself in the event of loss of control.

In addition to the DSP a Linux computer generates the joint trajectories and feedforward terms and transmits this data to the DSP's via serial cables. A windows computer is used to program the two DSP's in the C programming language using a Jtag emulator and Code Composer Studio software. Figure 7.1 shows an overview of the electrical system of the robot.

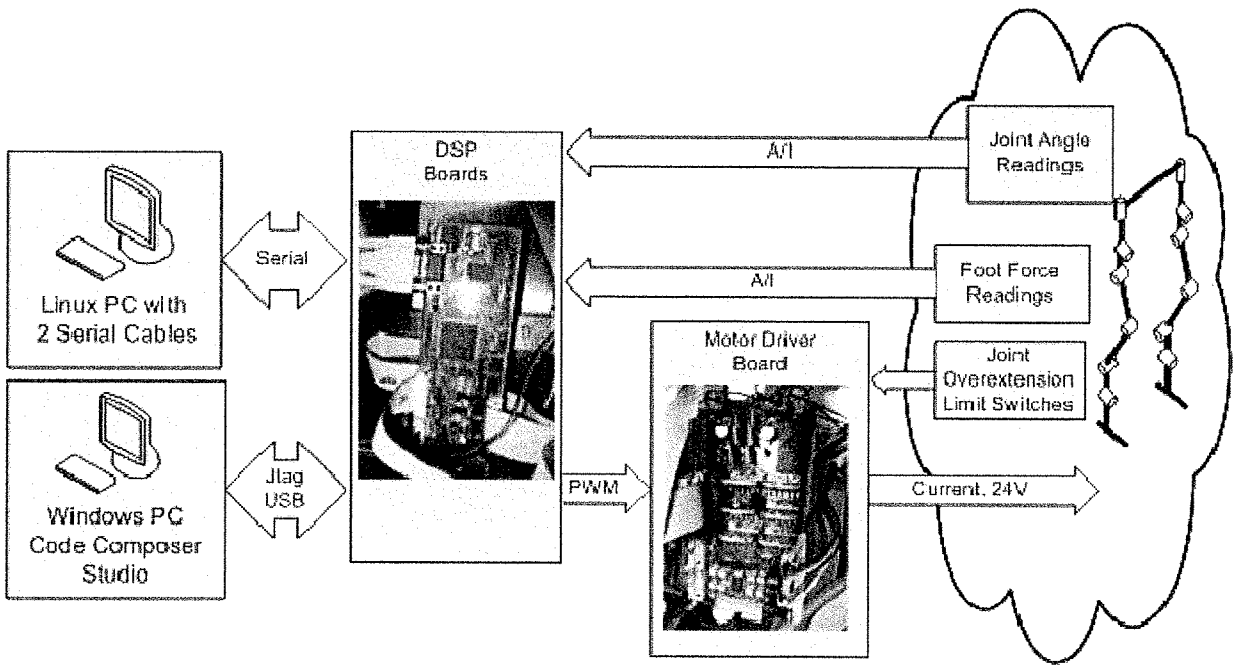

Figure 7.1: Electrical design overview

7.2 Sensors

7.2.1 Potentiometers

The most important source of feedback for the walking robot is the joint angle reading. For this purpose EVWAE4001B14 10kΩ potentiometers from Matsushita Electronic Components are selected. The potentiometers are small, light and eliminate the need for a homing routine that would be required if rotary encoders were to be used. Absolute encoders could have also been used; however their cost is much higher than that of potentiometers.

The downsides of the EVWAE4001B14 potentiometers are that they produce a noisy signal that requires filtering, and their weak physical structure is prone to mechanical failure.

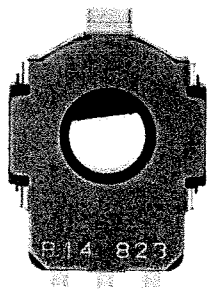

Figure 7.2: EVWAE4001B14 10kΩ potentiometers

7.2.2 Limit Switches

In addition to the potentiometers, small limit switches, model ESE 24 from Panasonic, are placed on each joint and wired to the overextension interlock on the motor driver circuit board. These limit switches are triggered by a plate glued to the shaft collar on each lazy shaft assembly.

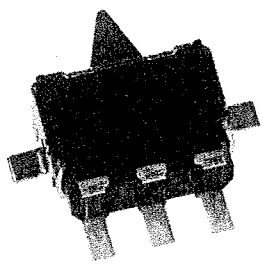

Figure 7.3: Panasonic ESE 24 limit switch

7.2.3 Force Sensors

In order to directly measure the zero moment point (ZMP) or centre of pressure (COP) of the biped robot it is necessary to use some form force sensor on the feet of the robot. In this design FC22 load cells from Measurement Specialties are used due to their small size, low noise and low cost. Four sensors are installed on each foot of the biped robot and used in the balance control algorithm.

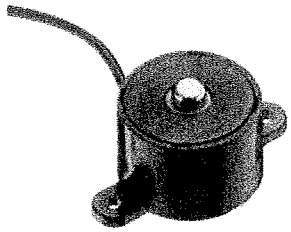

Figure 7.4: FC22 Load Cell from Measurement Specialties

7.3 Electronics

7.3.1 DSP Board

The TMS320F2812 DSP is used as the basis of the electrical design as it offers a large amount of input and outputs, it takes up little space, and is relatively low cost. The downside to the chip on the other hand is that it has a small memory size and slow computing speed. With 150 MHz clock frequency, and the flash memory expandable to only a maximum of 2MB[44], the DSP requires a separate computer to perform the computationally intensive tasks. In this design a desktop computer running Linux generates the joint trajectory and the feedforward terms using a C program, and then transmits the trajectories to the DSP's via serial cables. Table 5.1 outlines the specifications of the TMS320F2812 DSP.

Clock Speed	150 Mhz
Analog I/O	16 Channels, 12-Bit ADC
Digital I/O	56 Channels
RAM	On chip: 32kb Expandable to: 1024kb
Flash Memory	On Chip: 256kb Expandable to: 2056kb

Table 7.1: TMS320F2812 DSP specifications

7.3.2 Motor Driver Circuit Board

To drive the DC motors, LMD18200 3A H-Bridge motor driver chips are used. The motor divers work on an H-bridge principal, taking a discrete direction signal and pulse width modulation signal inputs to control the output motor current as per Figure 7.5 and Figure 7.6.

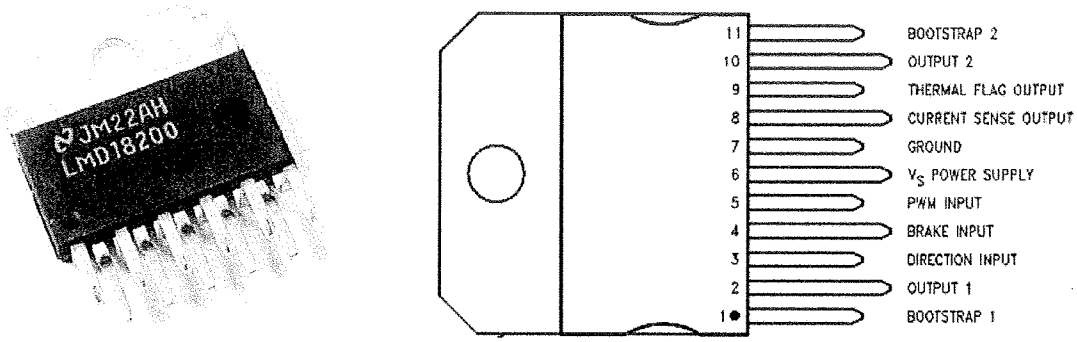

Figure 7.5: LMD18200 motor driver chip and pin outputs [45]

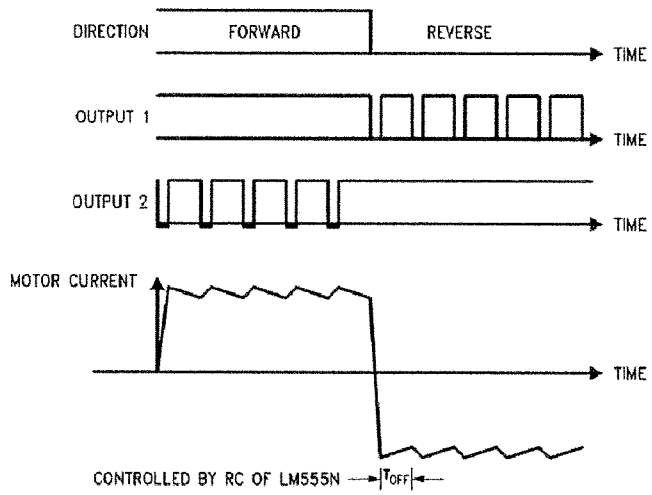

Figure 7.6: Operation waveforms of the motor driver chip [45]

8 Control System

8.1 Overview

The robot contains two control systems. The first control system is a computed torque scheme controller which ensures the robot follows the trajectory for each joint with a combination of a feedforward and feedback terms. The second control system on the robot is an active balance controller which helps keep the robot's feet flat on the ground and maintains an upright posture. It does this by contributing a PWM term to the ankle joint in the frontal plane while the robot is standing on one foot using feedback from the force sensors mounted on the four corners of each foot.

Figures 8.1 shows the block diagram for the control system of the ankle roll motor, consisting of PD controller, feedforward, and active balance control terms. Figure 8.2 shows the block diagram for the control system of the ankle pitch motor consisting of a PD controller and feedforward term. Figure 8.3 shows the block diagram for the control system of the knee, hip pitch and hip roll motors, consisting of a PID controller and feedforward term. Figure 8.4 shows the block diagram for the control system controlling the hip yaw motor consisting only of a PD controller.

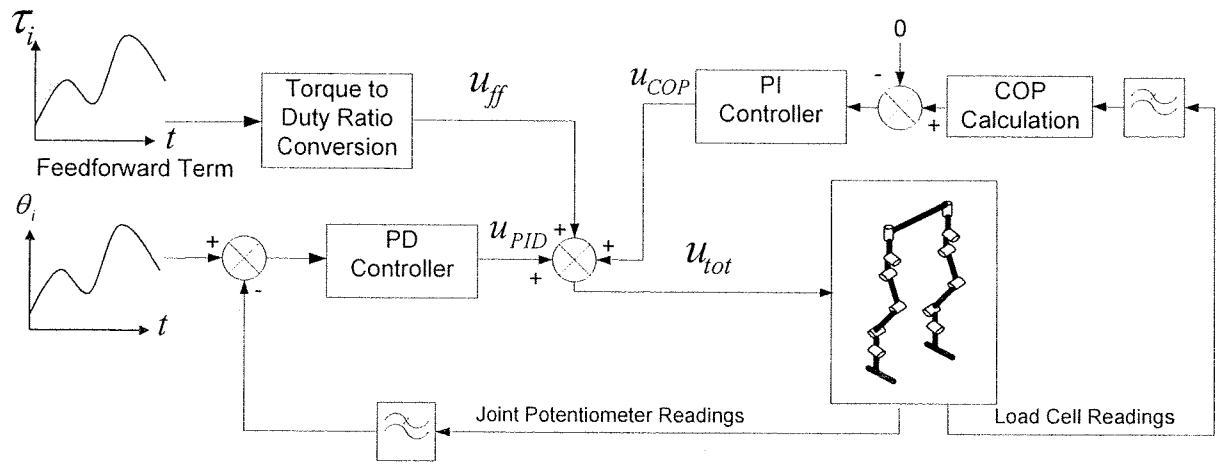

Figure 8.1: Block diagram of control system for the ankle roll motors

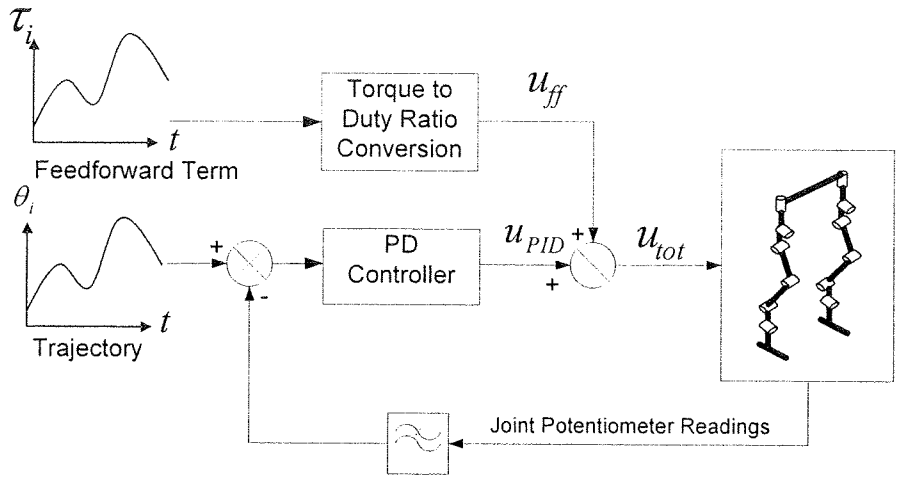

Figure 8.2: Block diagram of control system for ankle pitch motors

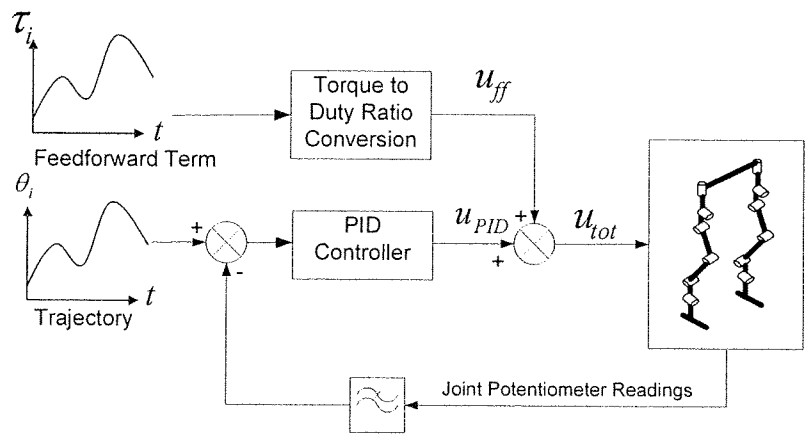

Figure 8.3: Block diagram of control system for the knee, hip pitch and hip roll motors

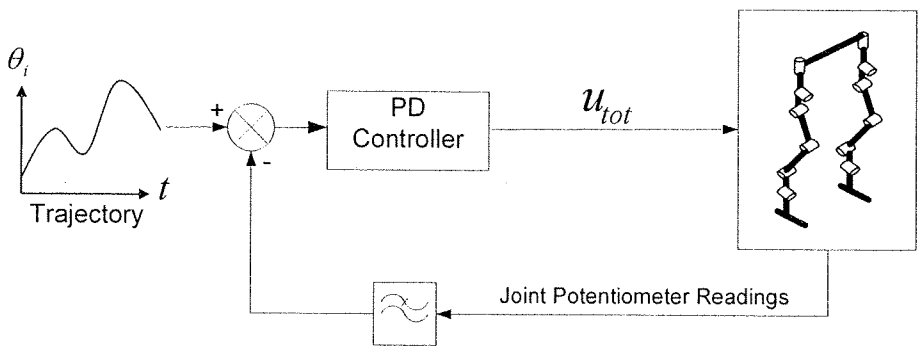

Figure 8.4: Block diagram of control system for the hip yaw motors

8.2 DC Motor Torque to PWM Relationship

From the overview of the control system we see that the computed feedforward term is attained by calculating the torque requirement at a given time. The units of this value are Newton-meters, thus must be converted to a pulse-width modulation duty ratio in order to use it as a signal for the motor driver circuit.

Figure 8.5 shows the schematic diagram for a DC motor. From this diagram we can derive Equation (8.1) which gives the formula for the current passing through the armature including losses from back emf. By taking into account of gearing, losses from gearing, and using the speed and torque constants of the motors we arrive at equations (8.4) and (8.5) which can be used to calculate the needed PWM signal for a desired torque. Table 8.1 lists the motor parameters used in calculating the feedforward term.

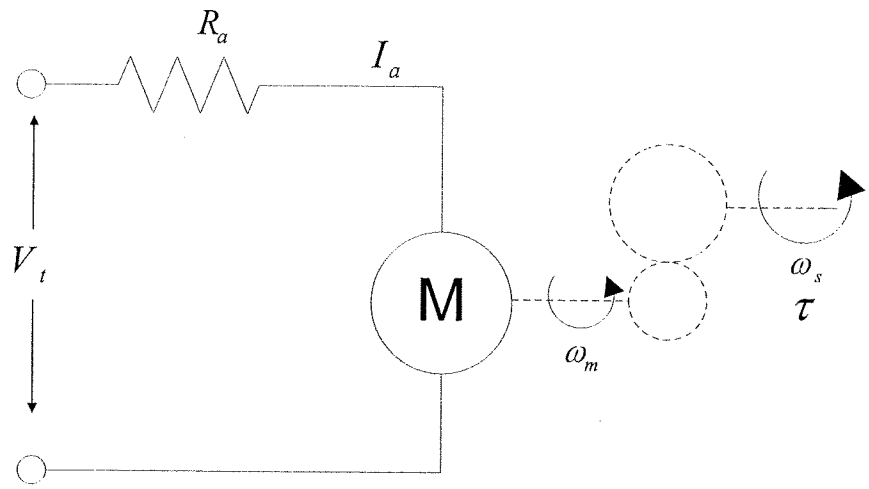

Figure 8.5: Schematic diagram of DC motor

$$I_a = \frac{V_t - {\omega_m}/{K_s}}{R_a} \tag{8.1}$$

$$K_T = \frac{1}{K_s} \tag{8.2}$$

$$\omega_s = \omega_m G_r \tag{8.3}$$

$$V_t = \frac{\tau R_a}{K_t G_r \eta} + \frac{\omega_s G_r K_t}{\eta} \tag{8.4}$$

$$D_{PWM} = \frac{V_t}{V_m} * 100 \tag{8.5}$$

Variable Definitions:

τ: The required torque, calculated using Recursive Newton Euler formulation
ω_s: Angular speed of the gear shaft
ω_m: Angular speed of the motor shaft
V_t: The terminal, or applied voltage
V_m: The nominal motor voltage
R_a: The armature resistance (Ω)
I_a: The armature current
K_T: The motor's torque constant (Nm/A)
K_s: The motor's speed constant (rad/s)
G_r: The motor gear ratio
η: The efficiency of the motor and gear
D_{PWM}: The PWM duty ratio during single support phase

Motor	Ankle Roll	Ankle Pitch	Knee	Hip Pitch	Hip Roll	Hip Yaw
K_T (Nm/A)	0.0259	0.0259	0.0259	0.0259	0.0259	0.0258
R_a (Ω)	0.611	0.611	0.611	0.611	0.611	2.36
η	20	20	25	25	25	25

Table 8.1: Motor parameters

8.3 Computing the Feedforward Term

A feedforward control term "*can be very beneficial in solving the problem of achieving a satisfactory performance both in the set-point following and in the load disturbance rejection task*" [42]. By anticipating what torque is required at a given time and by applying the correct PWM duty ratio, error can be minimized and overall system stability improved.

For the biped robot developed in this thesis, it was not possible for the robot to follow the given trajectory using only the tracking controller. The gains required for the robot to walk without the feed forward term were so high that they led to instability. The addition of a feedforward term to the control scheme results in acceptable performance without the need for high gains.

The feedforward term is generated by first starting with the Newton Euler Recursive formulation and converting the calculated torque to a PWM output. A gravity compensation term is added during the double support phase for the knee motor since while standing on two feet, this motor requires the largest amount of torque. Finally, a linear interpolation is made prior to and after the single support phase for motors which have a large jumps in PWM in order to emulate the robot's gradual shifting of its weight and to prevent instability that can result from a sudden application of a large feedforward term.

Formula 8.6 explains the construction of the feedforward term.

$$u_{ff} = \begin{cases} u_{DS}, & during\ double\ support\ for\ knee \\ u_{DS} + u_{slope}, & during\ transition\ for\ hip\ roll \\ u_{PWM}, & during\ single\ support \end{cases} \tag{8.6}$$

u_{DS}: The feedforward term for double support phase

u_{slope}: A linear interpolation from the double support feedforward term to the single support

u_{PWM}: The PWM duty ratio during single support phase (found with the Newton Euler formulation)

Figure 8.6 and Figure **8.7** show the feedforward terms used in the walking control of the robot for the left and right legs respectively.

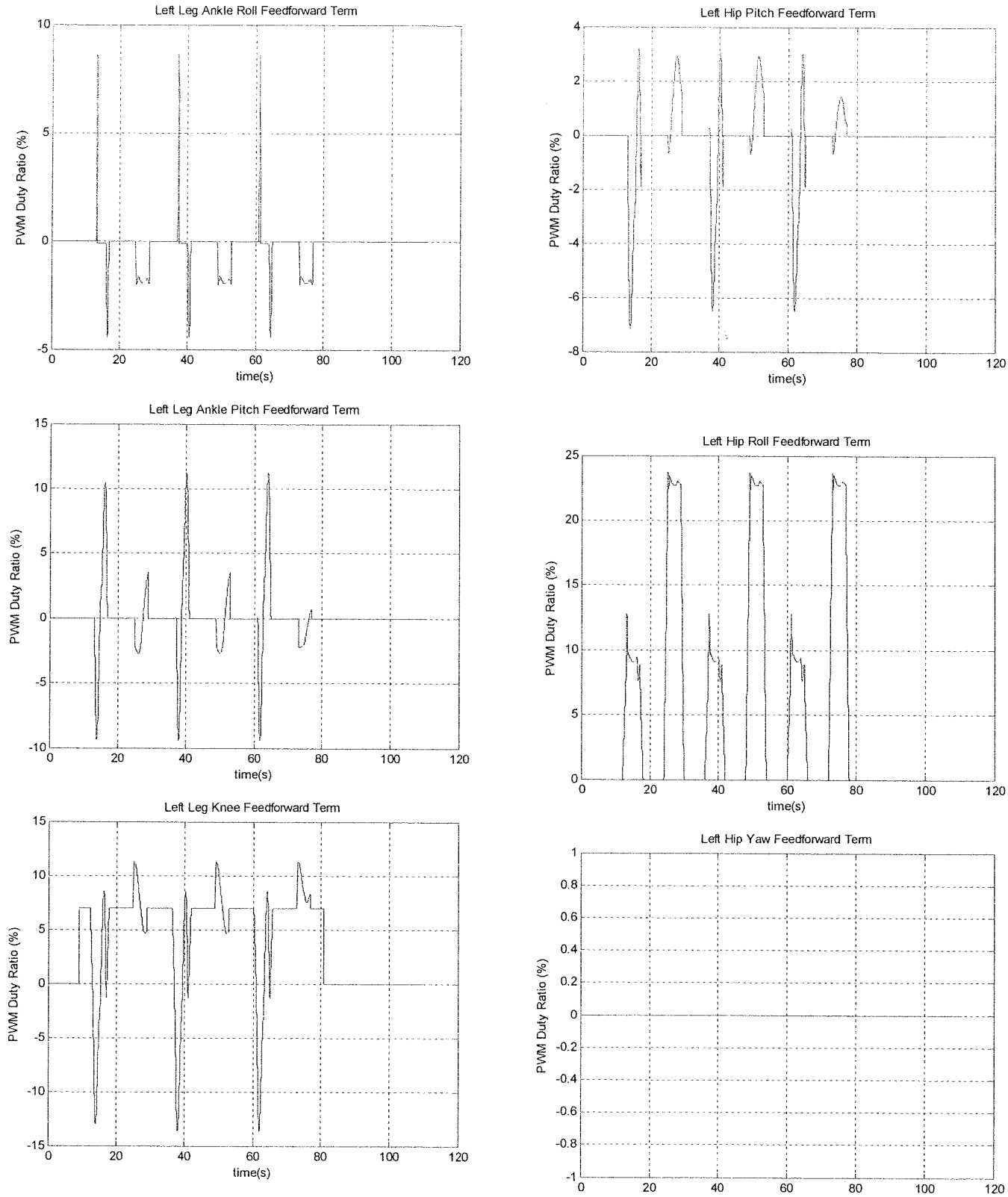

Figure 8.6: Left leg feedforward terms

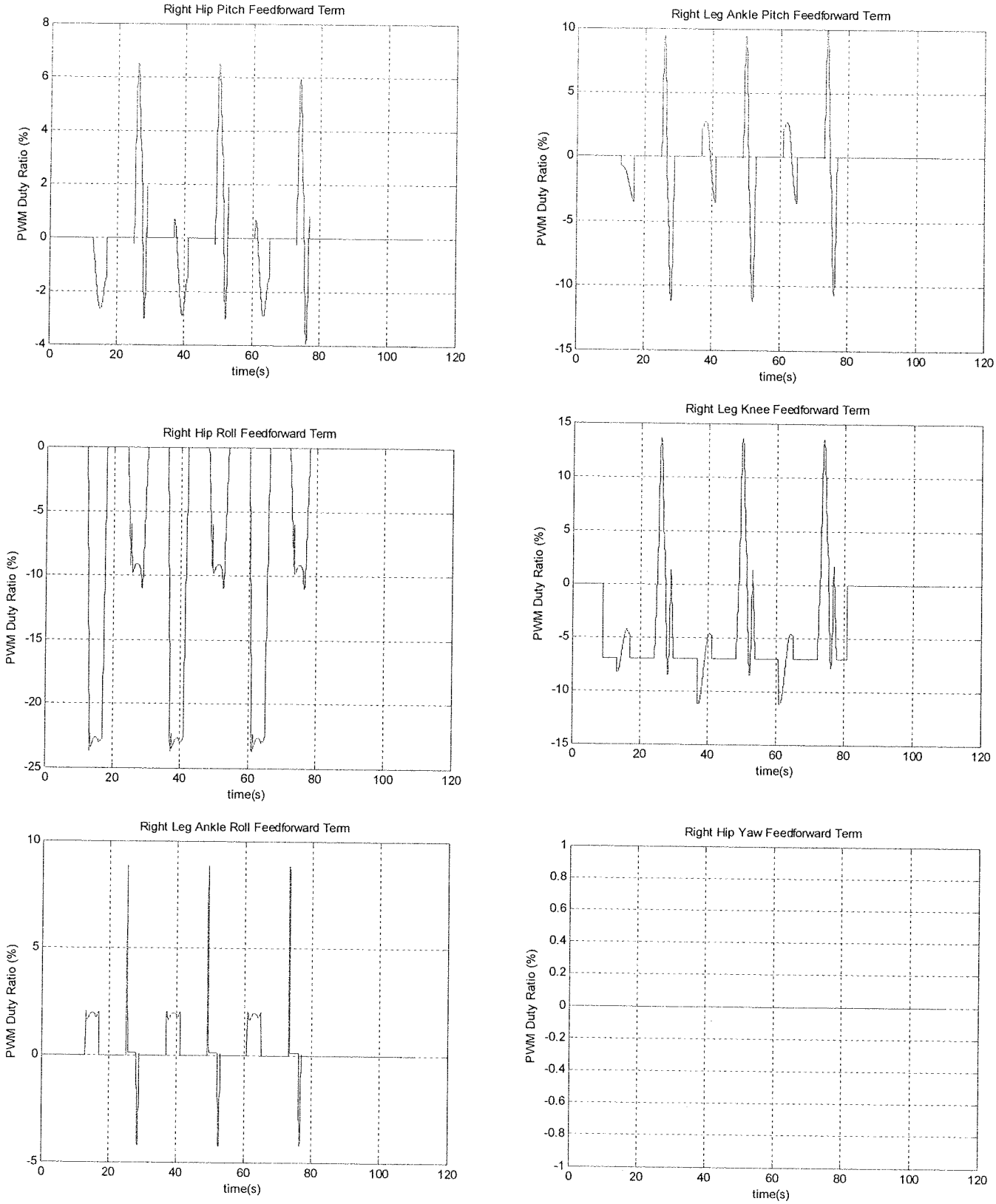

Figure 8.7: Right leg feedforward terms

8.4 Digital Filter Design

The electrical design of this robot contains many sources of noise in the analogue signals. These sources include: electrical interference in DSP circuit board, brushes on the potentiometer, internal DSP noise and unshielded wires to name a few. Although some of this noise could be reduced by means such as using shielded wires, or further refining the design of the circuit board, the noise from the within the DSP itself will still exist. For this reason appropriate filtering needs to be employed in order to have a usable signal for control purposes.

Figure 8.8 shows a plot of an unfiltered potentiometer reading containing noise corresponidng to roughly seven degrees of motion in the joint. Such spikes would cause a the derivative term in a PID controller to increase to the point that stability would be compromised. This can be contrasted to the filterd signals in section nine, the results section, which do not contain any noise larger than a fraction of one degree.

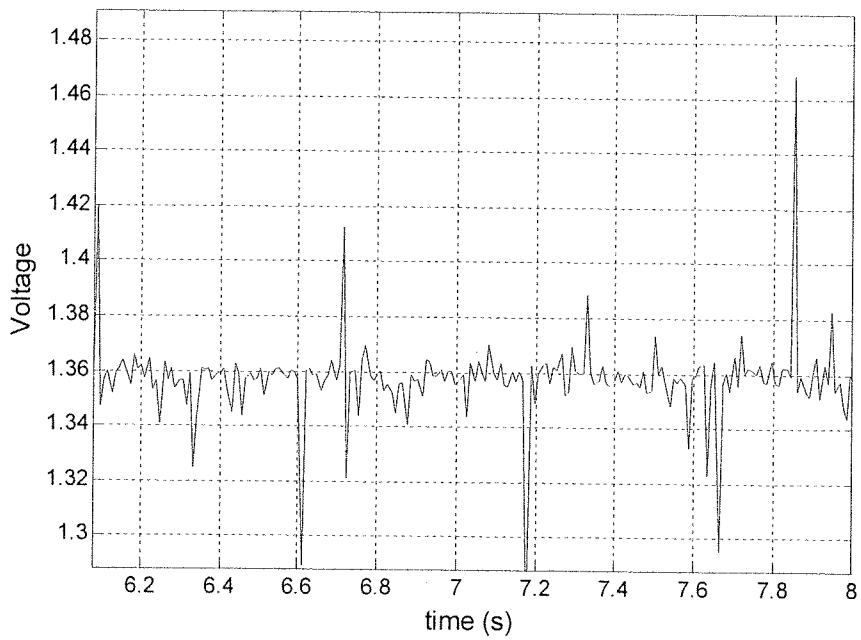

Figure 8.8: Unfiltered potentiometer signal

In order to address this problem appropriate digital filtering is employed. The filters used on the robot are designed with the competing goals of: cutting out noise, having a fast response time, and minimal computational overhead. A compromise between these goals is found by using second order Butterworth filters.

Butterworth filters roll off more slowly at the cutoff frequency than other infinite impulse response (IIR) filters such as the Chebyshev or Elliptic filter but contain no ripples in the

pass band. The Z-domain transfer function for a second order IIR filter is provided in Equation (8.7) , while the linear difference Equation is shown in Equation (8.8).

$$H(z) = \frac{Y(z)}{X(z)} = \frac{b_{0+}b_1 z^{-1} + b_2 z^{-2}}{1 + a_1 z^{-1} + a_2 z^{-2}} \tag{8.7}$$

$$y[n] = -\sum_{k=0}^{2} a_k\, y[n-k] + \sum_{k=0}^{2} b_k\, y[n-k] \tag{8.8}$$

The cut-off frequencies of the filters are selected by choosing a frequency that is low enough to eliminate most of high frequency noise, yet high enough that the step response is reasonable. The coefficients listed in Table 8.2 are attained by using the Filter Design and Analysis Tool included in Matlab. The same filter is used to filter the force sensors as well as the derivative signal. The step responses of the filters are shown in Figure 8.9 and Figure 8.10.

Filtered Signal	Filter Order	3dB Cut-Off Frequency	Coefficients	
Potentiometer Voltage	2nd	10 Hz	b_0	0.00094469184384015097
			b_1	0.0018893836876 80
			b_2	0.00094469184384015097
			a_0	1
			a_1	-1.9111970674260 73
			a_2	0.91497583480143363
Force Sensors Voltage And Derivative of Potentiometer Voltage	2nd	20 Hz	b_0	0.0036216815149286421
			b_1	0.007243363029857
			b_2	0.0036216815149286421
			a_0	1
			a_1	-1.8226949251963083
			a_2	0.83718165125602284

Table 8.2: Butterworth filter parameters

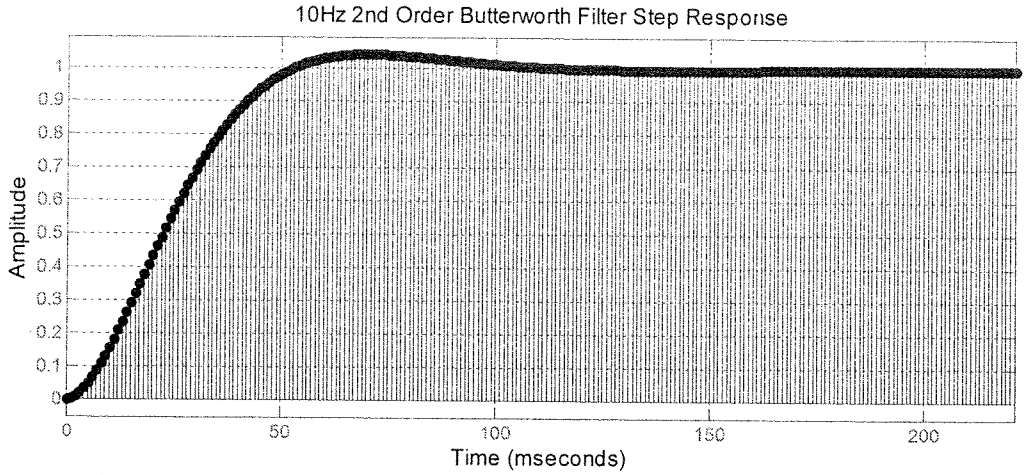

Figure 8.9: Step response plot for Butterworth low pass filter with a 3dB cutoff at 10Hz

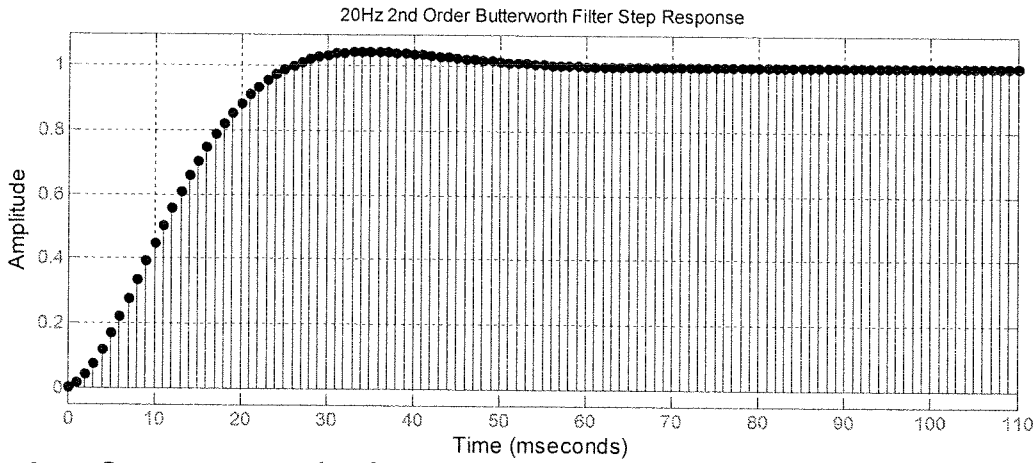

Figure 8.10: Step response plot for Butterworth low pass filter with a 3dB cutoff at 20Hz

8.5 PD and PID Controller Design

To control the joints PD and PID controllers are used. PD controllers are implemented on the ankle motors 1 and 2 as well as the hip yaw motor 6, while PID are implemented on the knee, hip pitch and hip roll (motors 3, 4, and 5 respectively). The integral term is not used on motors 1, 2 or 6, since maintaining stability is more crucial for these motors than eliminating steady state error.

These controllers are implemented using a parallel implementation or one where each of gains is set independently, and tuning is performed manually. The gains for each of the motors are listed in Table 8.3.

	K_p	K_d	K_i	**Integral Term Limit**
Motor 1	610	19	0	n/a
Motor 2	620	20	0	n/a
Motor 3	630	19	0.13	12
Motor 4	575	20	0.08	12
Motor 5	600	15	0.05	12
Motor 6	660	16	0	n/a

Table 8.3: Tracking controller gains and integral term limits

The formula for the frequency domain Equation for the controller is give in (8.9) and for the discrete implementation in (8.10) and (8.11).

$$u(s) = K_p + \frac{K_i}{s} + K_d s \tag{8.9}$$

$$u[n] = K_p e[n] + K_i \sum_{k=0}^{n} e[n-k] + K_d \frac{e[n-1]}{T_s} \tag{8.10}$$

$$e[n] = r[n] - y[n] \tag{8.11}$$

K_p: The proportional gain
K_d: The derivative gain
K_i: The integral gain
T_s: The sampling period
$e[n]$: The discrete error
$r[n]$: The reference angle error
$y[n]$: The measured angle
$u[n]$: The discrete control input.
$u_{PID}(s)$: The frequency domain control input from the PID controller.

The block diagram for the PD controller is shown in Figure 8.11, while the diagram for the PID controller is shown in Figure 8.12. Other than the two low pass filters on the diagram, the only other item of distinction is the anti integrator windup strategy prior to the integral gain.

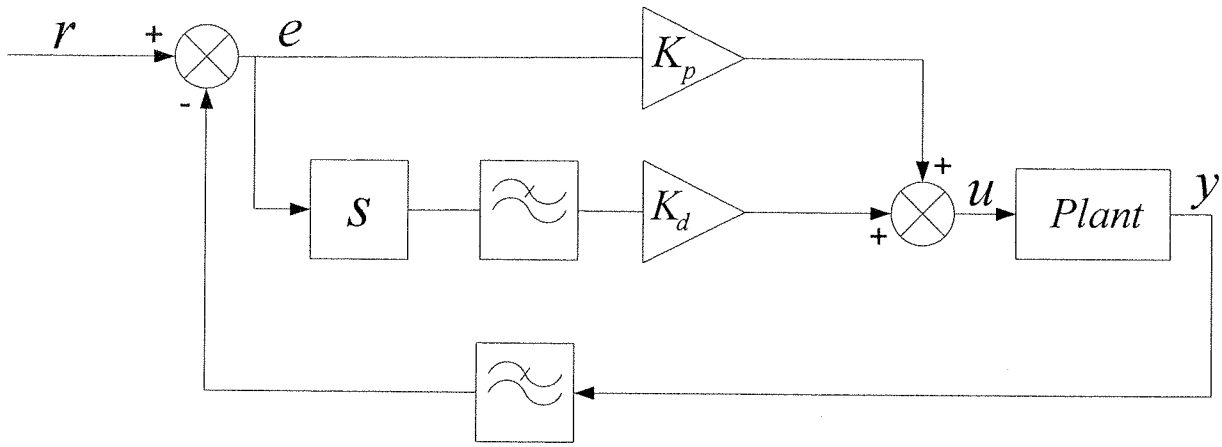

Figure 8.11: Block diagram for PD controller used on the ankle roll, ankle pitch and hip yaw motors

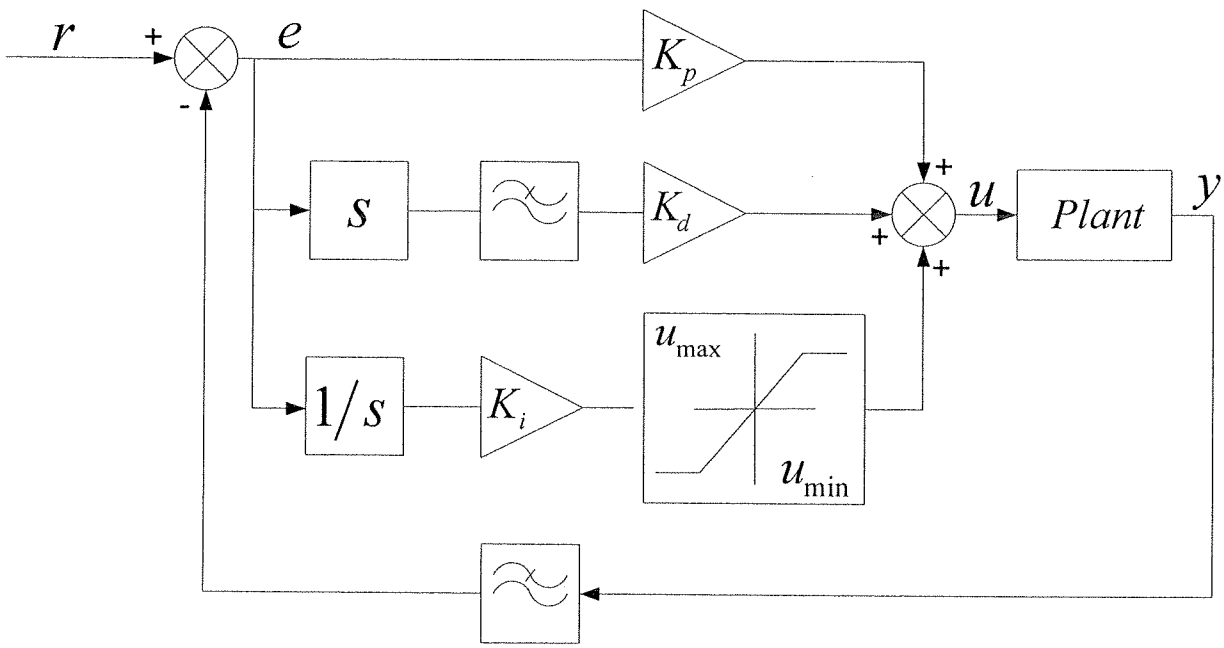

Figure 8.12: Block diagram for PID controller used on the knee, hip roll and hip pitch motors

8.5.1 Anti Windup Strategy for Integrator

To limit the amount of instability caused by the integral term, yet still have the benefit of a smaller steady state error, the error for the integral term is limited as to how large it can grow. Without this limitation the integral error could increase, or wind up, leading eventually to a large overshoot or instability.

8.6 Active Balance Control

8.6.1 Centre of Pressure Calculation

Since the planned trajectory of the centre of mass and zero moment point passes roughly through the centre of the foot during single support phase, it is possible to add a basic active balance controller to the robot in the frontal plane without having to follow a trajectory for the ZMP. This is done by using the force sensors located on the base of the each foot to calculate the centre of pressure (COP) in the y-axis, and to use this as the error signal.

The center of pressure is defined as *"The field of pressure forces (normal to the sole) is equivalent to a single resultant force, exerted at the point where the resultant moment is zero"* [20]. As long as the ground-sole contact occurs on a single plane surface, such as the biped robot walking along level ground, the COP and ZMP are the same point.

Equation (8.12), and Figure 8.13 details the calculation of the centre of pressure using force sensors mounted on the soles of the robot`s feet. Although the value for the COP corresponds to that of the ZMP [20], a distinction is made as the two have different definitions. While the COP can be thought of as sum of the forces exerted through contact between the ground and foot, the ZMP can be thought of as pertaining to forces that are transmitted without contact such as gravity and inertia [20].

$$o_{x,CoP} = \frac{\sum_{i=1}^{4} f_i r_{xi}}{\sum_{i=1}^{4} f_i} \qquad o_{y,CoP} = \frac{\sum_{i=1}^{4} f_i r_{yi}}{\sum_{i=1}^{4} f_i} \tag{8.12}$$

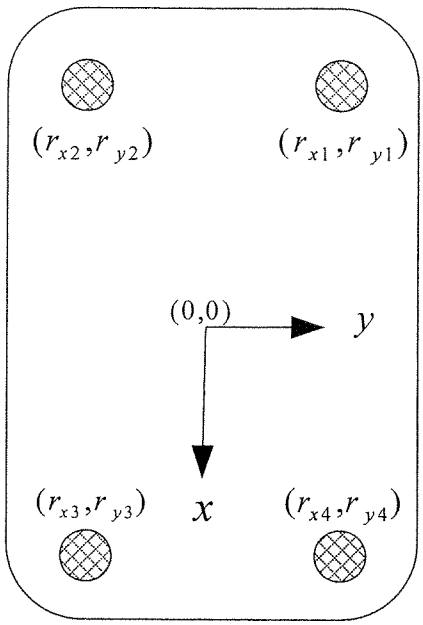

Figure 8.13: Force sensor location on the base of the foot

8.6.2 Proportional Integral Active Balance Control

The active balance controller works by using the centre of pressure in the y-axis calculated from the force sensors on the feet as an input. The controller then uses a proportional integral controller to create an additional control term contributed to the control of the ankle roll motor.

The controller itself is only activated when the robot is in single support phase and a force is detected on each of the sensors of the supporting foot indicating the foot is solidly placed. The controller has a weak proportional term, meaning most of the control is done via the integral term leading to a gradual change in the ankle angle, preventing instability.

$$u(s) = K_p + \frac{K_i}{s} \tag{8.13}$$

$$u[n] = K_p e[n] + K_i \sum_{k=0}^{n} e[n-k] \tag{8.14}$$

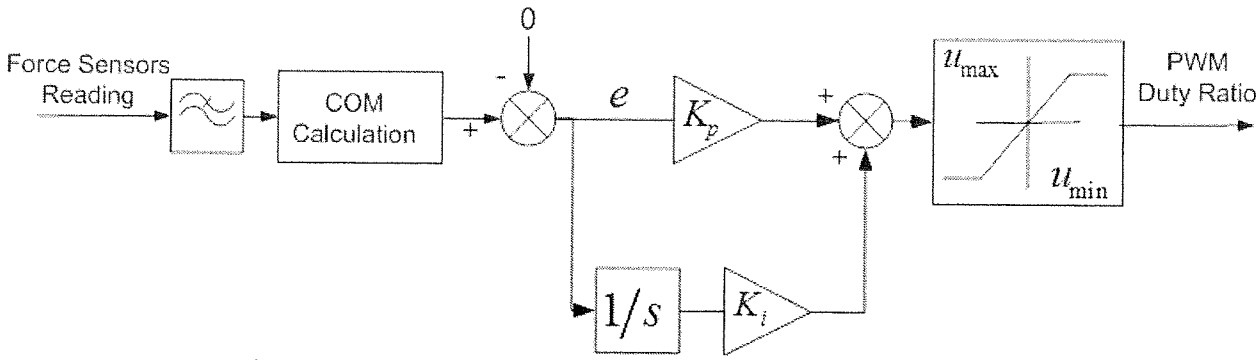

Figure 8.14: Block diagram for active balance controller

K_p	K_I	u_{max}/u_{min} (%)
20	0.35	15

Table 8.4: Balance controller gains and limits

9 Experimental Results

9.1 Introduction

Two sets of experiments were conducted on the control scheme implemented on this robot, the first to test walking control at the same time as the balance control, and the second to test just balance control. In the walking experiment the robot walks several steps while in the balance control experiment the robot balances on the right leg with the left leg lifted in the air.

9.2 Walking Control

Walking experiments were conducted on the robot in order to gauge the effectiveness of the computed torque scheme PID controller with active balance contribution to ankle roll motor.

Figure 9.1 and 9.2 show the tracking of the hips and the COM, respectively, in the X-axis. The plots show that the steps the robot takes are slightly shorter than planned due small tracking errors in the joint tracking.

Figure 9.3 - Figure 9.14 show the tracking performance, error and the applied duty ratio for all twelve motors as the robot takes six steps on level ground. Each step is ten centimeters long and the robot lifts its foot five centimeters. It takes the robot twelve seconds to take each step: 4 seconds to shift its weight onto the supporting foot, four seconds to lift and land each foot, and 4 seconds to shift its weight back to the centre.

From the graphs we see that the error is kept within two degrees for most of the trajectory, peaking at approximately three degrees occasionally. This controller allowed the robot steady bipedal locomotion consistently over the course of several trials.

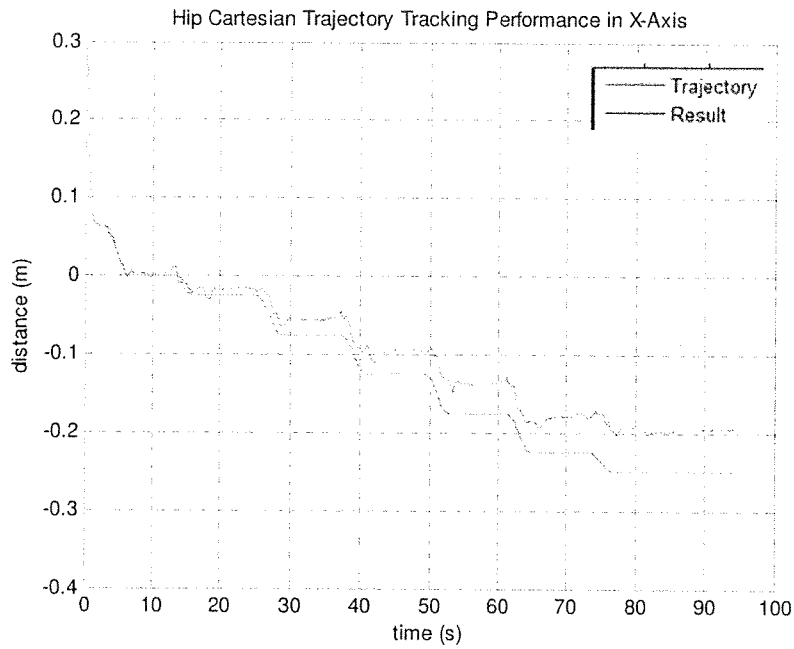

Figure 9.1: Hip Cartesian trajectory tracking performance in X-axis

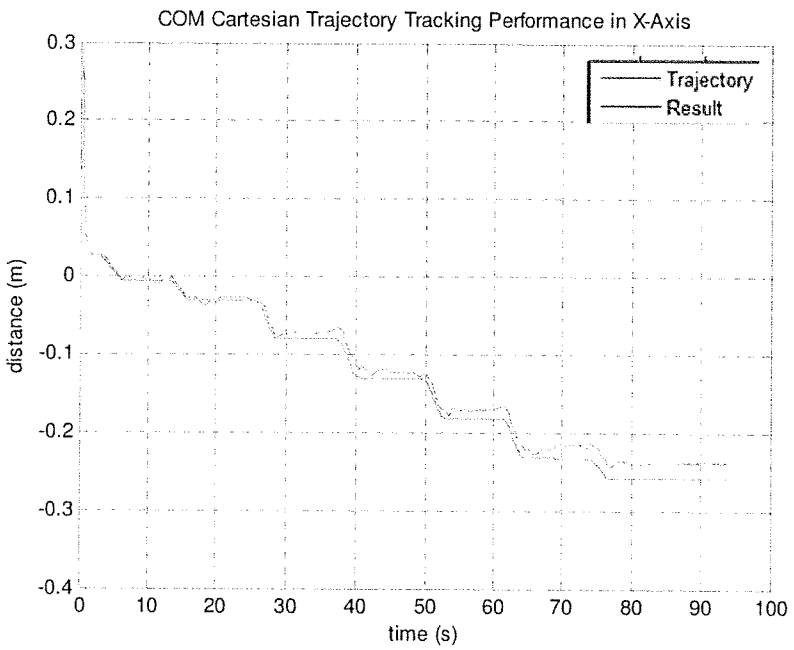

Figure 9.2: COM Cartesian trajectory tracking performance in Y-axis

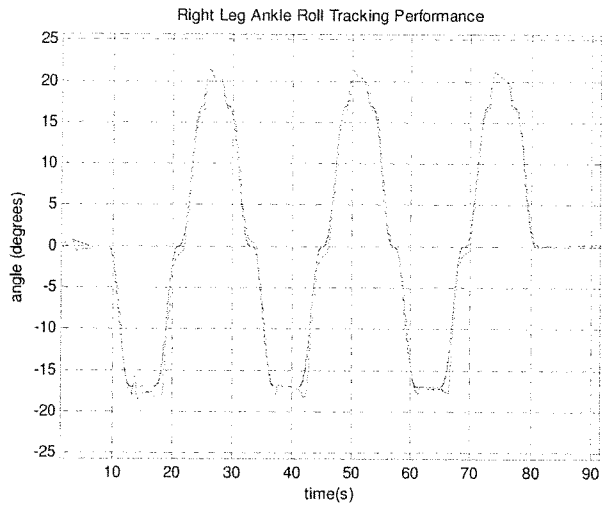

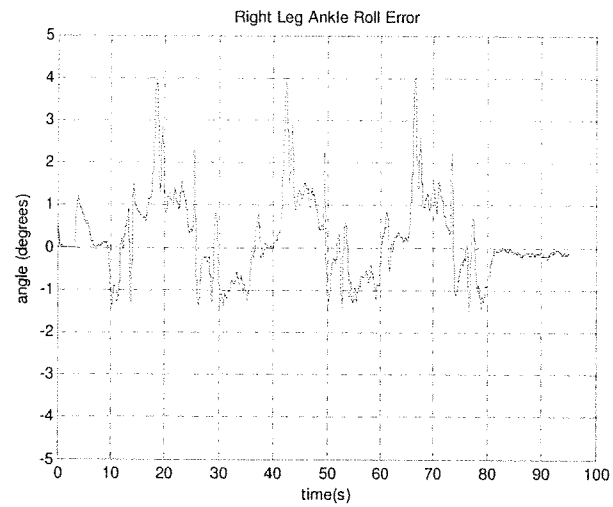

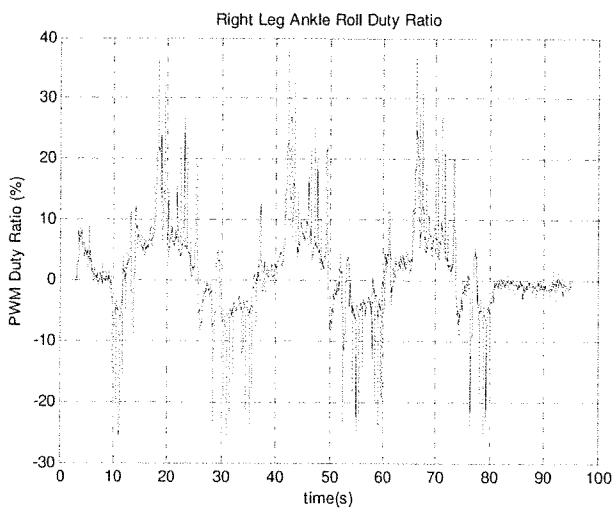

Figure 9.3: Right leg ankle roll joint performance graphs

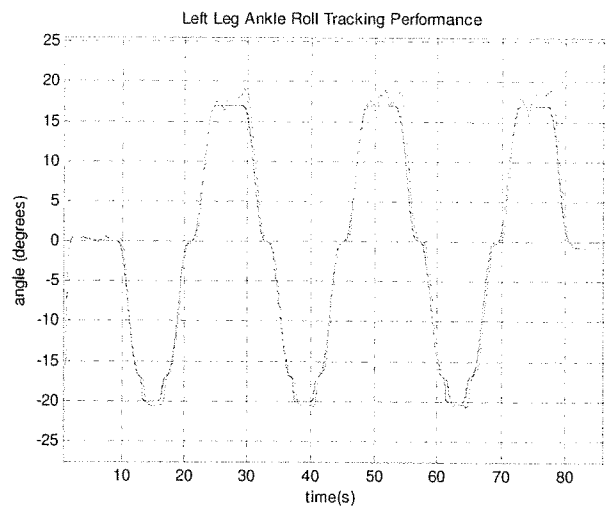

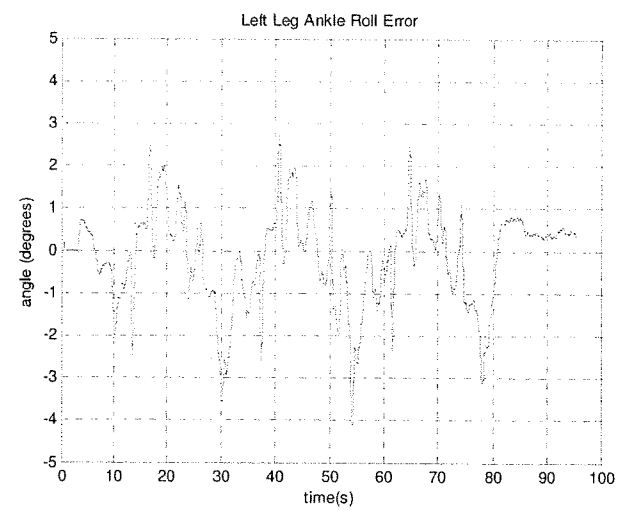

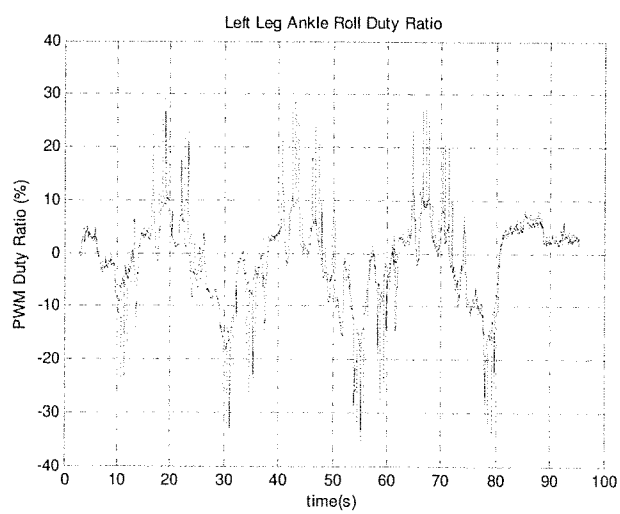

Figure 9.4: Left leg ankle roll joint performance graphs

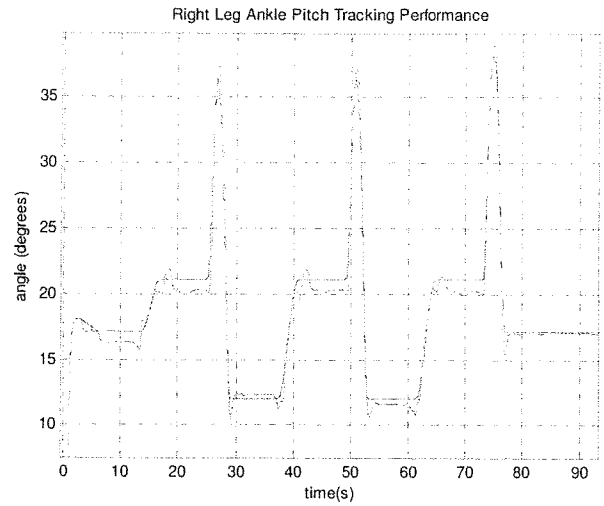

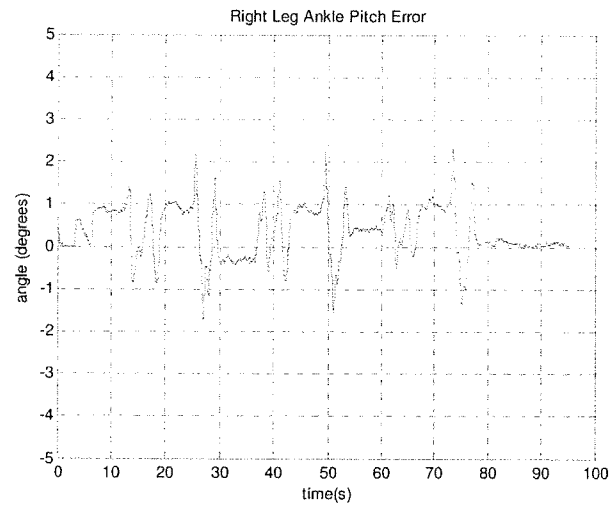

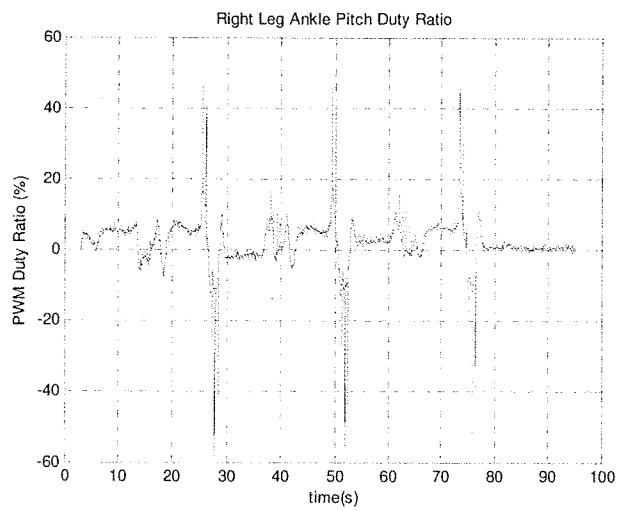

Figure 9.5: Right leg ankle pitch joint performance graphs

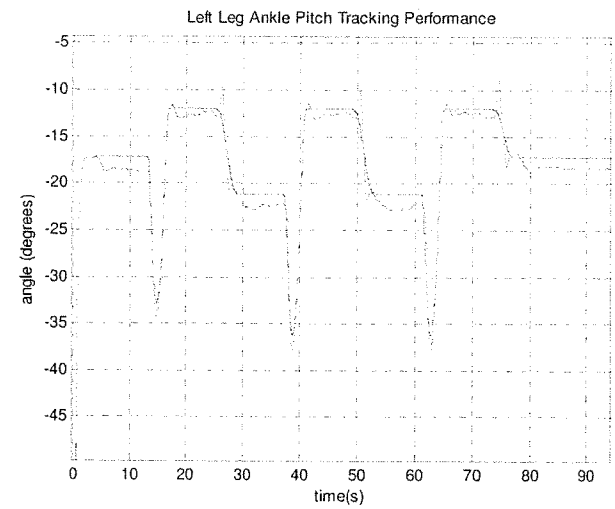

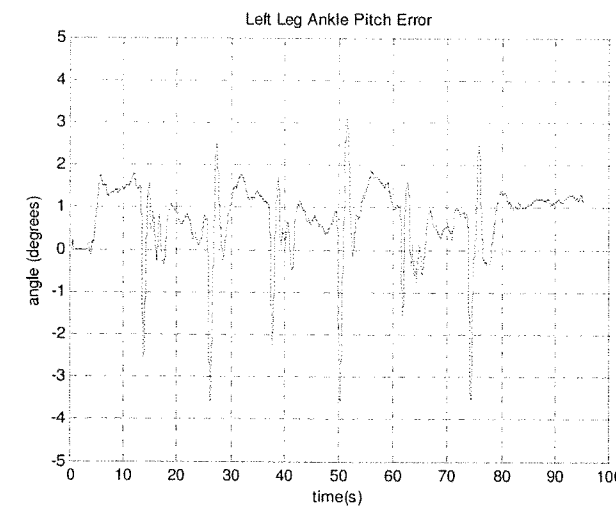

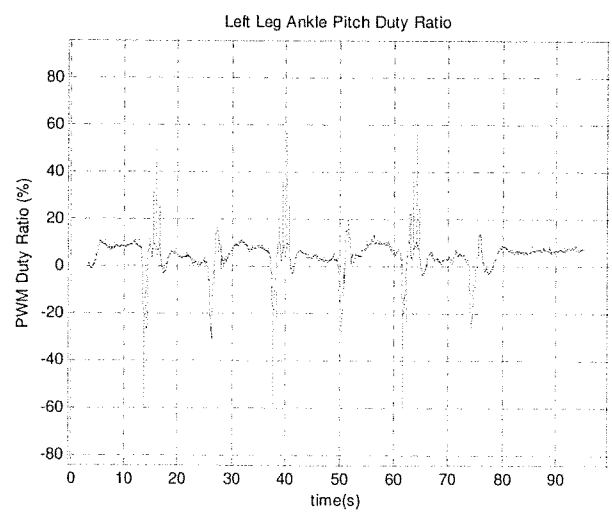

Figure 9.6: Left leg ankle pitch joint performance graphs

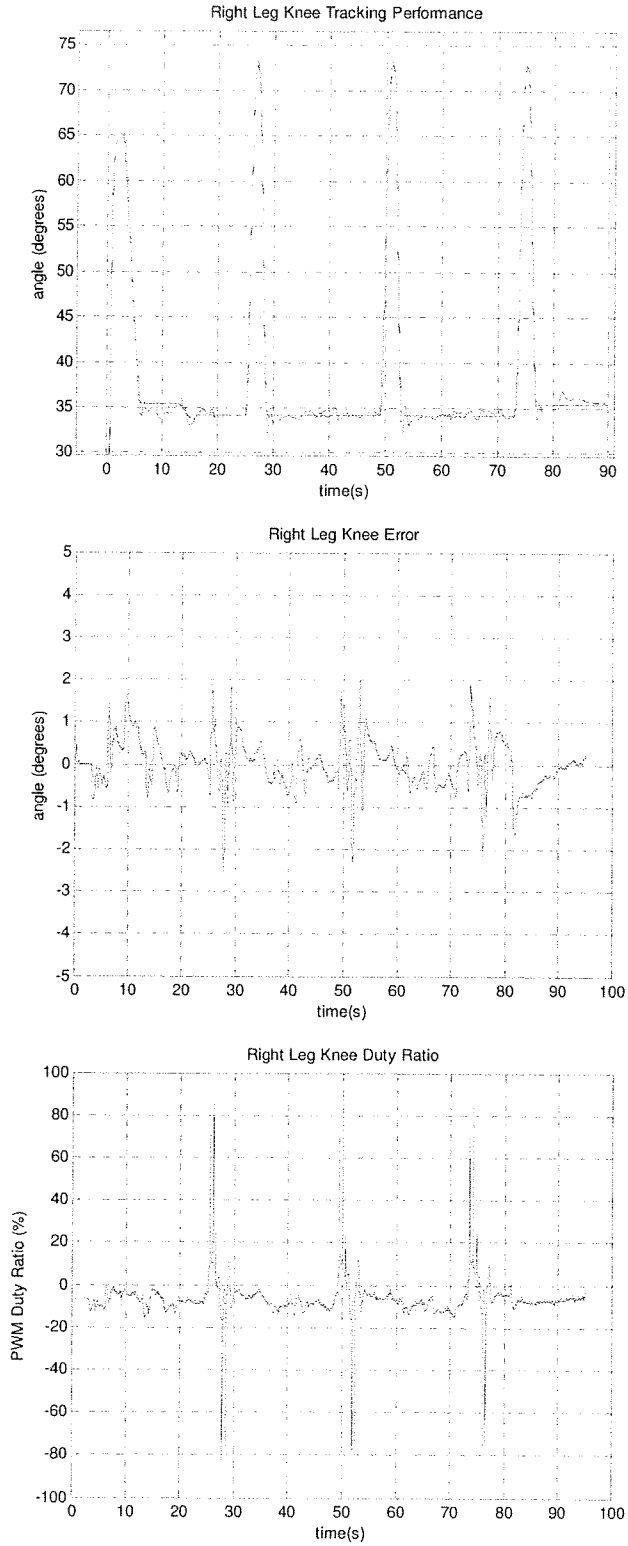

Figure 9.7: Right leg knee joint performance graphs

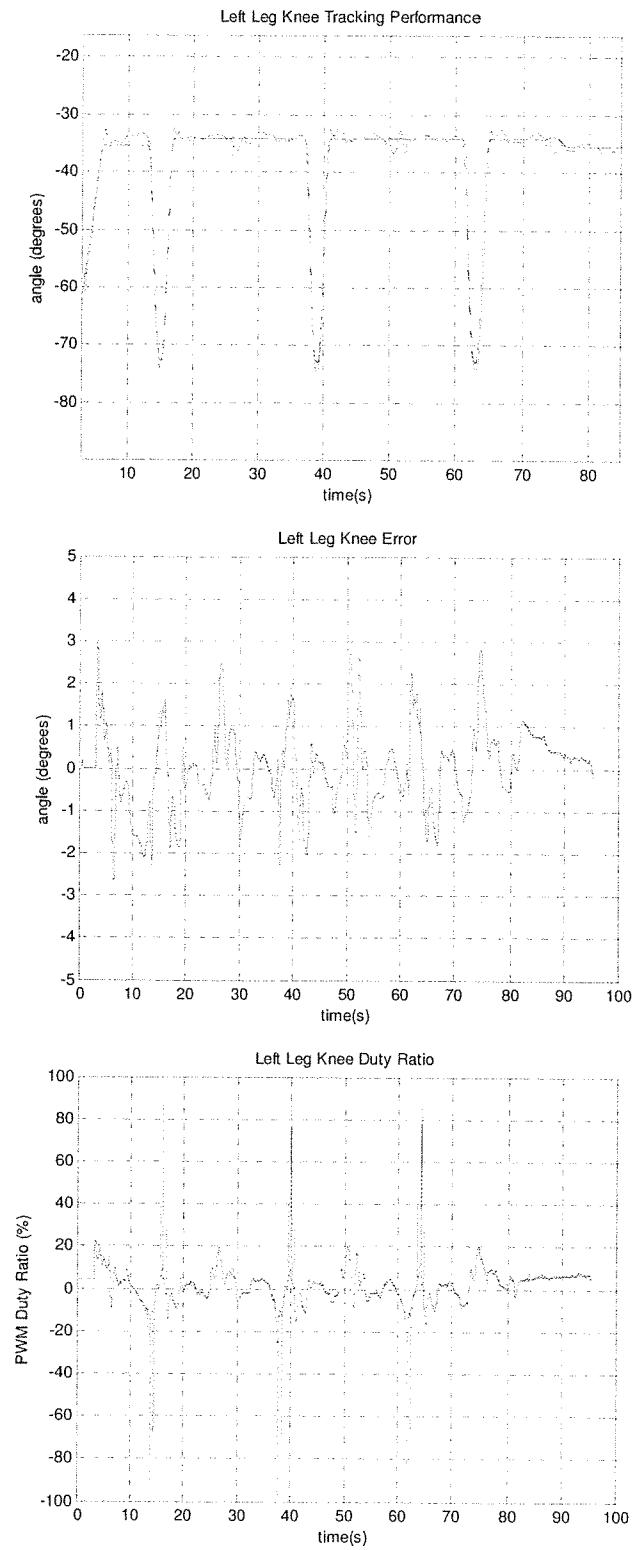

Figure 9.8: Left leg knee joint performance graphs

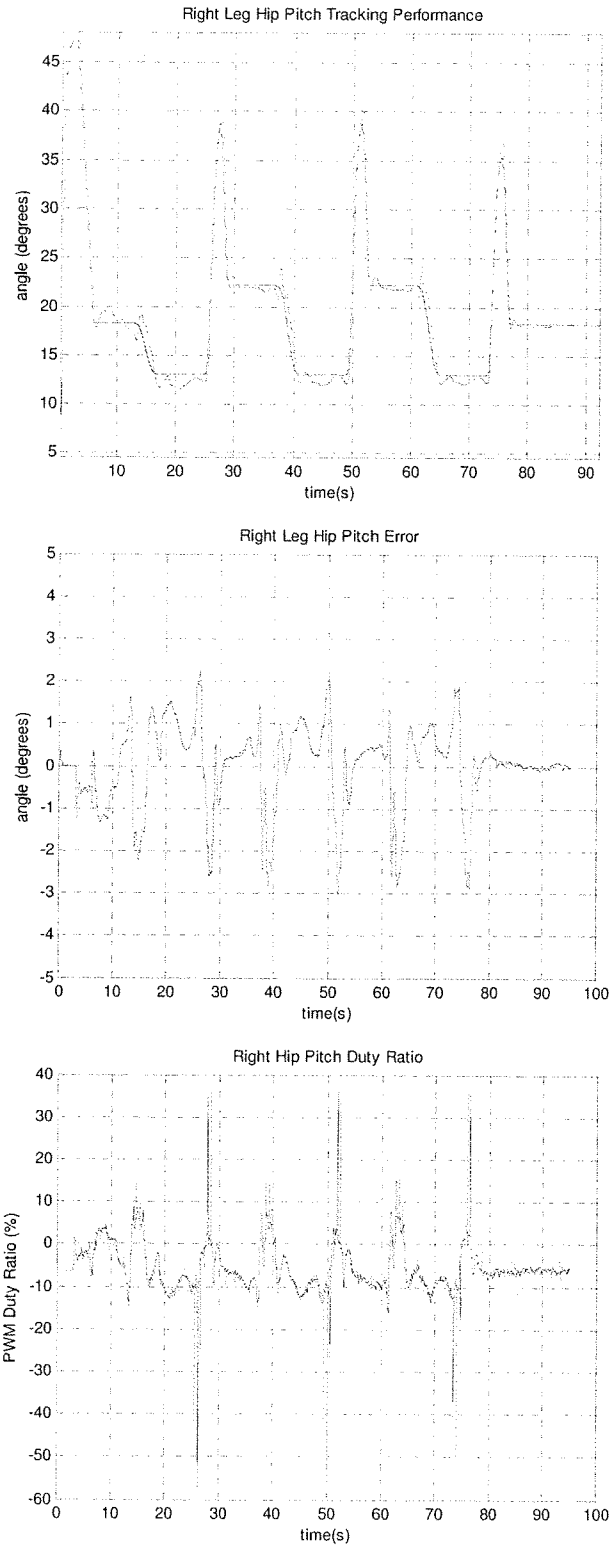

Figure 9.9: Right leg hip pitch joint performance graphs

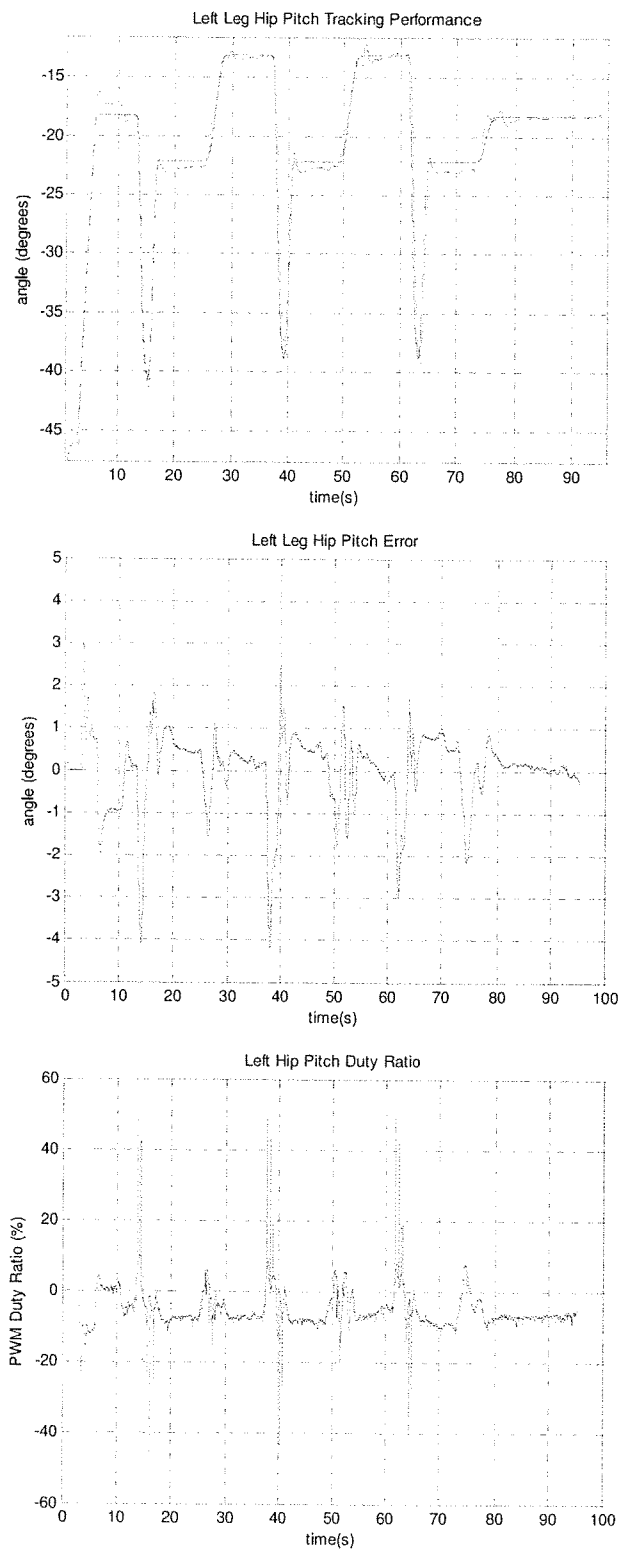

Figure 9.10: Left leg hip pitch joint performance graphs

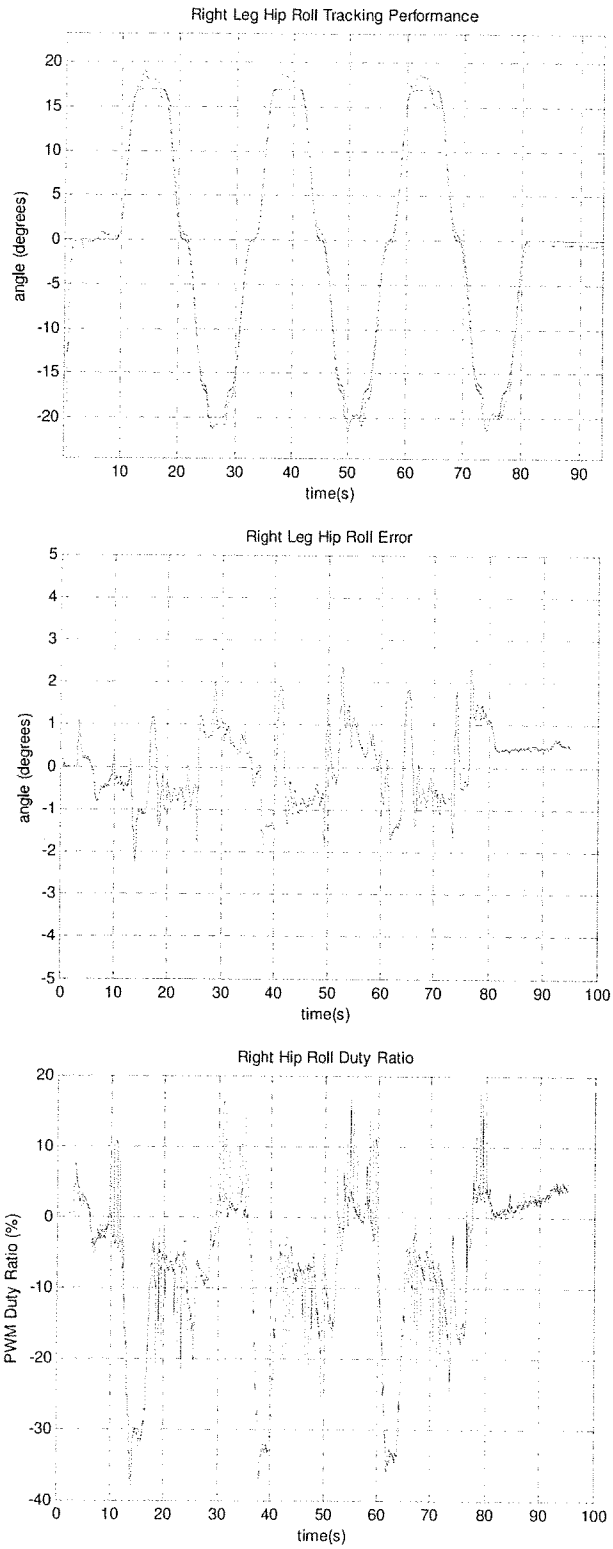

Figure 9.11: Right leg hip roll joint performance graphs

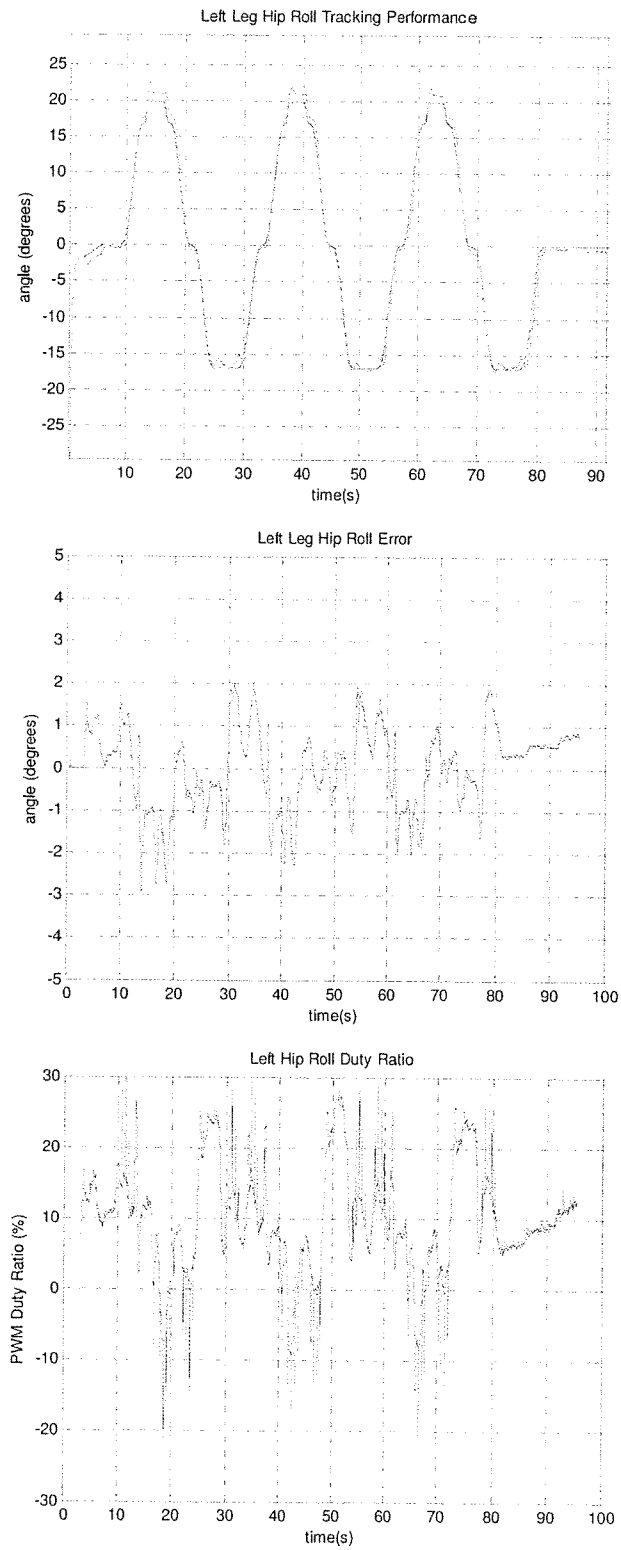

Figure 9.12: Left leg hip roll joint performance graphs

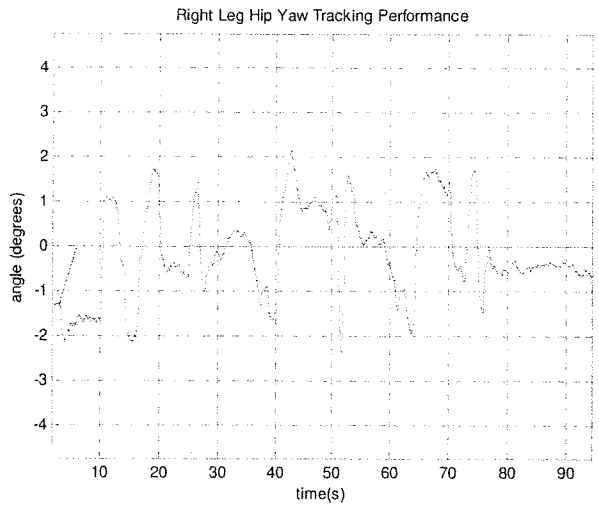

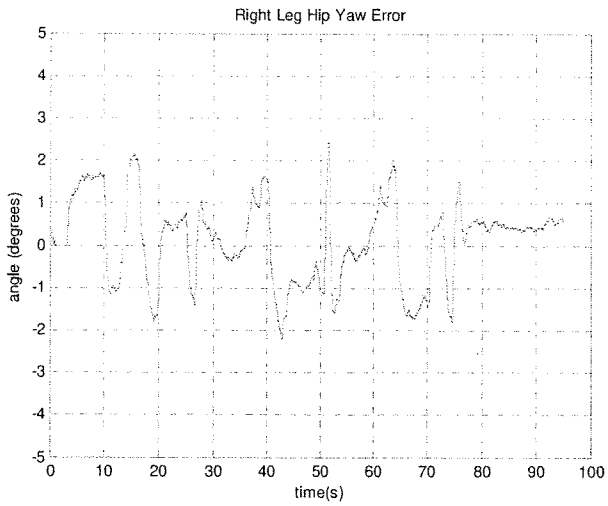

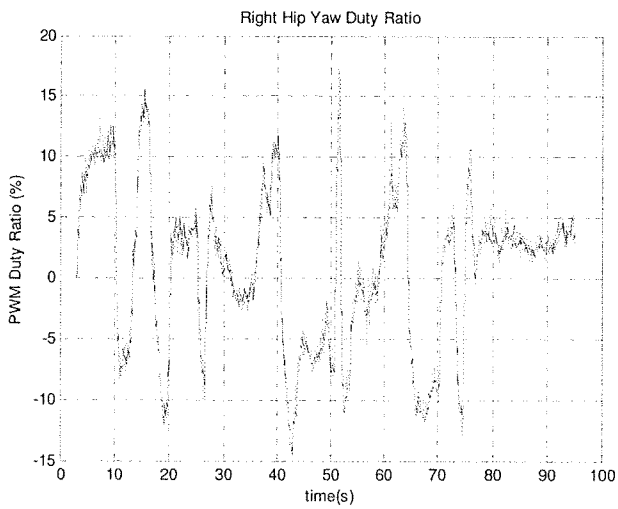

Figure 9.13: Right leg hip yaw joint performance graphs

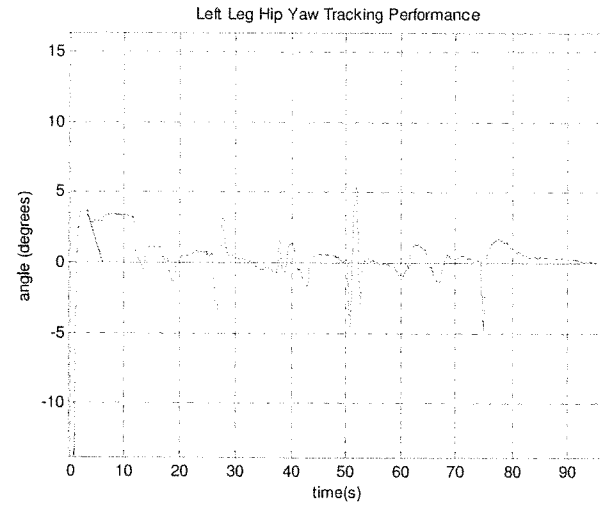

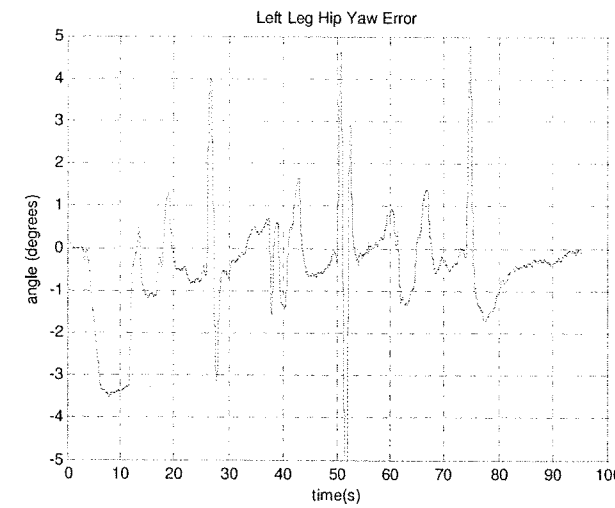

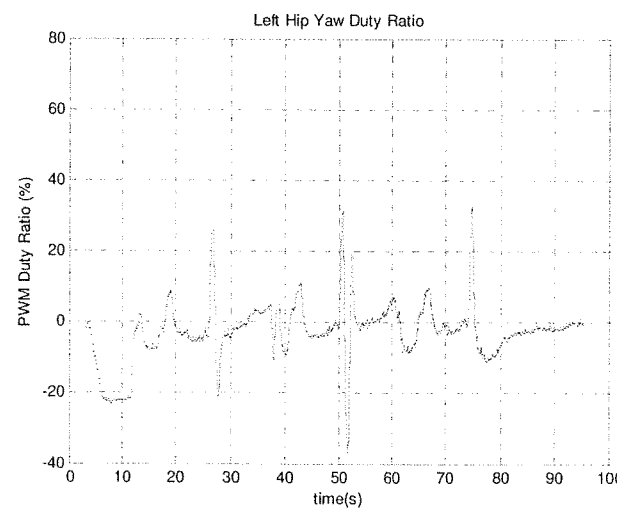

Figure 9.14: Left leg hip yaw joint performance grap

9.3 Active Balance Control

To test the balance controller the robot was given a trajectory to shift its weight on to the right leg and then to lift the left leg. In this position the robot was pushed three times to examine the performance of the balance controller. A photo of the balance control test setup is shown in Figure 9.15.

Figure 9.16, a plot of the COP in the y-axis, demonstrates that the robot is able to keep the center of pressure close to the center of the foot despite disturbances. Because the controller is not alone in controlling the ankle (the feedforward term and tracking controller also act on the joint), the balancing controller has a steady state error. Figure 9.17, a plot of the joint angle during the balance experiment, shows that the balancing controller changes the angle of the joint several degrees away from the planned trajectory in order to maintain a more stable center of pressure.

Figure 9.18 shows the COP location on right foot during the balance experiment. The rectangle in the figure is the outline of the base of the foot.

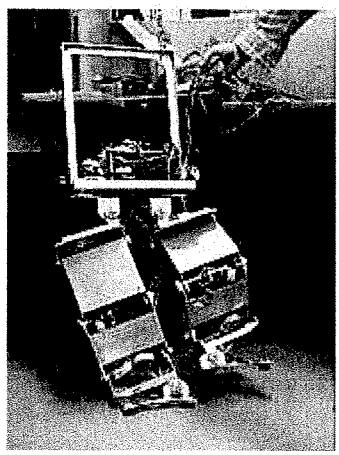

Figure 9.15: Experimental setup to test balance controller

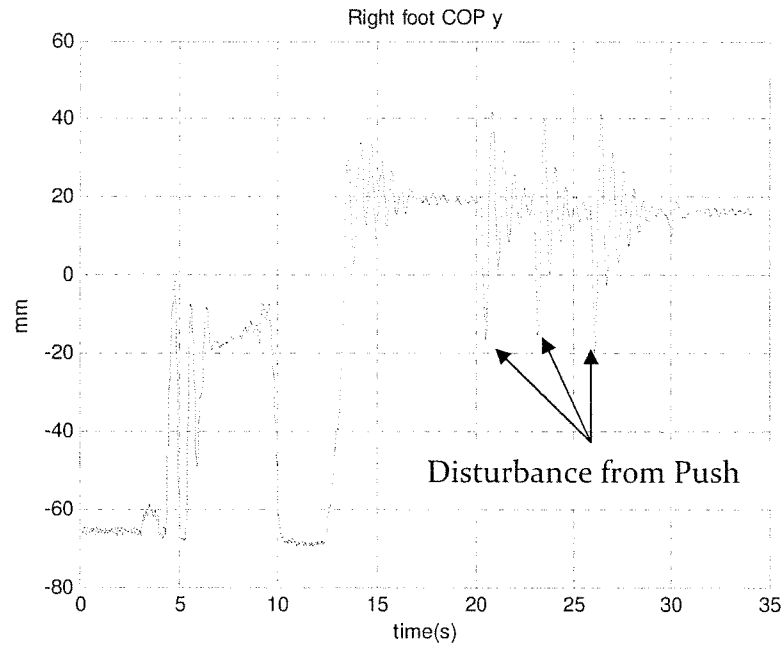

Figure 9.16: Right foot COP in y-axis with left leg lifted

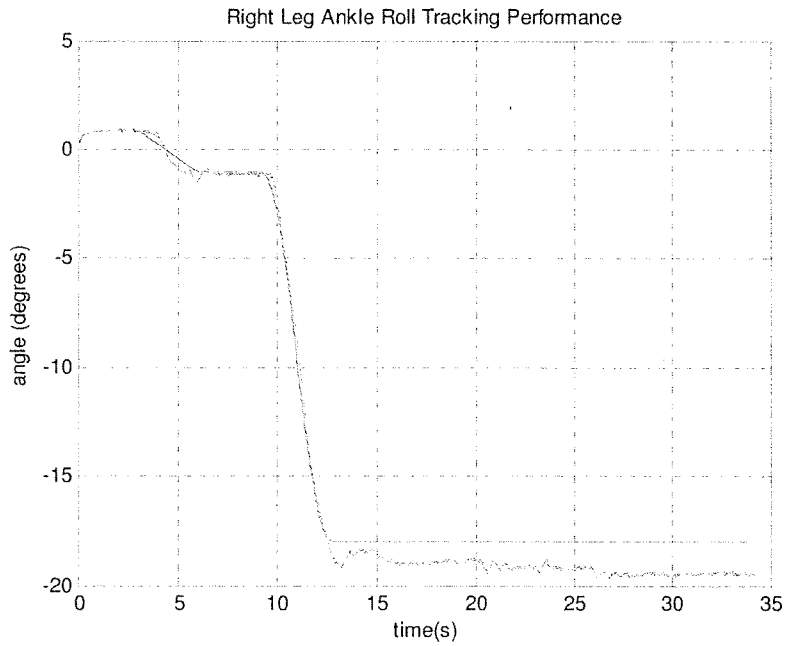

Figure 9.17: Right leg ankle roll joint tracking performance

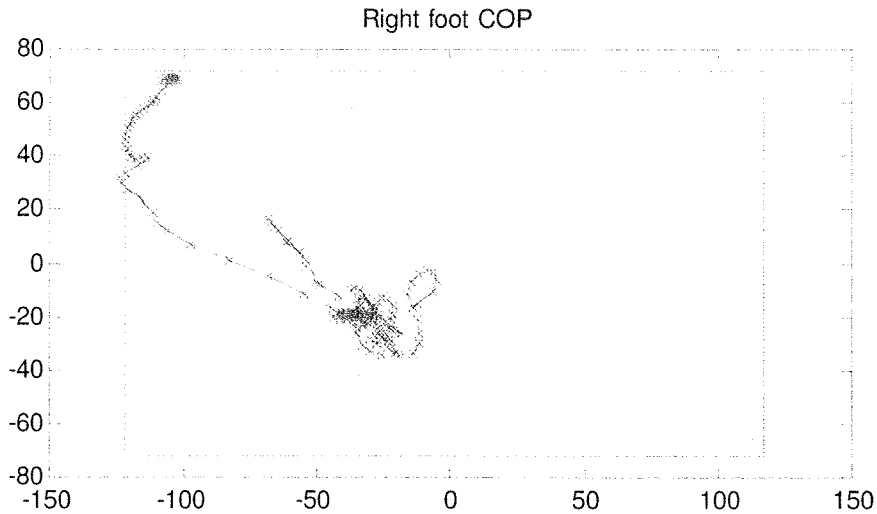

Figure 9.18: Right foot COP during balance experiment

10 Thesis Summary and Future Work

10.1 Thesis Summary

The twelve degree of freedom robot described in this work is able to passively walk on level ground at 25 cm/min. Active balance control from force sensors helps performance, and allows the robot to balance on one leg.

To accomplish this, the forward and inverse kinematic solutions are computed, and a trajectory is generated. To test the trajectory a computer animation is made which shows the anticipated robot movement as well as the location of the zero moment point and the centre of mass.

The robot is designed using 3D computer aided design software, Solidworks, and has a frame constructed of aluminum. The required joint torques are computed using the recursive Newton Euler formulation to ensure that designed structure and planned trajectory do not overload the motors.

Control of the robot is performed by using two TMS320F2812 Digital Signal Processors (DSP's) programmed in the C language on custom designed printed circuit boards. The motors are driven with H-Bridge motor drivers which receive their control signals from the DSP's.

The robot walks by having each joint follow a trajectory using PD and PID controllers with feedback coming from potentiometers at each joint and a feedforward term generated via the Newton Euler Recursive formulation. Force sensors on the feet are used to calculate the COP. The COP in the frontal plane is used by a PI balance controller which contributes to the control of the ankle roll motors, helping the robot balance.

10.2 Future Work

The main goal of future work should be to increase the speed of walking thereby moving the robot from a passive walker to a dynamic walker as well as development of a foot placement algorithm. To accomplish this, improvements would need to occur in four areas: the mechanical design, gait generation, the electrical design, and the control algorithm.

On the mechanical side, more rigid and lighter links could be designed and built by performing more static calculations and simulations on the mechanical design and by using space age materials such as titanium or carbon fiber for certain sections in order to reduce the weight of the structure. Furthermore, the centre of gravity of the robot should be shifted higher on the frame to minimize the amount of shifting needed to be done by the robot. Finally another large improvement in performance can be expected if the gears

on the robot are switched from planetary gears, which have backlash, to harmonic gears which have zero backlash.

Currently the robot's trajectory is generated first and then verified for stability by checking that the projection of the center of mass falls onto the support polygon. For the robot to walk dynamically a more sophisticated trajectory generation scheme needs to be used. This would consist of planning the path of the zero moment point and from this calculating the path of the center of mass using a simplified model such as the inverted pendulum. From the trajectory of the center of mass, the joint angles can be calculated with inverse kinematics.

The electrical design could be improved by centralizing the computation and control to a single processor. This could be done by using a single board computer with stacked pc-104 I/O cards, a programmable automation controller, or a more powerful DSP networked to weaker DSP's which serve as input and outputs. The electrical design could also benefit from more physically robust joint rotation sensors, potentially using more robust potentiometers, absolute encoders or regular encoders with a zeroing mechanism with the use of torque and level sensors on the robot.

Finally further work can be done on the control algorithm, by integrating other sensors such as torque and level sensors into a more sophisticated algorithm. Currently the active balance control is only done in the frontal plane due to limitations in the hardware, extending it to the sagittal plane could improve stability and allow the robot to walk on unlevel ground.

11 References

[1] B. Siciliano, L. Sciavicco, L. Villani and G. Oriolo, *Robotics Modelling, Planning and Control*, Glasgow, UK: Springer-Verlag London Limited, 2009.

[2] Honda Motor Company, "New Asimo - Running at 6km/h,"2005, http://world.honda.com/HDTV/ASIMO/New-ASIMO-run-6kmh/.

[3] A.D. Kuo, "Choosing Your Steps Carefully", *IEEE Robotics & Automation Magazine*, Vol. 14, No. 2, pp. 18-29, June 2007.

[4] S. H. Collins, A. Ruina, R. Tedrake, and M. Wisse, "Efficient Bipedal Robots Based on Passive-Dynamic Walkers," *Science*, Vol. 18, No. 307, pp. 1082-1085, February 2005.

[5] M.W. Spong and M. Vidyasagar, *Robot dynamics and control*, New York, New York, USA: John Wiley & Sons, 1989.

[6] A. Bélanger, L. Martel and E. Caron-Malenfant, "Population Projections for Canada, Provinces and Territories 2005-2031", Statistics Canada, Ottawa, Ontario Canada, December 2005.

[7] Honda Motor Company, "History of Humanoids", 2010, http://world.honda.com/ASIMO/history/history.html.

[8] Honda Motor Company, "Asimo Featuring Intelligence Technology", 2002, http://world.honda.com/ASIMO/technology/intelligence.html.

[9] Advanced institute of Science and Technology, 2009, http://www.aist.go.jp/aist_e/latest_research/2009/20090513/20090513.html.

[10] S. Collins, A. Ruina An, "A Bipedal Walking Robot with Efficient and Human-Like Gait", *Proceedings of the 2005 IEEE International Conference on Robotics and Automation*, Barcelona, Spain, pp. 1983-1988, April 2005.

[11] B. Vanderborght, "Dynamic Stabilization of the Biped Lucy Powered by Actuators with Controllable Stiffness", PhD Dissertation, Vrije University, Brussels, Belgium, 2007.

[12] H. Benbrahim, "Biped Dynamic Walking Using Reinforcement Learning", Ph. D. Dissertation, University of New Hampshire, Durham, New Hampshire, USA, 1996.

[13] M. Vukobratovic and B. Borovac, "Zero-moment point - Thirty Five Years

of its Life," *International Journal of Humanoid Robotics*, Vol. 1, pp. 157-173, 2004.

[14] A. Dasgupta and Y. Nakamura, "Making feasible walking motion of humanoid robots from human motion capture data," *IEEE International Conference on Robotics and Automation (ICRA 1999)*, Detroit, USA, Vol. 2, pp. 1044-1049, 1999.

[15] Alcoa, "6061 datasheet", http://www.alcoa.com/adip/catalog/pdf/Extruded_Alloy_6061.pdf.

[16] C. Shih, Y. Zhu, and W. A. Gruver, "Optimization of the Biped Robot Trajectory", *IEEE Proceedings International Conference on Systems, Man and Cybernetics*, Vol. 2, pp. 899-903, 1991.

[17] J. Hollerbach, "A Recursive Lagrangian Formulation of Manipulator Dynamics and a Comparative Study of Dynamics Formulation Complexity", *IEEE Transactions on Sysems, Man and Cybernetics*, Vol. SMC-10, pp. 730–736, Nov. 1980.

[18] D.Kim, S. J. Seo and G. T. Park "Zero-Moment Point Trajectory Modeling of a Biped Walking Robot Using an Adaptive Neuro-Fuzzy System", *IEEE Proceedings Control Theory Application*, Vol. 152, No. 4, pp. 411-426, July 2005,

[19] S.Ito and K. Moriki: "Robot Experiment of Torque Learning for Biped Balance with Respect to Periodic External Force", *SICE Annual Conference*, Okayama University, Japan, pp. 418-423, 2005.

[20] P. Sardain and G. Bessonnet, "Forces Acting On a Biped Robot: Centre of Pressure - Zero Moment Point", *IEEE Transactions on Systems*, Vol. 34, No 5, pp. 630-637, 2004.

[21] D. Hobbelen, T. Boer and M. Wisse, "System Overview of Bipedal Robots Flame and Tulip: Tailor-Made for Limit Cycle Walking", *IEEE/RSJ International Conference on Intelligent Robots and Systems*, Nice, France, pp. 2486-2491, 2008.

[22] A. Dasgupta and Y. Yakamura, "Making Feasible Walking Motion of Humanoid Robots from Human Motion Capture Data", *Proceedings of the 1999 IEEE International Conference on Robotics & Automation*, Detroit, Michigan, pp. 1044-1049, May 1999.

[23] J. H. Oh and J. Y. Kim and, "Walking Control of the Humanoid Platform KHR-1 Based on Torque Feedback Control," *IEEE International Conference on Robotics and Automation*, Vol. 1, pp. 623-628, May 2004.

[24] J. H. Oh, I. W. Park, J. Y. Kim, and J. Lee, "Mechanical Design of Humanoid Robot Platform KHR-3", *Proceedings of 2005 5th IEEE-RAS International Conference on Humanoid Robots*, pp. 321-326, 2005.

[25] J. H. Oh, D. Hanson, W. Kim Il, Y. Ha, J. Y. Kim, and I. W. Park, "Design of Android type Humanoid Robot Albert HUBO", *Proceedings of the 2006 IEEE/RSJ International Conference on Intelligent Robots and Systems,* Beijing, China, October, pp 1428-1433, 2006.

[26] Humanoid Robotics Institute, "Biped Walking Robot", Waseda University, http://www.humanoid.waseda.ac.jp/booklet/kato_4.html.

[27] G.T. Fallis, "Walking Toy". United States Patent Number 376,588, Washington, DC, 1887.

[28] T. McGeer, "Powered Fight, Child's Play, Silly wheels, and Walking Machines," *IEEE International Conference on Robotics and Automation,* pp. 1592-1597, 1989.

[29] C. L. Vaughan, "Theories of Bipedal Walking: an Odyssey", *Journal of Biomechanics,* Vol. 36, pp 513-523, 2003.

[30] Shadow Robot Company, "The Shadow Biped", 1999, http://www.shadow.org.uk/projects/biped.shtml.

[31] Anybots Company, "About the Robots", 2009, http://anybots.com.

[32] B.Verrelst, R. Van Ham, B. Vanderborght, F. Daerden, D. Lefeber And J. Vermeulen, "The Pneumatic Biped Lucy Actuated with Pleated Pneumatic Artificial Muscles", *Autonomous Robots*, Vol. 18, pp. 201–213, 2005.

[33] Boston Dynamics, "PETMAN - BigDog Gets a Big Brother", 2009, http://www.bostondynamics.com/robot_petman.html.

[34] J. Y. Kim, C. G. Atkeson, J. K. Hodgins, D. C. Bentivegna and S. J. Cho, "Online Gain Switching Algorithm for Joint Position Control of a Hydraulic Humanoid Robot", Carnegie Mellon University, Pittsburgh, PA, USA, 2007.

[35] R. Highfiel, "Robotic Exoskeleton Replicates Iron Man". Telegraph Media Group Limited, April, 2008, http://www.telegraph.co.uk/earth/main.jhtml?view=DETAILS&grid=&xml=/earth/2008/04/25/sciiron125.xml.

[36] Raytheon, "The Exoskeleton: Extreme Technological Innovation", 2009, http://www.raytheon.com/newsroom/technology/rtno8_exoskeleton/.

[37] J. J. Craig, *Introduction to Robotics*, 3rd Edition, Upper Saddle River, New Jersey, USA: Prentice Hall, 2005.

[38] P. I. Corke, "A Robotics Toolbox for MATLAB", *IEEE Robotics and Automation Magazine*, Vol. 3, pp. 24-32, September, 1996.

[39] W. Gu, "Design and Control of a 10 DOF Biped Robot", M.Sc. Dissertation, Lakehead University, Thunder Bay, Ontario, Canada, 2008.

[40] G.Tan, D.Mamadyl, H.He, and S. He, "On-line Computational Scheme for Dynamic Walking of Anthropomorphic Biped Robots II", *Proceedings of the 5th World Congress on Intelligent Control and Automation*, Hangzhou China, pp. 799-804, 2004.

[41] H. Benbrahim, "Biped Dynamic Walking Using Reinforcement Learning", Ph. D. Dissertation, University of New Hampshire, Durham, New Hampshire, USA, 1996.

[42] A. Visioli, *Practical PID Control*, Glasgow, UK: Springer-Verlag London Limited, 2006.

[43] S. Lohmeier, T. Buschmann, "Humanoid Robot LOLA", *IEEE International Conference on Robotics and Automation*, Kobe, Japan, May 12-17, pp.775-780, 2009.

[44] Texas Instruments, "TMS320F2810, TMS320F2811, TMS320F2812, TMS320C2810, TMS320C2811, TMS320C2812 Digital Signal Processors Data Manual", January, 2010, http://focus.ti.com/lit/ds/symlink/tms320f2812.pdf.

[45] National Instruments, *"LMD18200 - 3A, 55V H-Bridge", April, 2005,* http://www.national.com/ds/LM/LMD18200.pdf, *Data Sheet*.

[47] S. Kajita, F. Kahehiro, K. Kaneko, K. Fujiwara, K. Harada, K. Yokoi, and H. Hirukawa, "Biped Walking Pattern Generation using Preview Control of the Zero-Moment-Point," *IEEE International Conference on Robotics and Automation*, Vol. 2, Taipei, Taiwan, pp. 1620 – 1626, September 2003.

[48] Erbatur, K. and U. Seven, "An Inverted Pendulum Based Approach to Biped Trajectory Generation with Swing Leg Dynamics," *Proc. IEEE-RAS 7th International Conference on Humanoid Robots 2007*, Pittsburgh, USA, pp. 216-220, December 2007.

[49] Q. Huang, K. Yokoi, S. Kajita, K. Kaneko, H. Arai, N. Koyachi, and K. Taine, "Planning Walking Patterns for a Biped Robot," *IEEE Transactions on Robotics and Automation*, Vol. 17, No. 3, pp. 280-289, June 2001,

[50] J. Pratt and G. Pratt. "Intuitive Control of a Planar Bipedal Walking Robot", *IEEE Conference on Robotics and Automation*, pp. 2014-2021, 1998.

[51] K. Hirai, M. Hirose, Y. Haikawa, and T. Takenaka, "The Development of Honda Humanoid Robot," *IEEE International Conference on Robotics and Automations*, pp.1321-1326, 1998.

[52] M. Shibuya, T. Sato and K. Ohnishi, "Trajectory Generation of Biped Robots Using Linear Pendulum Mode with Virtual Supporting Point", *AMC '08. 10th IEEE International Workshop on Advanced Motion Control*, pp. 284 – 289, March 2008.

[53] S. K. Au, J. Weber, and H. Herr, "Powered Ankle–Foot Prosthesis Improves Walking Metabolic Economy", *IEEE Transactions on Robotics*, Vol. 25, No. 1, pp. 51-66, February 2009.

[54] Cyberdyne Inc., *"Robot Suit Hal"*, 2010. http://www.cyberdyne.jp/English/robotsuithal/index.html

[55] C. Azevedo, B. Espiau, B. Amblard, C. Assaiante, "Bipedal Locomotion: Toward Unified Concepts in Robotics and Neuroscience, *Biological Cybernetics*, Vol. 96 No. 2, pp. 209–228, 2007.

[56] S. Ha, Y. Han, and H. Hahn, "Natural Gait Generation of Biped Robot based on Captured Human Motion Image", *IEEE International Conference on Multisensor Fusion and Integration for Intelligent Systems Seoul*, Korea, August 20 - 22, pp. 522-525, 2008.

[57] K. Harada, K.Miura, M.Morisawa, K. Kaneko, S. Nakaoka, F. Kanehiro, T. Tsuji, and S. Kajita, "Toward Human-Like Walking Pattern Generator", IEEE/RSJ International Conference on Intelligent Robots and Systems, St. Louis, USA, October 11-15, pp. 1072-1077, 2009.

[58] R. C. Luo, C. W. Tzeng, P. C. and K. Lee, "Trajectory-Tracking of Nonlinear Biped Robot System Based on Adaptive Fuzzy Sliding Mode Control", The 33rd Annual Conference of the IEEE Industrial Electronics Society, Taipei Taiwan, pp. 2789-2794, 2007.